General Disclaimer

One or more of the Following Statements may affect this Document

- This document has been reproduced from the best copy furnished by the organizational source. It is being released in the interest of making available as much information as possible.

- This document may contain data, which exceeds the sheet parameters. It was furnished in this condition by the organizational source and is the best copy available.

- This document may contain tone-on-tone or color graphs, charts and/or pictures, which have been reproduced in black and white.

- This document is paginated as submitted by the original source.

- Portions of this document are not fully legible due to the historical nature of some of the material. However, it is the best reproduction available from the original submission.

COMPARISONS OF SEVERAL AERODYNAMIC METHODS
FOR APPLICATION TO DYNAMIC LOADS ANALYSES

Richard I. Kroll and Ronald D. Miller

July 1976

Final Report (Task IV, Item 3)

DEC 1976
RECEIVED
NASA STI FACILITY.
INPUT BRANCH

for
Ames Research Center
NATIONAL AERONAUTICS AND SPACE ADMINISTRATION

1. Report No. NASA CR-137720	2. Government Accession No.	3. Recipient's Catalog No.
4. Title and Subtitle COMPARISONS OF SEVERAL AERODYNAMIC METHODS FOR APPLICATION TO DYNAMIC LOADS ANALYSES		5. Report Date July 1976
		6. Performing Organization Code
7. Author(s) Richard I. Kroll and Ronald D. Miller		8. Performing Organization Report No. D6-44111
		10. Work Unit No.
9. Performing Organization Name and Address Boeing Commercial Airplane Company P.O. Box 3707 Seattle, Washington 98124		11. Contract or Grant No. NAS2-7729
		13. Type of Report and Period Covered Final Report
12. Sponsoring Agency Name and Address Ames Research Center National Aeronautics and Space Administration Moffett Field, California 94035		14. Sponsoring Agency Code

15. Supplementary Notes

16. Abstract

This report presents the results of a study in which the applicability at subsonic speeds of several aerodynamic methods for predicting dynamic gust loads on aircraft, including active control systems, was examined and compared. These aerodynamic methods varied from steady state to an advanced unsteady aerodynamic formulation.

Brief descriptions of the structural and aerodynamic representations and of the motion and load equations are presented. Comparisons of numerical results achieved using the various aerodynamic methods are shown in detail. From these results, aerodynamic representations suitable for dynamic gust analyses are identified.

It was concluded that several aerodynamic methods are satisfactory for dynamic gust analyses of configurations having either controls fixed or active control systems that primarily affect the low frequency rigid body aircraft response. If an active control system is included that primarily affects the elastic modes response, the more exact unsteady aerodynamic methods are required to provide the necessary accuracy for predicting both the magnitudes and phase angles of the modal responses.

17. Key Words (Suggested by Author(s)) Dynamic loads Quasi-steady aerodynamics Unsteady aerodynamics Frequency response	18. Distribution Statement Unclassified–Unlimited	
19. Security Classif. (of this report) Unclassified	20. Security Classif. (of this page) Unclassified	21. No. of Pages 22. Price*

CONTENTS

TABLES

FIGURES

FIGURES (Continued)

COMPARISONS OF SEVERAL AERODYNAMIC METHODS
FOR APPLICATION TO DYNAMIC LOADS ANALYSES

by Richard L. Kroll and Ronald D. Miller
Boeing Commercial Airplane Company

1.0 SUMMARY

This report presents the results of a study in which the applicability at subsonic speeds of several aerodynamic methods for predicting dynamic gust loads on aircraft, which include active control systems, was examined and compared. These aerodynamic methods varied from steady state to an advanced unsteady aerodynamic formulation. The study was performed under NASA contract NAS2-7729, "Development of a FLEXSTAB Computer Program," (task IV, item 3).

Brief descriptions of the structural and aerodynamic representations and of the motion and load equations are presented. Comparisons of numerical results achieved using the various aerodynamic methods are shown in detail. From these results, aerodynamic representations suitable for dynamic gust analyses are identified.

It was concluded that several aerodynamic methods are satisfactory for dynamic gust analyses of configurations having either controls fixed or active control systems that primarily affect the low frequency rigid body aircraft response. These include the FLEXSTAB steady state aerodynamics* modified with Küssner and Wagner indicial functions, strip theory aerodynamics** modified with Küssner and Wagner indicial functions, the Doublet Lattice unsteady method,** the vortex spline-kernel function unsteady method developed under this contract,** and the Rho unsteady kernel function aerodynamic method.** The approximations to the more exact unsteady representation, that are provided by the FLEXSTAB steady state and strip theory aerodynamic methods modified with Küssner and Wagner indicial functions, are suitable only because of the gust power attenuation at the higher frequencies. If an active control system is included that primarily affects the elastic modes response, only the Doublet Lattice, vortex spline-kernel function, and the Rho unsteady kernel function aerodynamic methods are suitable, because only the more exact unsteady aerodynamic methods can provide the required accuracy in predicting both the magnitudes and phase angles of the modal responses.

The only methods currently capable of providing a complete aerodynamic representation for three-dimensional aircraft configurations are the FLEXSTAB solution modified with Küssner and Wagner functions and the Doublet Lattice solution. The other aerodynamic methods are restricted to either planar surfaces and/or two-dimensional configurations, without including fuselage aerodynamics or interference effects.

---

*Applicable to both subsonic and supersonic flow.
**Subsonic flow.

2.0 INTRODUCTION

In aircraft design, differences in the unsteady aerodynamic methods used for predicting the interactive coupling between the aerodynamics and structural motions of lifting surfaces can dramatically affect the calculated stability of the system and, therefore, the calculated elastic response and structural loads. These methods must accurately predict both phase angle and magnitude of the pressures for each of the elastic modes. This requirement becomes less important at higher frequencies for dynamic gust analyses if controls are fixed or if the control motions are used only to influence the rigid body motions, because of the large attenuation of the gust power at the higher frequencies. However, this requirement becomes critical with the inclusion of active control systems that are designed to alter the elastic structural motions in a prescribed manner as in a modal suppression system.

Every unsteady aerodynamic method is based on a numerical scheme containing approximations. The influence of these approximations on the predictions of dynamic loads and response of an aircraft is not adequately ascertained by simply examining the real and imaginary parts of predicted pressure distributions. Small differences in predicted pressure magnitudes and phase angles may dramatically affect the dynamic response and loads due to coupling effects between modes. To reliably assess the relative accuracy of particular methods in obtaining the interactions and resulting response, it is necessary to perform a full dynamic analysis of an aircraft including aerodynamic, structural, and control system representations. Comparisons can then be made with results predicted by previously validated aerodynamic methods.

The purpose of this study was to compare the accuracy of several unsteady aerodynamic methods by using each method in performing dynamic loads analyses. The aerodynamic methods compared were: (1) an "s" plane* (Küssner-Wagner) modification of the steady flow method employed in the present FLEXSTAB program (ref. 1); (2) the steady flow method plus the low frequency, constant pressure panel method of the existing FLEXSTAB program; (3) vortex spline-kernel function method developed under contract NAS2-7729, task IV, item 2 (ref. 2); and (4) the Rho unsteady kernel function method (ref. 3). In addition, results from a separate study (conducted under the Boeing IR&D program) involving two other aerodynamic methods are included for comparison.** They are the lifting line (strip theory) aerodynamics*** modified with Küssner and Wagner functions and the Doublet Lattice method of reference 4. The validity of all of these methods was measured using the Rho unsteady kernel function method (ref. 3), a current advanced state-of-the-art unsteady aerodynamic representation, as a basis for comparison.

---

*LaPlace transform parameter.

**Richard, M. and Kroll, R. I., "Limitations of the Doublet Lattice Method–Application to a High Aspect Ratio Wing," Boeing document D6-42395, 1975.

***Richmond, L. D., "A Rational Method of Obtaining Three-Dimensional Unsteady Aerodynamic Derivatives of Intersecting Airfoils in Subsonic Flow," Boeing document D6-7401, 1962.

3.0 SYMBOLS AND ABBREVIATIONS

$\bar{A}$	gust response factor (σ_r/σ_g), response/unit velocity
AIC	aerodynamic influence coefficient
A_{in}, A_{out}	acceleration (g's), inboard and outboard nacelles, respectively
AR	aspect ratio
A_{root}, A_{tip}	acceleration (g's), wing root and wingtip, respectively
a_1, b_1, c_1, d_1	coefficients of Wagner function
a_2, b_2, c_2, d_2	coefficients of Küssner function
b_r	wing root semichord = 326 in.
c.g.	center of gravity
$\{C_1\}$, $\{C_2\}$	real and complex generalized forcing function coefficients, respectively
$\{\bar{C}_1\}$, $\{\bar{C}_2\}$	real and complex coefficients of loads due to the forcing function, respectively
F	forcing function
F_c	compressibility factor
f_n	natural frequency, cps
g	acceleration due to gravity
I	mass moment of inertia
k	reduced frequency, $\left(\dfrac{\omega b_r}{V}\right)$, rad/s
L	scale of turbulence, ft
M	Mach number
MAC	mean aerodynamic chord
m	mass
M_{in}, M_{out}, M_{root}	bending moment (in-lb), inboard nacelle, outboard nacelle, and wing root, respectively

$[M_1]$	generalized structural stiffness matrix
$[M_3]$	generalized structural inertia matrix
$[M_4]$	generalized aerodynamic stiffness matrix
$[M_5]$	generalized aerodynamic damping matrix
$[\overline{M}_3]$	inertia force coefficients
$[\overline{M}_4]$	aerodynamic stiffness force coefficients
$[\overline{M}_5]$	aerodynamic damping force coefficients
N_0	number of zero crossings with positive slope/ft
$\{P\}$	complex surface pressure matrix, force/unit area
$[P_{Re}], [P_{Im}]$	real and imaginary pressure matrix coefficients, respectively
PSD	power spectral density
$\{Q\}$	complex generalized force matrix
q	generalized coordinates
$[Q_{Re}], [Q_{Im}]$	real and imaginary coefficient matrices of the generalized forces, respectively
rms	root mean square
$T(i\Omega)$	complex load frequency response function
V	airplane forward true speed, length/s
$V_{in}, V_{out}, V_{root}$	shear (lb), inboard nacelle, outboard nacelle, and wing root, respectively
W	downwash (w/v)
w	velocity normal to lifting surface, length/s
WBL	wing buttock line
x, y	surface coordinates, length
α_g	function of gust angle

$\alpha_1, \beta_1, \gamma_1$	coefficients of Wagner function
$\alpha_2, \beta_2, \gamma_2$	coefficients of Küssner function
Δp	surface pressure, force/unit area
ζ	damping ratio (c/c_c)
η, ξ	surface integration variables, length
ρ	density of air, mass/unit volume
σ_g	rms of gust velocity, length/s
σ_r	rms of response
$\Phi(i\Omega)$	response quantity spectrum
$\Phi(\Omega)$	gust spectrum
$\Phi(t)$	Wagner function
ϕ	mode shape
$\psi(t)$	Küssner function
Ω	spatial function (ω/v), rad/unit length
ω	frequency, rad/s
$*$	indicial convolution

Subscripts

Bdg	bending
g	gust
Im	imaginary
r	response
Re	real
Tors	torsion

4.0 ANALYSIS

In order to effectively compare each aerodynamic method employed in the dynamic analysis, the differences in the analysis results must be reflected only from the various aerodynamics. Thus, the structural model, structural modal interpolation routines, formulation of the equations of motion and load equations, and solution routines should remain fixed while only the aerodynamic methods are varied.

Since the formulation and solution routines used in dynamic gust analyses involving active control system effects are based on linear analysis techniques, it is possible to separate the solution into two separate analyses: (1) dynamic gust loads analysis performed in the frequency domain with controls fixed and (2) dynamic loads analysis performed in the frequency domain with the excitation function consisting of an oscillatory control surface. The different aerodynamic methods were employed in each analysis where applicable, thus, enabling comparisons of the ability of each aerodynamic method to model two basic types of dynamic analyses. The airplane configuration chosen for this study was a simplified model of a large subsonic jet aircraft. Other parameters used in relation to the study were:

Speed	359 kn
Mach number	0.8
Altitude	20 000 ft
Weight	753 000 lb
C.G. location	16.2% MAC (MAC = 327.75 in.)
Aspect ratio (AR)	6.96

4.1 STRUCTURAL REPRESENTATION

In order to simplify the structural model but maintain a meaningful dynamic analysis, the airplane structural model was represented by using only the wing elastic degrees of freedom. The body, empennage, and nacelles were considered to be rigid. The wing was modeled as a finite number of lumped masses, rotary inertias, and beam segments. The generalized mass and stiffness matrices were obtained for the first eight free-free modes of this model which consisted of two rigid body modes (vertical translation and pitch) and six wing elastic modes. This representation of the generalized mass and stiffness was used with each aerodynamic method in formulating the equations of motion. A more detailed description of the structural model is presented in appendix A.

4.2 AERODYNAMIC REPRESENTATION

The aerodynamic representation was dependent on the aerodynamic method employed. Following is a brief description of each method.

4.2.1 FLEXSTAB AERODYNAMICS

The panel-type aerodynamic method (ref. 1) in FLEXSTAB calculates either subsonic or supersonic steady state aerodynamic influence coefficient (AIC) matrices relating surface pressure to flow incidence, and a low frequency approximation to an unsteady AIC matrix relating surface pressure to flow incidence time rate of change. The aerodynamic theory considers linear potential flow in both subsonic and supersonic regimes. Solutions are written as integral equations involving the strengths of flow singularities distributed over aerodynamic mean surfaces and mean lines. Strengths of the flow singularity distributions are determined using approximations based on those used in the finite element method of Woodward. Thin body and interference body mean surfaces are represented by panels, each panel having a constant strength vortex flow singularity. The aerodynamic grid used for this method is shown in figure 1.

The low frequency approximation to unsteady aerodynamics used in FLEXSTAB has severe frequency limitations and is generally suitable only for calculation of dynamic stability derivatives. The restrictions are based on reduced frequency and an AR-Mach number relationship ($k<<1$, $k<<(1-M^2)/M^2$, $k|\ln k|<<2/AR\sqrt{1-M^2}$ for subsonic, and $k<<1$, $k<<(M^2-1)/M^2$ for supersonic flow).

4.2.2 VORTEX SPLINE-KERNEL FUNCTION UNSTEADY AERODYNAMICS

This panel-type method (ref. 2) is an unsteady adaptation of the steady vortex spline-kernel function method of reference 5. The integral equation relating pressure and normal wash on a lifting surface is solved using localized spline-type functions to represent the pressure distribution. These pressure functions are defined over a local portion of the aerodynamic surface, and a spline technique is employed to ensure continuity across adjacent panels. A modified version of the Rho unsteady aerodynamic method (ref. 3) for evaluating the kernel function is employed using these pressure functions with the spline technique. This finite element method is in its early development stages and is presently restricted to single planar surfaces in subsonic flow. The paneling scheme used for this method is shown in figure 2.

4.2.3 RHO UNSTEADY KERNEL FUNCTION AERODYNAMIC METHOD

The Rho unsteady kernel function aerodynamic method (ref. 3) solves the classic boundary value problem by equating the kinematical downwash to the integral downwash expression as shown in equation (1).

$$\frac{W}{V} = \frac{1}{4\pi\rho V^2} \iint \Delta p\,(\xi, \eta)\, K\,(x, \xi, y, \eta, k, M)\, d\xi\, d\eta \qquad (1)$$

First, the singularities in the integral expression are isolated and evaluated individually. Next, pressure loading functions that account for discontinuities in the downwash due to the control surface are assumed. These pressure functions are then substituted into the integral downwash expression with the proper discontinuities to calculate a mathematical downwash which is used to remove the discontinuities in the kinematic downwash, resulting in a modified kinematical downwash that contains no discontinuities. A second set of pressure functions are then assumed which contain

7

unknown coefficients. These coefficients are determined using the modified kinematical downwash in the solution. The total unsteady pressure loading becomes the sum of all the pressure functions.

Although this method is presently the most exact theoretical formulation of subsonic unsteady aerodynamics available, it is restricted to single planar surfaces. This severely restricts its use in dynamic loads analysis where the total airplane must be represented.

The Kho unsteady method is a collocation point method. The distribution of the collocation points used over the wing surface is shown in figure 3.

4.2.4 DOUBLET LATTICE

The Doublet Lattice method (ref. 4) evaluates the integral equations relating pressure and normal wash on lifting surfaces. Landahl's representation of a nonplanar kernel function is used. Streamlined closed-body aerodynamics are represented with Mile's slender body theory. Woodward's method of interference surfaces is applied to determine the lifting-surface slender-body interaction effects. The Doublet Lattice method is a subsonic panel-type method which can be used to represent the aerodynamics on the total airplane. The primary restrictions are that the aspect ratio of each panel should be approximately unity and that the number of panel divisions in the chordwise direction must increase with reduced frequency. Figure 4 shows the panel distribution used for the gust excitation problem; figure 5 illustrates the paneling scheme used in the oscillatory aileron case.

4.2.5 STRIP THEORY (LIFTING LINE)

This aerodynamic method* is based on two-dimensional incompressible flow in formulating the aerodynamic lift curve slopes. These two-dimensional lift curve slopes can be modified with compressibility factors (F_c) and wind tunnel test data where applicable. Steady state three-dimensional lift is obtained by modifying the two-dimensional lift coefficients with a static induction matrix based on the method developed in reference 6 to include three-dimensional effects. Strip theory aerodynamics are restricted to high AR lifting surfaces. The paneling used for this aerodynamic method is shown in figure 6.

4.2.6 KÜSSNER AND WAGNER LIFT GROWTH FUNCTIONS
AS APPLIED TO THE STEADY STATE AERODYNAMIC
FORMULATIONS OF FLEXSTAB AND STRIP THEORY

One method of formulating the unsteady aerodynamic problem is to use the FLEXSTAB or strip theory steady state aerodynamic formulations with the Küssner and Wagner lift growth functions. This approach is discussed extensively in reference 7. Briefly, the circulatory portion of the aerodynamic forces is obtained by multiplying the steady state lift and moment by the convolution of the normal wash (the velocity normal to the

---

*Richmond, L. D., "A Rational Method of Obtaining Three-Dimensional Unsteady Aerodynamic Derivatives of Intersecting Airfoils in Subsonic Flow." Boeing document D6-7401, 1962.

lifting surface) with either the Küssner or Wagner lift growth function. Normal wash caused by structural motion is convoluted with the Wagner lift growth function which was derived assuming a step change in angle of attack. This convolution multiplied by the steady state aerodynamics gives the circulatory portion of the response aerodynamics. The circulatory part of the gust aerodynamic forces is calculated using the normal wash, resulting from a gust encounter, convoluted with the Küssner lift growth function. The Küssner function was derived assumming a sharp-edge gust. The exact form of the Küssner-Wagner functions is not expressible in terms of well known functions; therefore, approximate representations are used:

$$\phi(t) = a_1 - b_1 e^{-\alpha_1 t} - c_1 e^{-\beta_1 t} - d_1 e^{-\gamma_1 t} \quad \text{(Wagner)} \tag{2}$$

$$\psi(t) = a_2 - b_2 e^{-\alpha_2 t} - c_2 e^{-\beta_2 t} - d_2 e^{-\gamma_2 t} \quad \text{(Küssner)} \tag{3}$$

The values of the coefficients used in equations (2) and (3) are dependent on aspect ratio and Mach number. References 8 and 9 present the development of the approximations and the tabular data for selecting the coefficient values. For this study, the coefficients were selected based on an aspect ratio of six and a Mach number equal to zero. The numerical values used for the Küssner and Wagner functions are shown in appendix B.

4.3 EQUATIONS OF MOTION AND LOAD EQUATIONS FORMULATION

The form of the equations of motion and load equations are presented in appendix B. In summary, two basic forms were used depending on the aerodynamic representation: (1) constant coefficient equations which are formed by utilizing steady state aerodynamic representations, and approximating unsteady aerodynamics with either Küssner and Wagner indicial lift growth functions or the low frequency representation of FLEXSTAB; and (2) nonconstant coefficient equations with respect to frequency, that are formed utilizing the more exact unsteady aerodynamic methods. The constant coefficient generalized structural inertia and stiffness forces were obtained from the structural representation and used in conjunction with both of the two basic forms of the aerodynamic force equations. The structural damping force was set equal to zero.

Since it was the purpose of this study to obtain a comparison between several aerodynamic methods when used with a dynamical system, it was felt that the omission of structural damping would yield the clearest comparison of differences between the several methods in predicting both magnitudes and phase angle relationships. Admittedly, the addition of structural damping would have effect on the overall response of the system and, therefore, could change the magnitude of the relative differences between several aerodynamic methods calculated without structural damping.

The load equation formulation used the force summation technique (ref. 10). Shears and bending moments were obtained at three wing locations; wing buttock line (WBL) 105, 470, and 837, which correspond to wing span stations at approximately the wing root, inboard nacelle, and outboard nacelle, respectively. Accelerations were obtained at four wing stations; WBL 1132, 837, 470, and 64, which approximately correspond to wingtip, outboard nacelle, inboard nacelle, and wing root, respectively (fig. 7).

9

The acceleration equation coefficients are only a function of the mode shape. Shear and bending moments are a function both of the inertia load and aerodynamic forces. The inertia load coefficients were calculated using the mass and geometry data and then combined with the aerodynamic load coefficients to produce a total load representation.

The methods of calculating the aerodynamic load coefficients for the different aerodynamic theories were similar with only slight differences caused by the variation of the location and form of the aerodynamic panel forces. For the strip theory representation, forces and moments are determined at a point on the elastic axis and at the midspan point of each strip. The FLEXSTAB, Doublet Lattice, and vortex spline-kernel function methods define forces that are constant over each panel and act at the panel centroids. The vortex spline-kernel function also defines moments at the centroid of each panel. The Rho unsteady kernel function method used a simplified integration of pressures to define lifts and moments on streamwise aerodynamic panels at the quarter chord.

4.4 SOLUTION TECHNIQUES

The method of solution of the equations of motion are identical whether the equations have either frequency dependent or constant coefficients. The equations are solved for the generalized coordinates at discrete frequencies producing frequency response functions in terms of magnitude and phase angles for sinusoidal excitation functions.

The excitation functions include aerodynamic forces resulting from either a continuous sinusoidal gust encounter (ref. 9) or a sinusoidal aileron oscillation. Once the generalized coordinate frequency responses were obtained, then the load equation frequency response functions were obtained by direct multiplication of the load coefficients by the generalized coordinate responses. Appendix B contains a more detailed discussion of the equations of motion and load equation formulation.

In utilizing the continuous sinusoidal gust excitation function, a comparison of the load parameters obtained by statistical methods produced a means of examining the adequacy of the aerodynamic methods for dynamic gust design loads with controls fixed. The two parameters of interest are $\overline{A}$ and N_0 (refs. 11 and 12).

$$\overline{A} = \left[\int_0^\infty |T(i\Omega)|^2 \, \Phi(\Omega) d\Omega \right]^{1/2} \tag{4}$$

is the ratio of the root mean square (rms) value of the load to the rms value of the gust velocity.

$$N_0 = \frac{1}{2\pi\overline{A}} \left[\int_0^\infty \Omega^2 \Phi(\Omega) \, |T(i\Omega)|^2 d\Omega \right]^{1/2} \tag{5}$$

is the average number of times per unit distance that load crosses the value zero with positive slope;

where:

$T(i\Omega)$ = load frequency response function
$\Phi(\Omega)$ = gust spectrum

Note: The integrations in these expressions, though defined from zero to positive infinity, were actually performed from zero to 16 cycles per second (cps).

The accepted gust spectrum for commercial airplane design purposes has been the Von Karman (fig. 8) which has the expression

$$\frac{\Phi(\Omega)}{\sigma^2_g} = \frac{L}{\pi} \frac{1 + \frac{8}{3}(1.339\ L\Omega)^2}{\left[1 + (1.339\ L\Omega)^2\right]^{11/6}} \tag{6}$$

where:

L = scale of turbulence, ft
Ω = ω/v, spatial frequency, rad/ft
ω = frequency, rad/s
v = velocity, ft/s

$\bar{A}$ and N_0 can give an indication of the adequacy of the different aerodynamic methods when dealing with continuous turbulence. However, these parameters are not able to give insight into the differences in magnitude and phase angle prediction between the different aerodynamic theories. These differences can become critical in the design of active control systems for modal suppression, stability augmentation, or load alleviation. A clearer picture of the differences arising from the different methods can be obtained by examining the generalized coordinate and load frequency response functions resulting from gust and aileron excitation.

Although two separate computer programs* were used depending on whether the coefficients to the equations were constant or nonconstant, the solution routines and output of each computer program are identical—only the input routines differ. Thus, commonality was maintained wherever possible so that any differences were a result of only the aerodynamic methods.

---

*Clemmons, R. E., A Power Spectral Digital Computer Program to Determine Dynamic Loads Due to Random Gusts—PSDSYS (TEV156)—User's Guide, BCS-60235-1, June 1973.

Sidewell, K. W., Solution Program System (TEV114) for the Analysis of the Response of a Flexible Airplane to Vertical Turbulence, D6-29669TN, Vol. 1, March 1969.

5.0 RESULTS AND DISCUSSION

As discussed earlier, the aerodynamic methods used to generate equations of motion and load equations and which were compared are the:

1. Quasi-steady* formulation of the FLEXSTAB steady state aerodynamics

2. Quasi-steady formulation of the FLEXSTAB steady state aerodynamics with the instantaneous angle of incidence modified with Küssner and Wagner indicial lift growth functions

3. Quasi-steady formulation of the FLEXSTAB steady state and low frequency approximation aerodynamics used both for response (motion induced) and gust aerodynamic forces

4. Quasi-steady formulation of the FLEXSTAB steady state aerodynamics used for gust aerodynamic forces, and both FLEXSTAB steady state and low frequency approximation aerodynamics used for response (motion induced) aerodynamic forces

    Note: This method is the aerodynamics developed in FLEXSTAB and used in method 3 but with only the low frequency approximation aerodynamics on the response forces included. With the aerodynamic gust forces due to the flow incidence time rate of change eliminated, this method is theortically incomplete. However, it is useful for some stability and control analyses when evaluating the stability of the system. Thus, it was included as an aerodynamic method for use in comparison.

5. Quasi-steady formulation of the strip theory aerodynamics corrected to match wind tunnel steady state data, and the instantaneous angle of incidence modified with Küssner and Wagner indicial lift growth functions

6. Rho unsteady kernel function aerodynamics

7. Vortex spline-kernel function unsteady aerodynamics

8. Doublet Lattice unsteady aerodynamics

The solution of second-order differential equations becomes cumbersome and time-consuming when the coefficients of the equation are nonconstant with respect to frequency compared to an equation having constant coefficients. Unfortunately, the more exact unsteady aerodynamic methods listed as items 6, 7, and 8 produce frequency dependent equations (nonconstant coefficients) when used in dynamic loads analyses. Consequently, these methods have not been used extensively for dynamic loads predictions.

---

*The quasi-steady formulation neglects the influence of the wake vorticies on the flow. This is equivalent to setting the Theordorsen function, $C(k)$, equal to one (ref. 10).

12

The accepted and most commonly used method has been the method listed as item 5. This method accounts for the unsteady aerodynamics in an approximate manner with lift growth functions but still retains its ease and speed in the equation solutions; the results are generally conservative for use in the design process. In addition, the theoretical aerodynamics can be modified in a simple manner with wind tunnel or flight test results. Unfortunately, this method is not suitable for airplanes with low AR lifting surfaces.

An analogous method to the strip theory (method 5) is the FLEXSTAB panel-type steady state aerodynamics modified with Küssner and Wagner indicial lift growth functions (method 2) to approximate unsteady aerodynamics. This method is applicable to airplanes with low AR lifting surfaces but has a disadvantage that it cannot presently be correctly modified to reflect wind tunnel or flight test results.

The aerodynamic methods listed as items 1, 3, and 4 were considered in order to conclusively determine their adequacy or inadequacy for use in any type of dynamic loads analyses. The type of dynamic analysis that was performed with each aerodynamic method is shown in table 1. Note, for the oscillating aileron excitation, methods 3 and 4 are equivalent since these methods only differ in their approximation of the unsteadiness caused by the gust-forcing function. Method 1 was not run with the oscillatory aileron excitation because of the bad agreement with the unsteady Rho method in the gust excitation case (see fig. 9).

The relative accuracy of these aerodynamic methods is ascertained by using the Rho unsteady kernel function aerodynamics as a basis for comparison. The roots of the characteristic equations for each of the aerodynamic theories, which yield constant coefficients, are shown in table 2. Since the other aerodynamic theories are frequency dependent, the roots of the equation vary with frequency and cannot be compared directly.

Certain points of interest arise in studying the results shown in table 2. First, methods 3 and 4 yield the same results. This should be expected since the difference between the two methods lies only in the approximation of the unsteadiness produced by the gust force which does not enter into the problem when rooting the equations of motion. Second, although the predicted frequencies are all approximately the same, there is considerable variation in the predicted damping. Third, when comparing each method over the range of modes, clear trends do not appear; therefore, no definite conclusions can be determined as to the relative accuracy of the prediction of loads by examining roots alone. It becomes necessary to turn to the comparisons of power spectral density (PSD) load parameters, frequency response function magnitudes and phase angles predicted by each method.

5.1 PSD DYNAMIC GUST LOADS ANALYSIS, CONTROLS FIXED

Table 3 shows the PSD load parameters for gust analyses with control surfaces fixed, obtained using random harmonic analysis techniques. The FLEXSTAB steady state and low frequency approximation aerodynamics (method 3) used for both response and gust aerodynamic forces produce PSD load parameters whose values diverge with increasing frequency. This is primarily caused by the effect of the low frequency approximation on

13

gust angle, α_g. This produces a generalized coordinate acceleration frequency response function that increases with increasing frequency. Since load is a function of inertia forces which are in turn a function of coordinate acceleration, the divergence of the load frequency response functions and $\bar{A}$ and N_0 can be expected. Figure 9, which has plots of the magnitudes of wing root bending moment and wingtip acceleration frequency response functions due to continuous sinusoidal gust, demonstrates the effect of exceeding the reduced frequency restrictions for the low frequency approximations which were previously stated in section 4.2.1. In this section, the frequency restrictions were stated as:

$$k \ll 1$$

$$k \ll (1 - M^2)/M^2 \qquad (7)$$

$$k|\ln k| \ll 2/AR\sqrt{1 - M^2}$$

For the present analysis case, the Mach number was 0.8 and the aspect ratio was 6.29. This results in the reduced frequency being restricted to a value much less than 0.56 radians and which corresponds to a cyclic frequency of 2.7 cps. Thus, the consideration of frequencies above 2 cps becomes meaningless for this method and, therefore, its use was discontinued.

Using the Rho unsteady aerodynamics as a basis for comparison, the rms load/rms gust ($\bar{A}$) percent difference for each aerodynamic method and each type of load is shown in table 4.

Typical comparison of load magnitude frequency response plots due to gust excitation for the various aerodynamic methods, except method 3, with Rho unsteady aerodynamics is shown in figures 10a through 12a.* The corresponding comparison of the phase angle relationships is shown in figures 10b through 12b.** For completeness, all of the comparisons of frequency response plots (magnitude and phase angle) for the generalized coordinates and loads are shown in appendix C (figs. C-1 through C-18). The corresponding PSD comparisons of figures 10 through 12 are shown in figures 13 through 15 for the response due to the Von Karman gust spectrum. These figures are determined by the expression:

$$\Phi_{out} = |T|^2\ \Phi(\Omega) \qquad (8)$$

---

*See table 5 for a guide of plot contents.
**The ordinates of the phase angle figures represent the difference in phase angles predicted by method i minus the phase angle predicted by Rho unsteady aerodynamics (method 6).

where:

$|T|$ = magnitude of load frequency response functions (figs. 10 through 12)

$\Phi(\Omega)$ = Von Karman's gust spectrum

Φ_{out} = spectrum of the response quantity

The PSD plots for such gust input are weighted at the low frequencies because of the gust spectrum.

From the values of the PSD load parameters ($\overline{A}$ and N_0) given in table 3 (obtained from integration of the PSD plots), it can be concluded that for PSD gust loads calculated for the controls fixed configuration only the Doublet Lattice unsteady aerodynamics (method 8), the vortex spline-kernel function unsteady aerodynamics (method 7), strip theory aerodynamics modified with Küssner and Wagner indicial functions (method 5), and the FLEXSTAB steady state aerodynamics modified with Küssner and Wagner indicial functions (method 2) produce fairly satisfactory results compared to the Rho unsteady aerodynamics. However, this is only because of the large attenuation of the gust power at the higher frequencies (fig. 8). The other aerodynamic methods produce differences in $\overline{A}$ which, in some cases, become too large for design purposes. This becomes apparent when looking at the load frequency response plots (figs. 10 through 12); the comparison of each aerodynamic method with Rho unsteady aerodynamics varies from fair to good for the frequency range from zero to approximately 2 cps.

From 2 cps and higher, the comparison of all the aerodynamic methods with Rho unsteady aerodynamics (based on the magnitude of the frequency response function) is poor except for the vortex spline-kernel function and the Doublet Lattice aerodynamic representations which compare very favorably with Rho unsteady aerodynamics. The load frequency response phase angle plots (figs. 10b through 12b) also show appreciable differences over the entire frequency range between all of the aerodynamic methods and Rho unsteady aerodynamics, except for the vortex spline-kernel function and Doublet Lattice aerodynamics which generally compare favorably.

At the several frequencies where the phase angle comparisons of the vortex spline-kernel function and the Doublet Lattice aerodynamic methods are poor, the magnitude of the load responses is near zero; e.g., compare figure 10a with 10b. This discrepancy in the phase angles occurs because small differences in the magnitude of the near zero load responses can result in large phase angle differences. However, since the load response magnitudes are small at these frequencies, it is expected that they would have little effect on an active control analysis regardless of the phase angle differences.

5.2 DYNAMIC LOADS ANALYSIS, OSCILLATING CONTROL SURFACE

Typical comparison of load magnitude frequency response plots due to an oscillating inboard aileron for aerodynamic methods 2, 4, 7, and 8 with Rho unsteady aerodynamics

(method 6) is shown in figures 16a through 18a.[*] The corresponding comparison of the phase angle relationship is shown in figures 16b through 18b. For completeness, all of the comparisons of frequency response plots (magnitude and phase angle) for the generalized coordinates and loads are shown in appendix C (figs. C-19 through C-36).

From the load frequency response plots (both magnitude and phase angle), only the results from the vortex spline-kernel function method and the Doublet Lattice method agree satisfactorily with the Rho unsteady aerodynamic results. Even with these unsteady aerodynamic methods, the agreement varies from excellent to only acceptable. It is apparent from these figures and those from section 5.1 that the aerodynamics are much more sensitive to an oscillating control surface than to a gust.

Figures 16 through 18 also show that the agreement of the FLEXSTAB results (methods 2 and 4) with the Rho unsteady results is very poor when using an oscillation control surface. Examination of these figures shows a number of interesting occurrences concerning the three unsteady aerodynamic methods (methods 6, 7, and 8). First for oscillatory aileron excitation, the Doublet Lattice method, when compared to the Rho method, predicts higher frequency response function magnitudes for frequencies less than 3 cps; but for frequencies above 3 cps, the Doublet Lattice method underestimates the magnitudes. A study conduced at Boeing[**] showed that the underestimation was a result of the paneling choosen.

The Doublet Lattice method is a panel-type aerodynamic method and is sensitive to the paneling scheme used. It was found in the Boeing study that the number of chordwise divisions must increase as the upper reduced frquency of interest increases in order to minimize potential error. For example, if the highest reduced frequency of interest were $k = 0.5$, then four chordwise divisions would be sufficient; whereas, if the highest k value of interest were $k = 1.0$, then eight chordwise divisions would be required. As shown in figure 5, six chordwise divisions were used over the majority of the wing in this study. Using the study of reference 4 as a guide, the highest k value which could be analyzed without considerable error is 0.7. In terms of the flight condition used in this study, a k value of 0.7 is equivalent to a cyclic frequency of 3.4 cps. Therefore, the disagreement above 3 cps can be expected and its cause shown to be a result of the paneling scheme used.

An examination of figures 10 through 12, which are the frequency response functions for continuous gust excitation, shows that this discrepancy between Rho and Doublet Lattice above 3 cps does occur but is not as marked. This too is reasonable since a continuous gust excitation will tend to excite the higher modes less than a concentrated force such as an oscillating control surface.

---

[*]For oscillatory control excitation, methods 3 and 4 are equivalent (see discussion in sec. 5.0) Method 5 was omitted because of the difficulty in modeling the oscillatory control using strip theory aerodynamics. Method 1 was left out because of its lack of agreement with Rho aerodynamics when using gust excitation.

[**] Richard, M. and Kroll, R. I., "Limitations of the Doublet Lattice Method–Application to a High Aspect Ratio Wing." Boeing document D6-42395. 1975.

The reason for the low frequency disagreement between Rho and Doublet Lattice when using an oscillatory control excitation can only be a matter of conjecture at this time. Again, an examination of figures 10 through 12 shows that Rho and Doublet Lattice agree extremely well in the low frequency region when using a gust excitation; yet for an oscillatory control excitation (figs. 16 through 18), the agreement is not as good. Control surface deflections introduce high pressure gradients in the region of control surface boundaries. To model these gradients sufficiently with panel-type aerodynamics requires a fine grid in the control surface boundary region. The panel scheme for the oscillatory control surface case, shown in figure 5, may not have been changed as much as required in the region of the control surface.

A second point of interest in examining figures 16 through 18 is that the vortex spline-kernel function aerodynamics (method 7) consistently overestimates the response magnitudes. Looking to figures 10 through 12 for the gust excitation case shows that the agreement between Rho and this method is very good over the entire frequency range. Because the paneling scheme for this method (shown in fig. 2) was not changed between the two cases, it seems safe to assume that much of the disagreement is caused by the type of paneling scheme used. This assumption is supported by reference 2.

The third point of interest is the phase angle differences shown in figures 16b through 18b. In general, the phase angles agree quite well over the entire frequency range. The large sharp peaks and abrupt sign changes in phase difference curves are not significant, since they occur at very small magnitudes and are associated with the problem of division by small numbers.

A final note of interest concerns the amount of aerodynamic damping predicted by the various methods when compared to Rho. From examination of the response plots due to gust and, even more so, due to oscillatory aileron, all aerodynamic methods above 3 cps in general predict less aerodynamic damping than Rho as seen by their overestimation of response magnitudes. The approximate unsteady aerodynamic methods tend to predict less damping than the unsteady aerodynamic methods.

A complete summary of figures 9 through 18 is given in table 5.

17

6.0 CONCLUSIONS AND RECOMMENDATIONS

Applicability of the various aerodynamic methods for use in dynamic loads analyses was ascertained by comparing results to those obtained using the Rho unsteady kernel function aerodynamic method which was used as a basis for comparison. The sensitivity of the results to the use of some of the various aerodynamic methods (methods 2, 5, 6, and 7) is not as critical when calculating controls fixed PSD gust loads versus loads due to active controls. This is because of the large attenuation of the gust-forcing function power at the higher frequencies. However, even with this relaxed sensitivity to the aerodynamic representation, only the PSD gust loads ($\overline{A}$) calculated using the vortex spline-kernel function (method 7) and the Doublet Lattice aerodynamics (method 8) differed less than 10%* from those calculated using Rho unsteady aerodynamics (method 6). RMS loads ($\overline{A}$) calculated with strip theory and FLEXSTAB steady state aerodynamics modified with Küssner and Wagner functions differed from -12% to +18%. The remaining aerodynamic methods, FLEXSTAB steady state (method 1), FLEXSTAB steady state plus low frequency approximation on response aerodynamics only (method 4), and FLEXSTAB steady state plus low frequency approximation on both the gust and response aerodynamics (method 3), produce $\overline{A}$'s which varied much above 20% with results from the latter method actually diverging.

When active controls are used to influence elastic structural motions, none of the quasi-steady state aerodynamic representations are satisfactory even with unsteady effects represented with indicial lift growth functions. To properly represent the aerodynamics resulting from an oscillating control surface, more exact unsteady aerodynamic methods must be employed.

There are some advantages in using the approximate methods in representing unsteady aerodynamics. These methods are less expensive to use than the full unsteady methods because they yield equations of motion which are easier to formulate and solve. In addition, the modal responses tend to be less damped than those using unsteady aerodynamics and result in more conservative loads. The disadvantages are that the response and loads, magnitudes and phase angles are inaccurate at higher frequencies and cannot be used for active control design with any amount of confidence.

This study used an advanced state-of-the-art unsteady aerodynamic method as a basis to determine the validity of various aerodynamic theories. It is assumed that this theory satisfactorily matches the actual aerodynamics on a planar surface. There have been very few oscillatory aerodynamic wind tunnel tests performed on lifting surfaces to credit or discredit any exact unsteady aerodynamic methods at oscillatory frequencies other than zero.

---

*The vortex spline-kernel function method results differ by ≤3% from the Rho aerodynamic method.

A logical extension of this present study would be to perform a theoretical dynamic vertical gust analysis on an airplane employing total airplane flexibility and a sufficient number of modes to adequately cover the gust bandwidth as defined from flight test results. The theoretical gust analysis load frequency response functions would then be compared to the load frequency responses obtained from gust loads survey flight test results. Several aerodynamic theories could be used in the theoretical vertical gust analysis to verify their adequacy in gust loads predictions on the total airplane and indications of their adequacy for active controls representations. The aerodynamic theories are (1) Doublet Lattice unsteady aerodynamic method and (2) quasi-steady formulation of the FLEXSTAB steady state aerodynamics modified with Küssner and Wagner indicial lift coefficients.

Table 1.—Type of Dynamic Analysis Performed With Each Aerodynamic Method

Method	Aerodynamics based on	Gust excitation function		Oscillating aileron excitation function	
		Loads and responses		Loads and responses	
		Magnitude	Phase angle	Magnitude	Phase angle
1	FLEXSTAB steady state	√	√		
2	FLEXSTAB steady state modified with Küssner and Wagner Functions	√	√	√	√
3[a]	FLEXSTAB steady state plus low frequency approximation used both for response and gust forces	√			
4[a]	FLEXSTAB steady state for gust forces and both FLEXSTAB steady state plus low frequency approximation for response forces	√	√	√	√
5	Strip theory corrected to wind tunnel data and modified with Küssner and Wagner functions	√	√		
6	Rho unsteady kernel function	√	√	√	√
7	Vortex spline-kernel function	√	√	√	√
8	Doublet lattice	√	√	√	√

[a]The difference between methods 3 and 4 is only how the gust excitation force is used.

Table 2.—Equations of Motion Roots[a]

| Aerodynamic method / Modes | Basic structural frequencies and damping (in vacuo) | | FLEXSTAB aerodynamics | | | | | | | | 5 Strip theory corrected to wind tunnel data with Küssner and Wagner k = 0 | |
| | | | 1 Steady state[b] without Küssner and Wagner | | 2 Steady state with Küssner and Wagner | | 3 Steady state + low freq approx aero on response and gust aero | | 4 Steady state + low freq approx aero on response aero | | | |
	f_n, cps	$\zeta = c/c_c$	f_n, cps	$\zeta = c/c_c$	f_n, cps	$\zeta = c/c_c$	f_n, cps	$\zeta = c/c_c$	f_n, cps	$\zeta = c/c_c$	f_n, cps	$\zeta = c/c_c$
Translation	0.0	0.0	0.0	0.0	0.0	0.0	0.0	0.0	0.0	0.0	0.0	0.0
Pitch	0.0	0.0	0.233	0.479	0.235	0.475	0.234	0.489	0.234	0.489	0.261	0.461
First elastic mode	1.00	0.0	1.16	0.097	1.17	0.085	1.17	0.073	1.17	0.078	1.16	0.093
Second elastic mode	2.15	0.0	2.49	0.061	2.48	0.033	2.51	0.060	2.51	0.060	2.35	0.058
Third elastic mode	3.04	0.0	3.11	0.059	3.13	0.045	3.07	0.082	3.07	0.082	3.08	0.056
Fourth elastic mode	4.16	0.0	4.13	0.007	4.14	0.007	4.09	0.024	4.09	0.024	4.12	0.008
Fifth elastic mode	6.17	0.0	6.28	0.028	6.28	0.017	6.26	0.036	6.26	0.036	6.18	0.032
Sixth elastic mode	8.25	0.0	8.30	0.018	8.31	0.012	8.20	0.035	8.20	0.035	8.18	0.026

[a]Based on large subsonic jet airplane: weight = 753 000 lb; altitude = 20 000 ft; Mach = 0.8; eight free-free mode (vertical translation, pitch, and six elastic wing modes).

[b]Quasi-steady approach (see sec. 5.0).

Table 3.—PSD Load Parameter Comparisons[a]

Aerodynamic method / Loads	FLEXSTAB aerodynamics							
	1		2		3[b]		4	
	Steady state without Küssner and Wagner		Steady state with Küssner and Wagner		Steady state + low freq approx aero on response and gust aero		Steady state + low freq approx aero on response aero	
	$\overline{A}$	N_0	$\overline{A}$	N_0	$\overline{A}$	N_0	$\overline{A}$	N_0
	Load per fps	Zero crossings per feet	Load per fps	Zero crossings per feet	Load per fps	Zero crossings per feet	Load per fps	Zero crossings per feet
Shear, lb								
Root	2072	0.00317	1924	0.00258	5002	0.01144	1943	0.00237
Outbd of inbd nac	1568	0.00146	1599	0.00138	2174	0.01033	1705	0.00139
Outbd of outbd nac	551	0.00166	546	0.00135	1246	0.01094	576	0.00157
Bending moment, in-lb x 10^6								
Root	1.1100	0.00196	1.1020	0.00163	2.629	0.01111	1.1650	0.00147
Outbd of inbd nac	0.5530	0.00137	0.5620	0.00128	1.229	0.01062	0.6090	0.00131
Outbd of outbd nac	0.0921	0.00280	0.0837	0.00230	0.197	0.01103	0.0926	0.00234
Acceleration, g's								
Wingtip	0.1870	0.00690	0.1480	0.00580	0.2650	0.00912	0.1720	0.00694
Outbd of outbd nac	0.0519	0.00417	0.0505	0.00328	0.0676	0.00652	0.0570	0.00371
Outbd of inbd nac	0.0232	0.00603	0.0198	0.00478	0.0289	0.00851	0.0213	0.00607
Root	0.0138	0.00268	0.0131	0.00208	0.0142	0.00316	0.0134	0.00210

[a]Based on large subsonic jet airplane: weight = 753 000 lb; altitude = 20 000 ft; Mach = 0.8; eight free-free mode (vertical translation, pitch, and six elastic wing modes).

[b]Loads have not converged.

Note: cutoff frequency is 16 cps.

Table 3.—(Concluded)

	5 Strip theory corrected to wind tunnel data with Küssner and Wagner k = 0		6 Rho unsteady aerodynamics		7 Vortex spline-kernel function nonsteady aerodynamics		8 Doublet lattice unsteady aerodynamics	
Aerodynamic method / Loads	$\overline{A}$ Load per fps	N_0 Zero crossings per feet	$\overline{A}$ Load per fps	N_0 Zero crossings per feet	$\overline{A}$ Load per fps	N_0 Zero crossings per feet	$\overline{A}$ Load per fps	N_0 Zero crossings per feet
Shear								
Root	1830	0.00259	1708	0.00226	1705	0.00226	1686	0.00221
Outbd of inbd nac	1474	0.00127	1513	0.00116	1481	0.00116	1558	0.00114
Outbd of outbd nac	514	0.00119	516	0.00112	515	0.00114	536	0.00105
Bending moment, in-lb x 10^6								
Root	0.9350	0.0020	1.05	0.00132	1.03	0.00134	1.07	0.00135
Outbd of inbd nac	0.5270	0.0013	0.547	0.00125	0.543	0.00122	0.567	0.00120
Outbd of outbd nac	0.0841	0.0018	0.075	0.00225	0.077	0.00215	0.081	0.00195
Acceleration, g's								
Wingtip	0.1170	0.00507	0.1336	0.00687	0.1316	0.00676	0.1294	0.00653
Outbd of outbd nac	0.0429	0.00266	0.0437	0.00351	0.0431	0.00346	0.0447	0.00335
Outbd of inbd nac	0.0177	0.00409	0.0179	0.00673	0.0175	0.00656	0.0175	0.00631
Root	0.0136	0.00198	0.0126	0.00188	0.0122	0.00195	0.0123	0.00187

Note: cutoff frequency is 16 cps

Table 4.—Percent Difference in Load of Each Aerodynamic Method Compared to Rho Unsteady Aerodynamic Method

Method	Aerodynamic method	$\overline{A}$ percent difference from Rho (method 6)									
		Wing shear at			Wing bending moment at			Wing acceleration at			
		Root	Inbd nacelle	Outbd nacelle	Root	Inbd nacelle	Outbd nacelle	Tip	Outbd nacelle	Inbd nacelle	Root
1	FLEXSTAB steady state	21.0	4.0	7.0	6.0	1.0	23.0	40.0	19.0	30.0	10.0
2	FLEXSTAB steady state with Küssner and Wagner indicial lift growth functions	13.0	6.0	6.0	5.0	3.0	18.0	11.0	16.0	11.0	4.0
3	FLEXSTAB steady state plus low frequency approximation on response and gust aerodynamics	193.0	116.0	141.0	150.0	125.0	163.0	98.0	55.0	61.0	13.0
4	FLEXSTAB steady state and low frequency approximation on response aerodynamic	14.0	13.0	12.0	11.0	11.0	23.0	29.0	30.0	19.0	6.0
5	Strip theory with Küssner and Wagner indicial lift growth functions	7.0	-3.0	0.0	-11.0	-4.0	12.0	-12.0	-2.0	-1.0	8.0
7	Vortex spline-kernel function	0.0	-2.0	0.0	-2.0	-1.0	3.0	-1.0	-1.0	-2.0	-3.0
8	Doublet lattice	-1.0	3.0	4.0	2.0	4.0	8.0	-3.0	2.0	-2.0	-2.0

24

Table 5.—Contents of Comparison Plots in Figures 9 Through 18

Response Description (Two Rigid Body Modes and Six Elastic Modes)

Figure	Response variable			Frequency response due to gust excitation			Power spectral density due to Von Karman Input	Frequency response due to oscillating inboard aileron	
	A_{tip}	V_{root}	M_{root}	Methods 3 and 6	All methods except 3		All methods except 3	Methods 2, 4, 6, 7, and 8	
				Magnitude	Magnitude	Phase angle		Magnitude	Phase angle
9	✓		✓	✓					
10		✓			✓	✓			
11			✓		✓	✓			
12	✓				✓	✓			
13		✓					✓		
14			✓				✓		
15	✓						✓		
16		✓						✓	✓
17			✓					✓	✓
18	✓							✓	✓

Figure 1.—Aerodynamic Grid Used for FLEXSTAB Aerodynamic Method

26
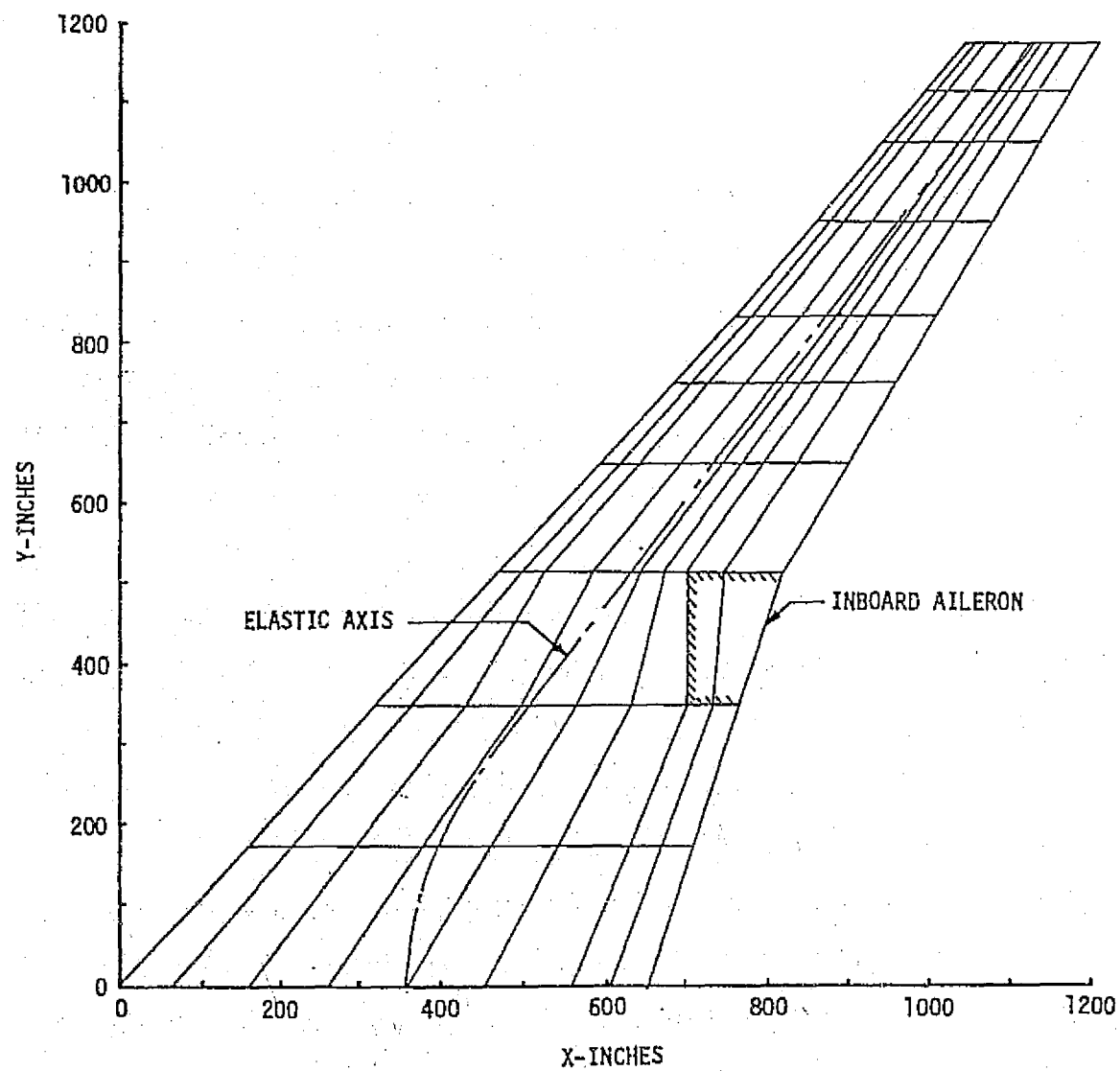
Figure 2.—Aerodynamic Grid Used for Vortex Spline-Kernel Function Aerodynamic Method

27
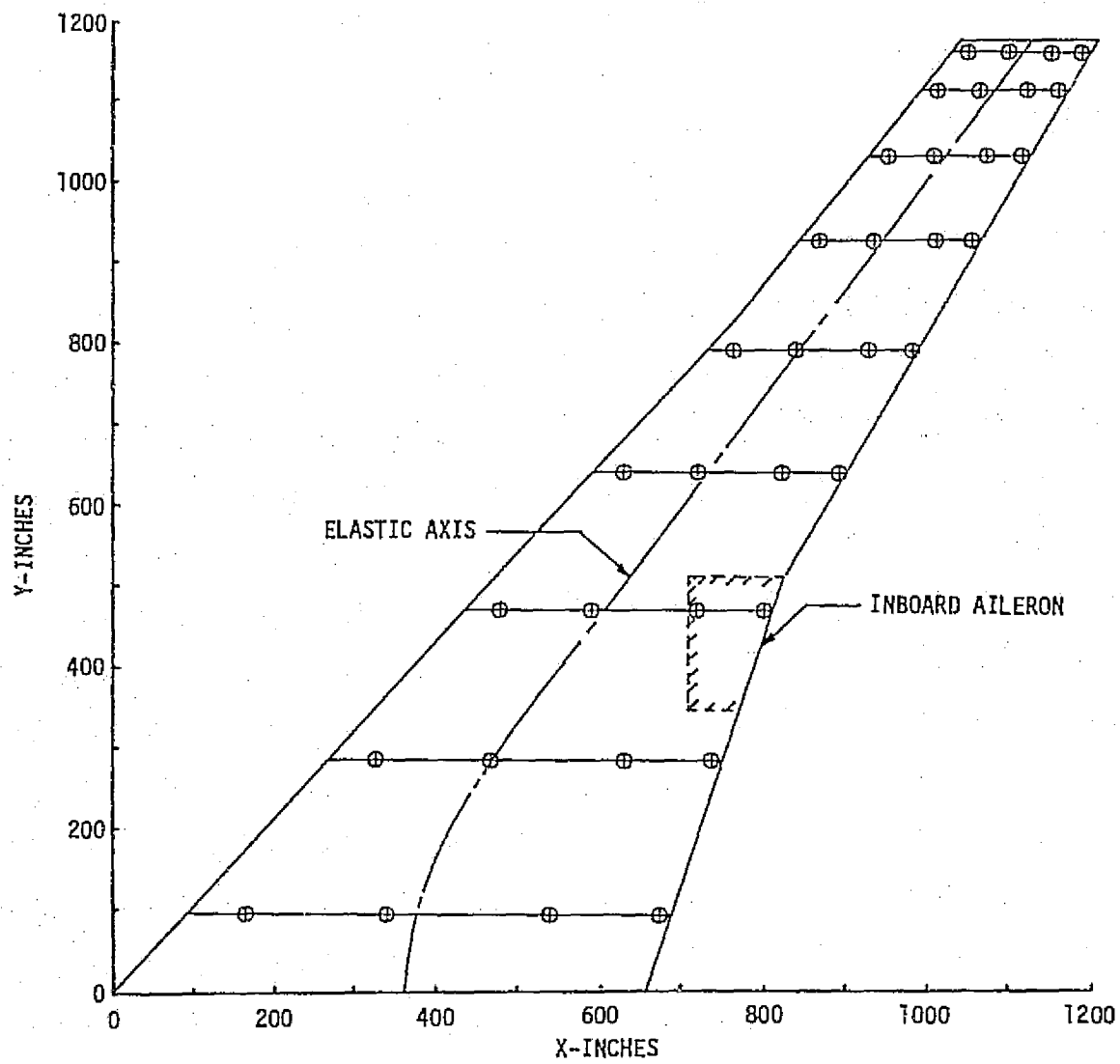
Figure 3.—Collocation Point Distribution Used for Rho Aerodynamic Method
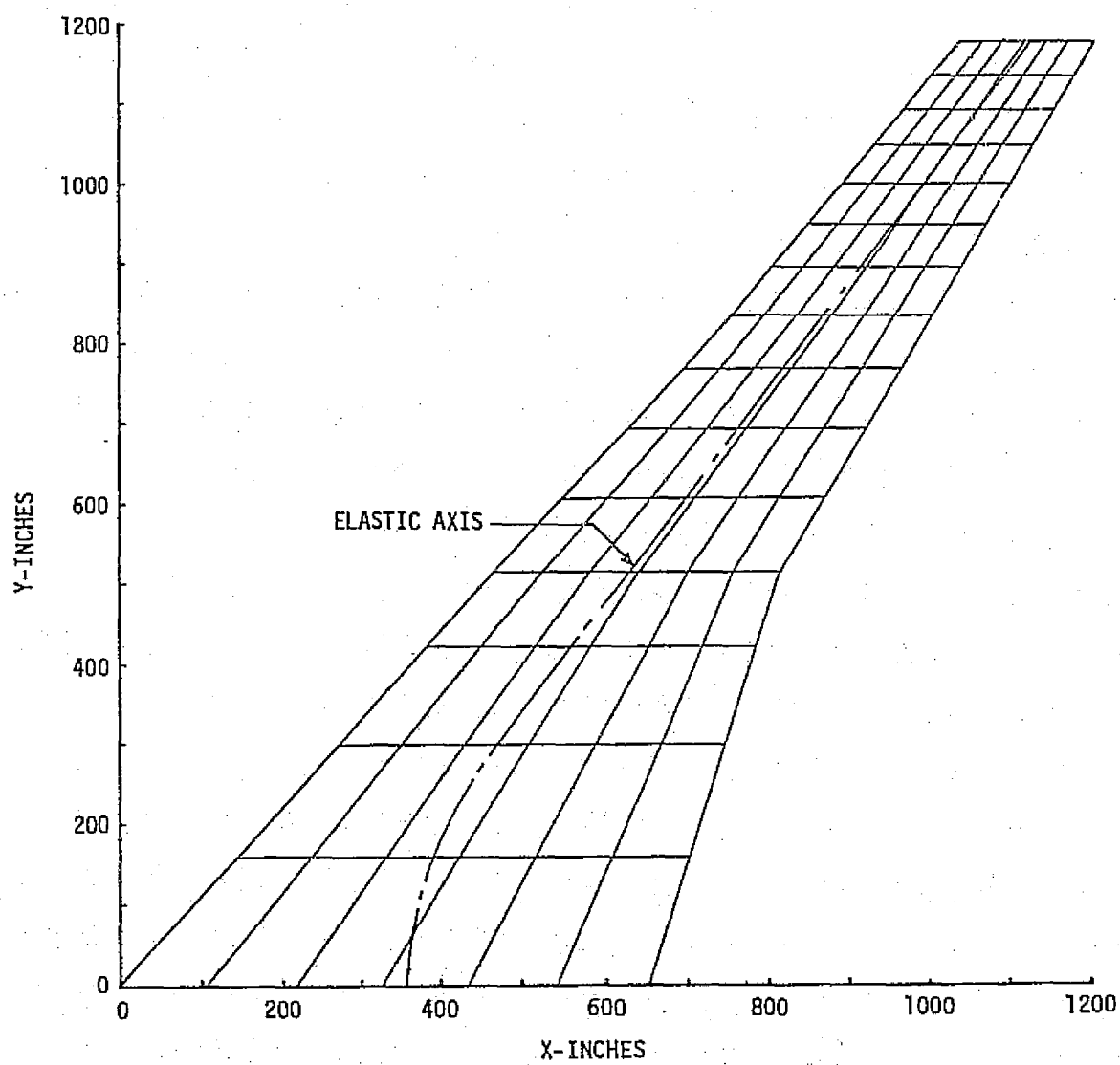
Figure 4.—Aerodynamic Grid Used for Doublet Lattice Gust Excitation
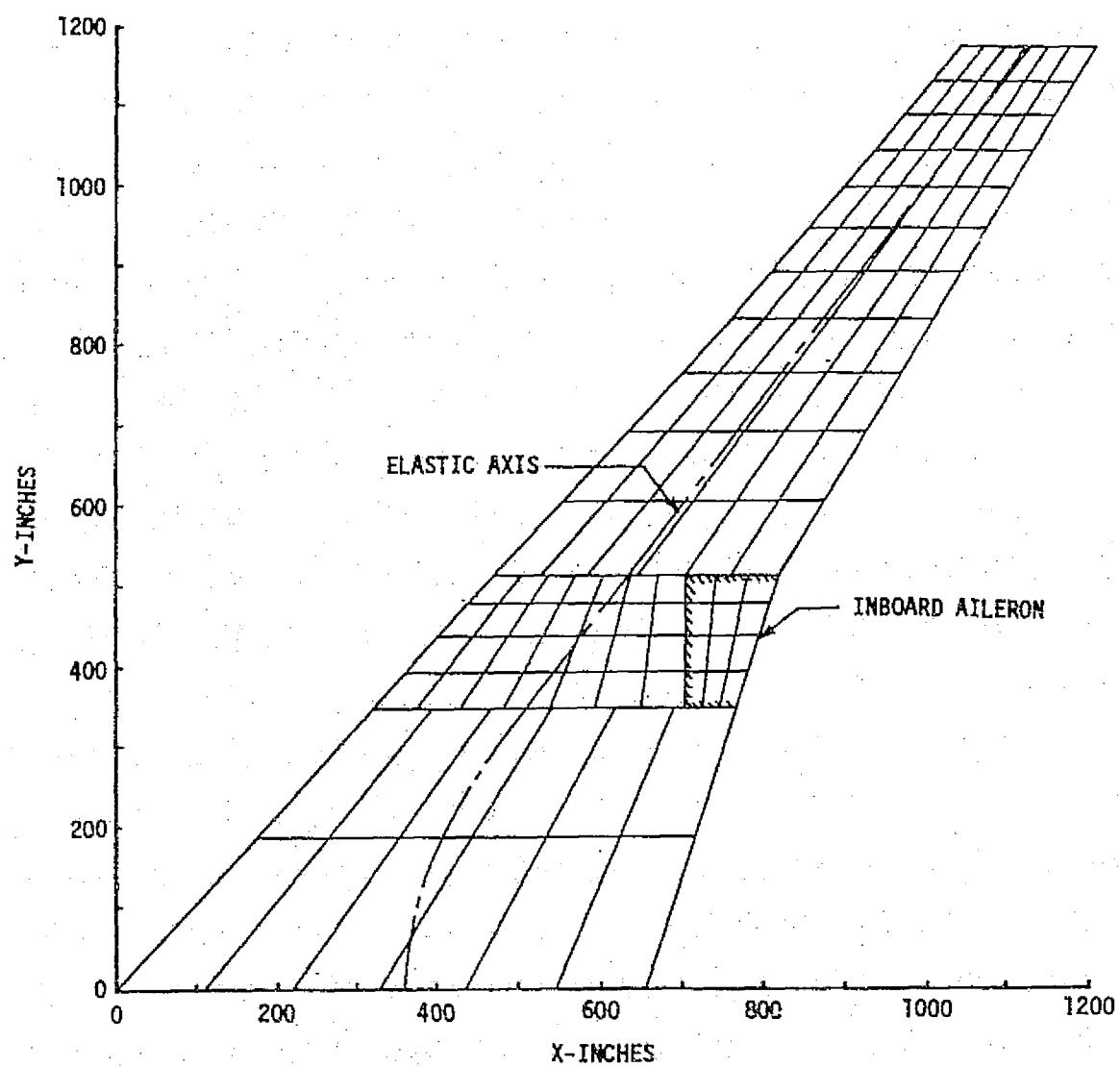
Figure 5.—Aerodynamic Grid Used for Doublet Lattice Oscillatory Aileron Excitation
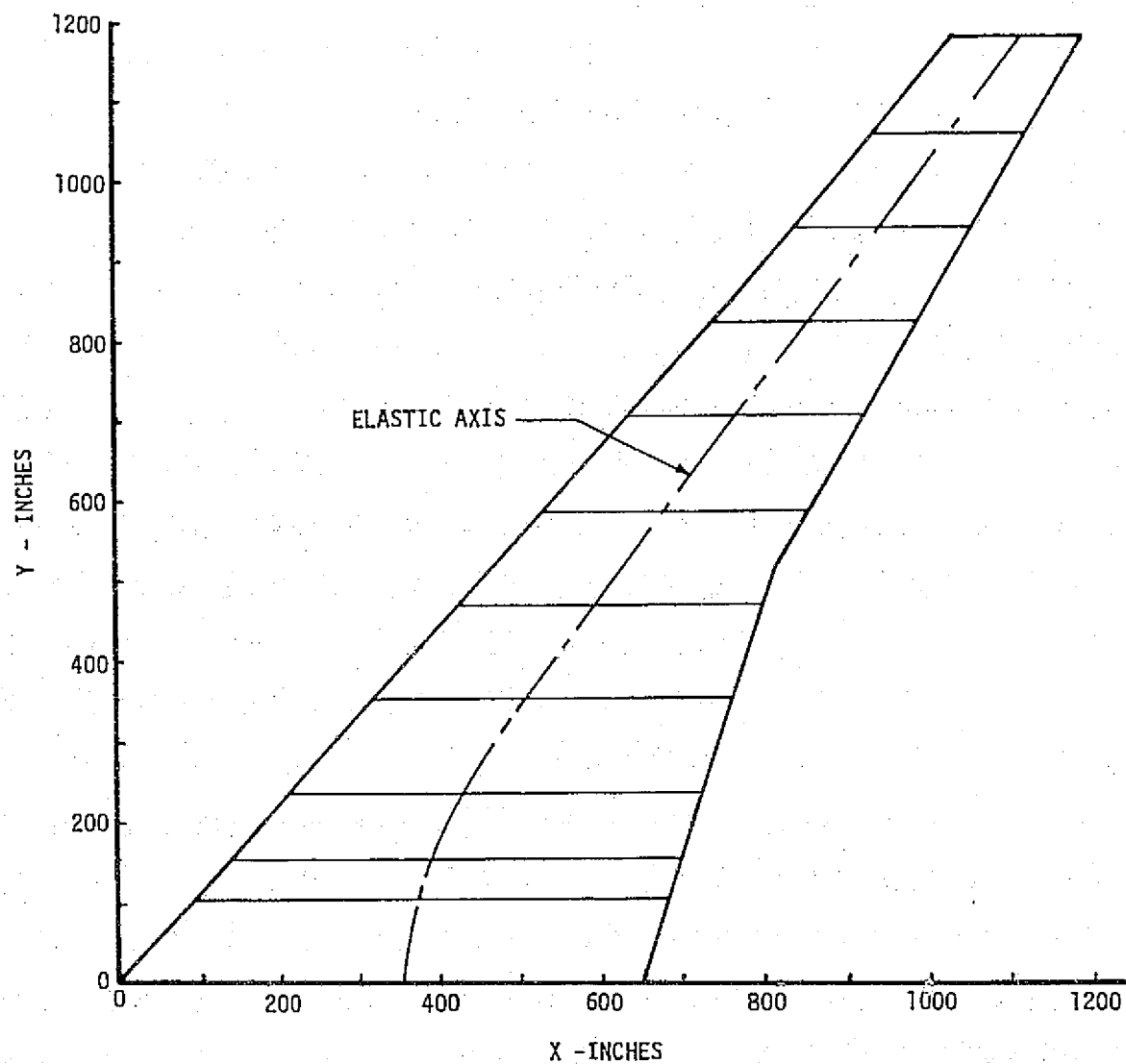
Figure 6.—Aerodynamic Paneling Used for Strip Theory (Lifting Line) Aerodynamic Method
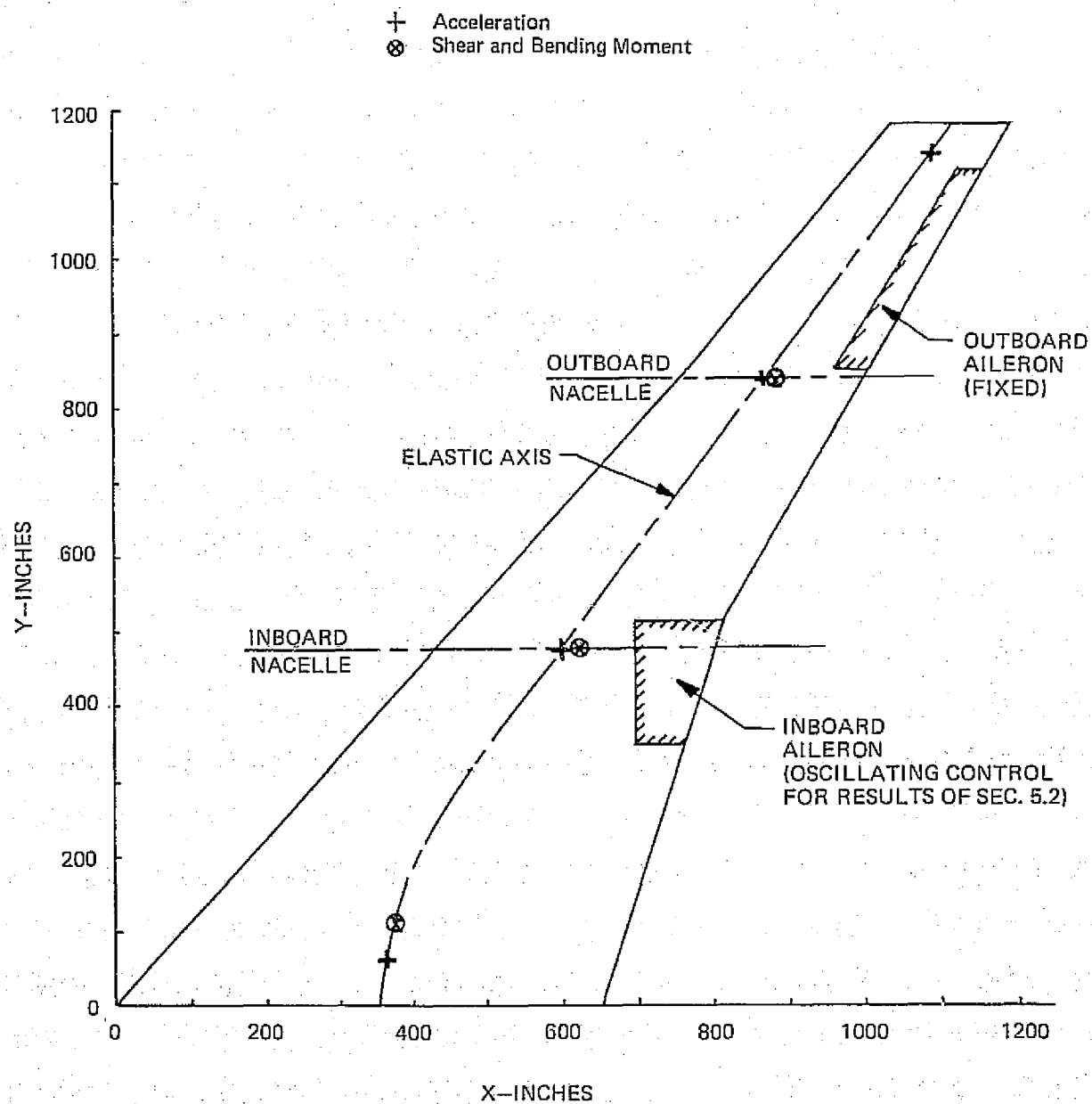
Figure 7.—Load Station Locations
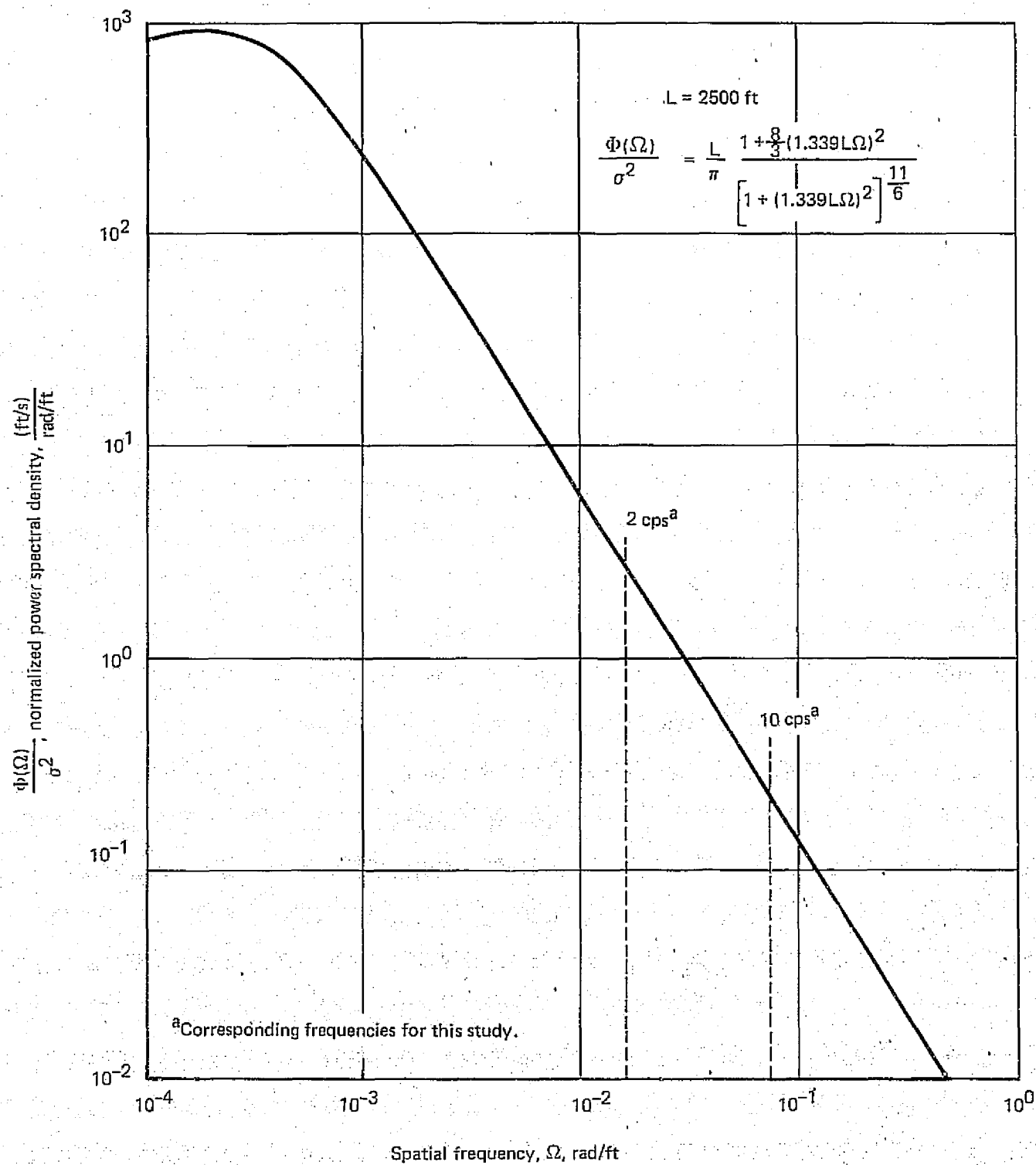
Figure 8.—Atmospheric Turbulence Spectrum—Von Karman Representation
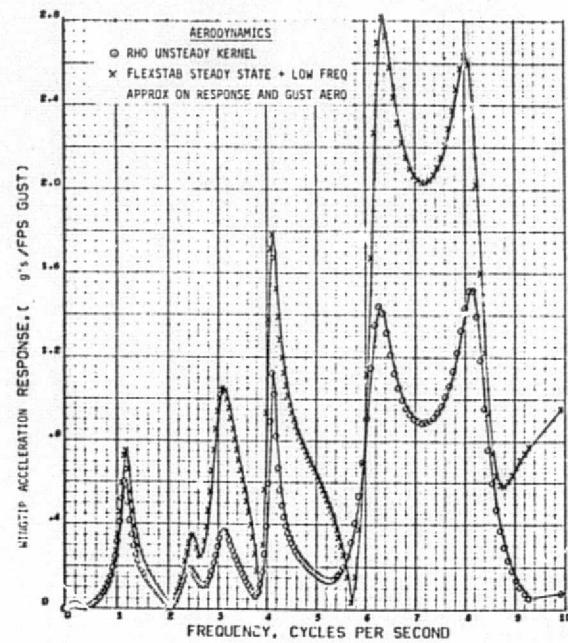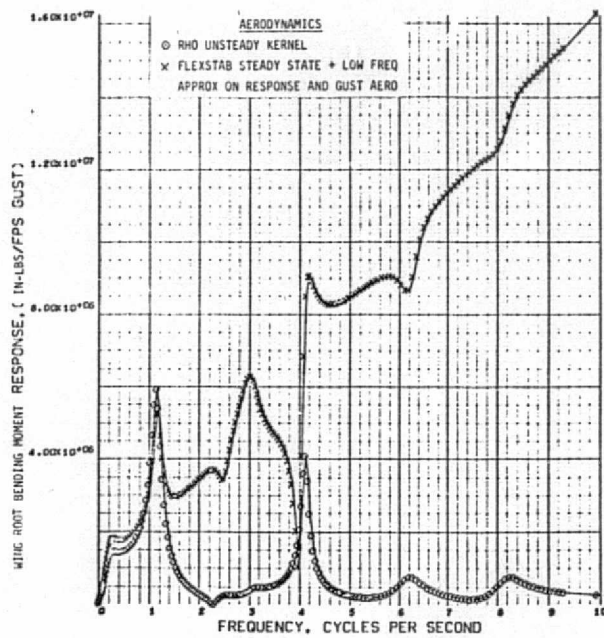
Figure 9.—Load Frequency Response Function Magnitudes Due to Gust Excitation
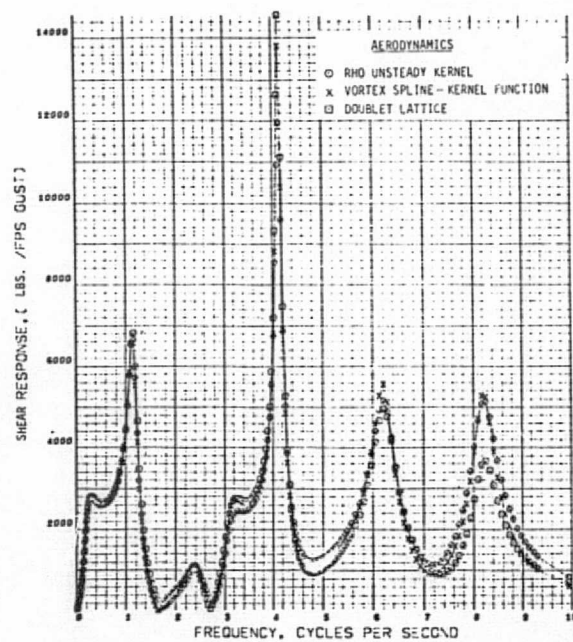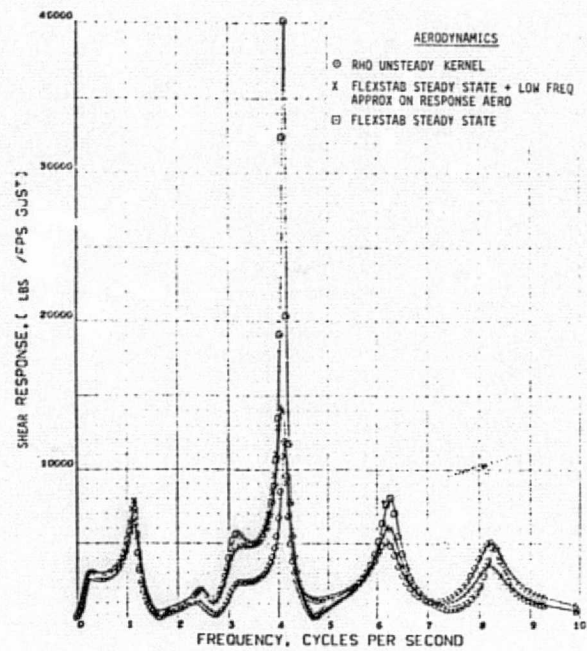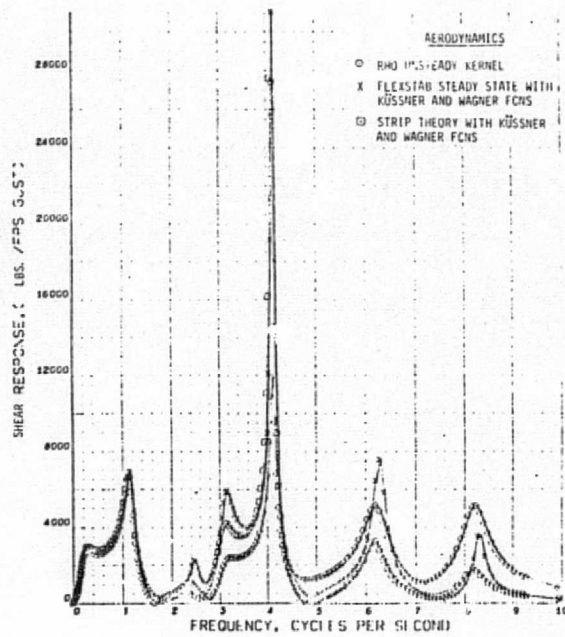
(a) Magnitudes

Figure 10.—Comparison of Wing Root Shear Frequency Response Function Due to Gust Excitation

35
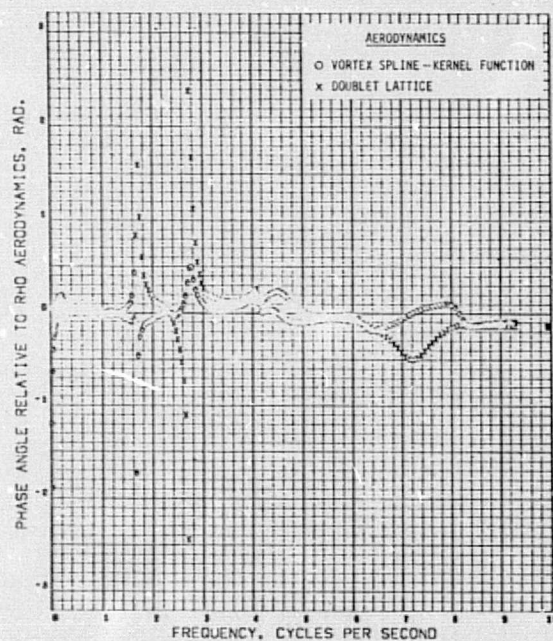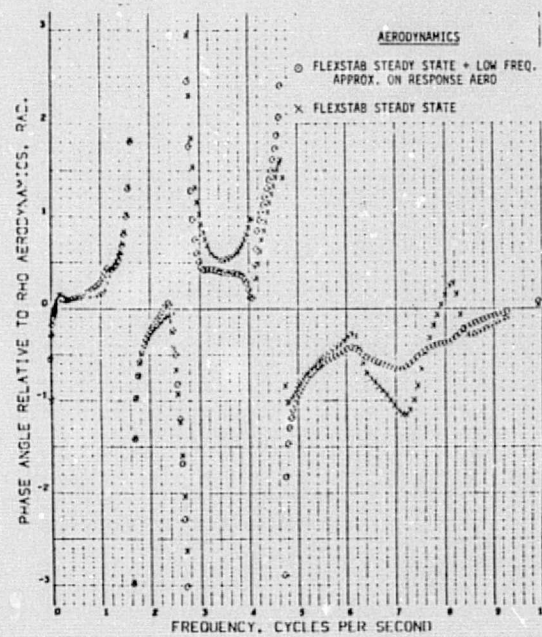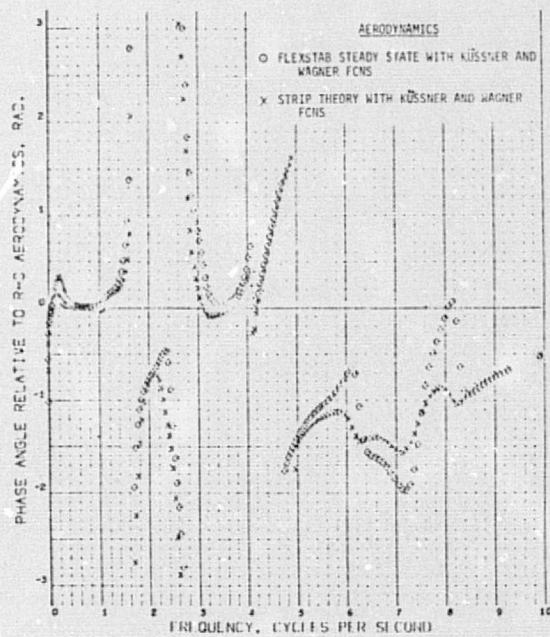
(b) Phase Angles

Figure 10.—(Concluded)

36
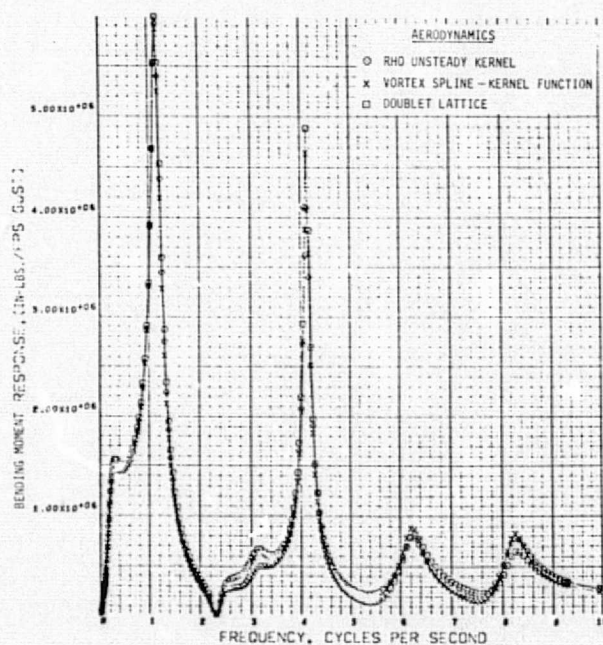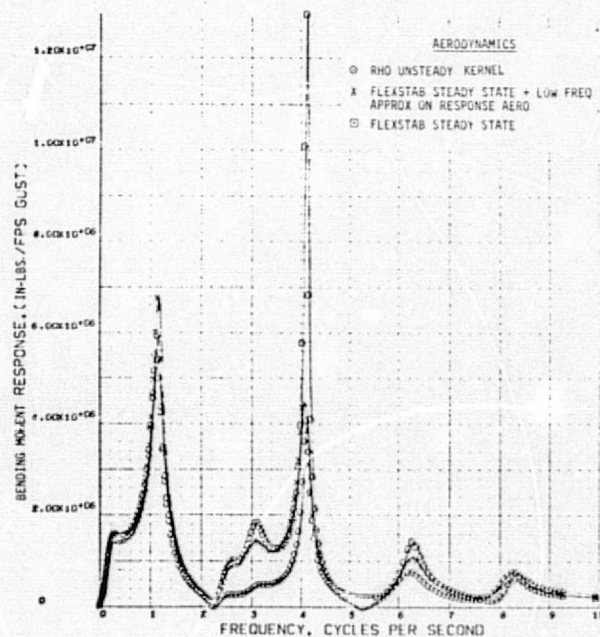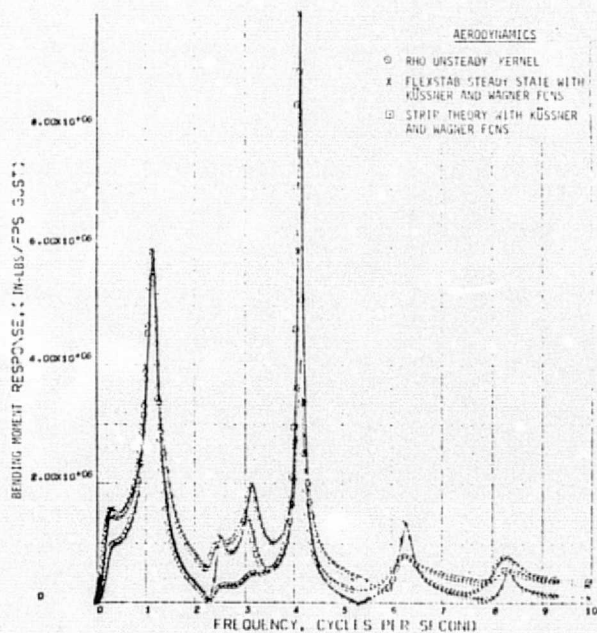
(a) Magnitudes

Figure 11.—Comparison of Wing Root Bending Moment Frequency Response Function
Due to Gust Excitation

37
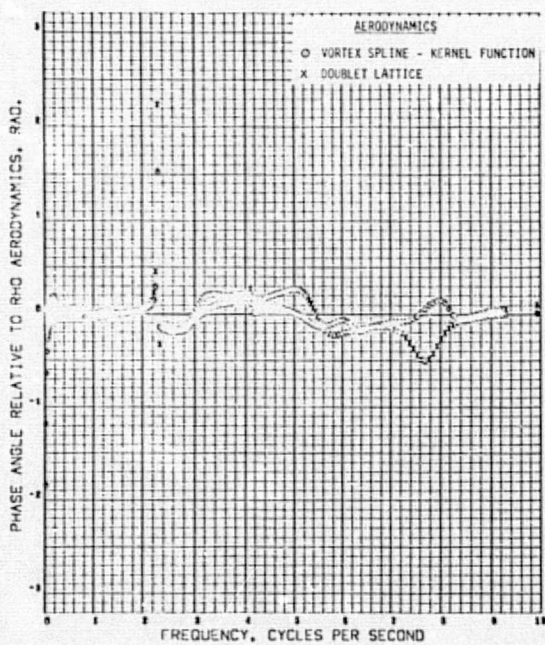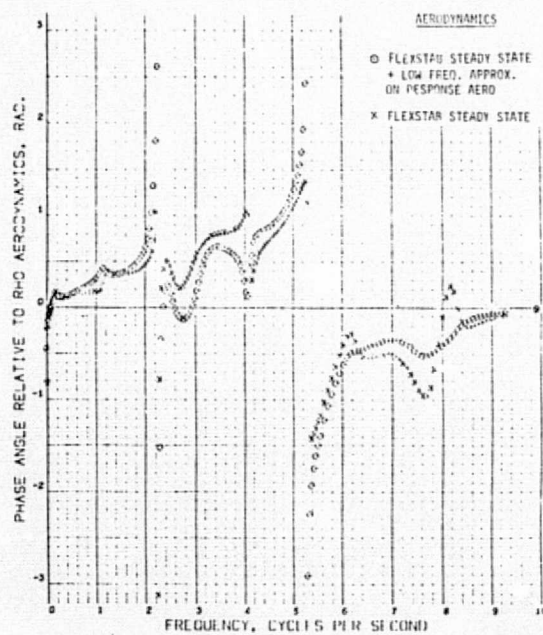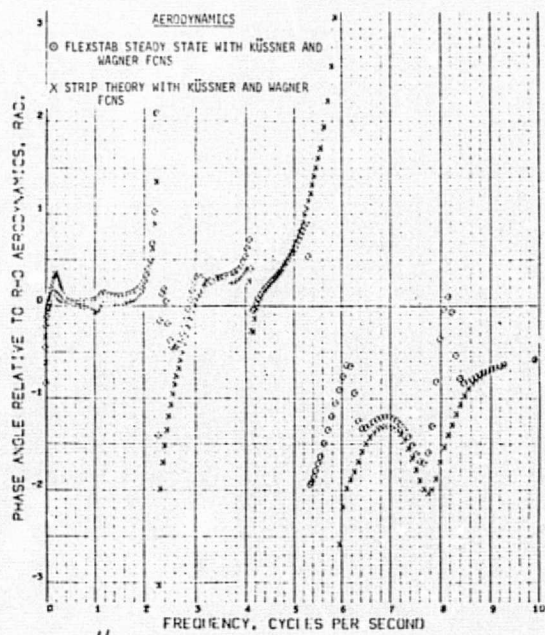
(b) Phase Angles

Figure 11.—(Concluded)

38
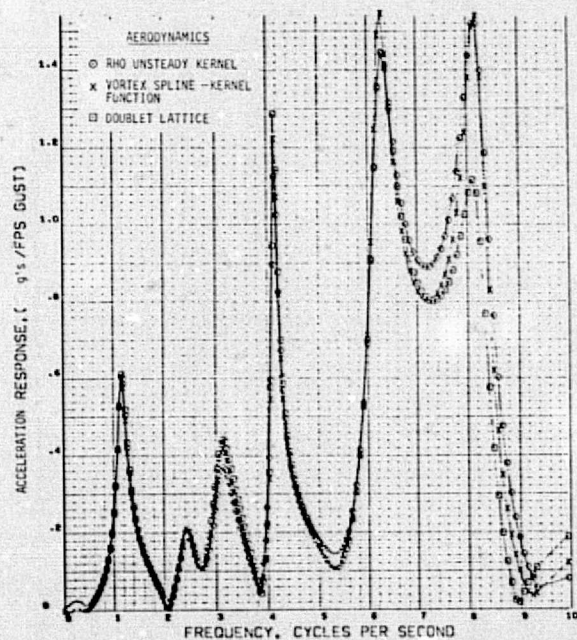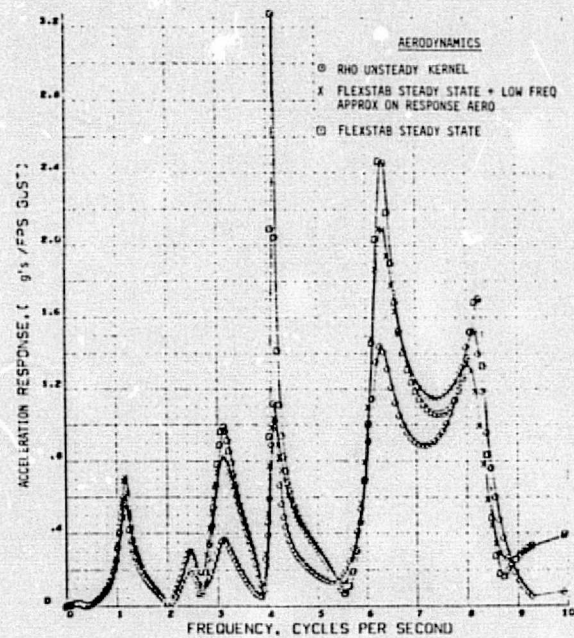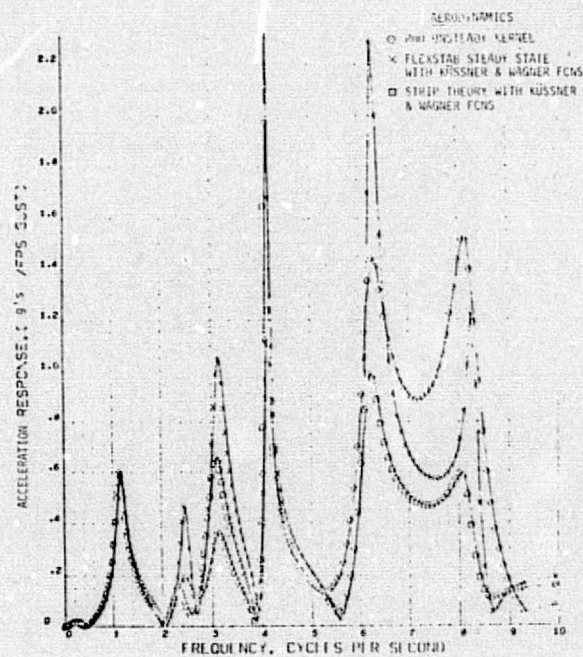
(a) Magnitudes

Figure 12.—Comparison of Wingtip Acceleration Frequency Response Function Due to Gust Excitation
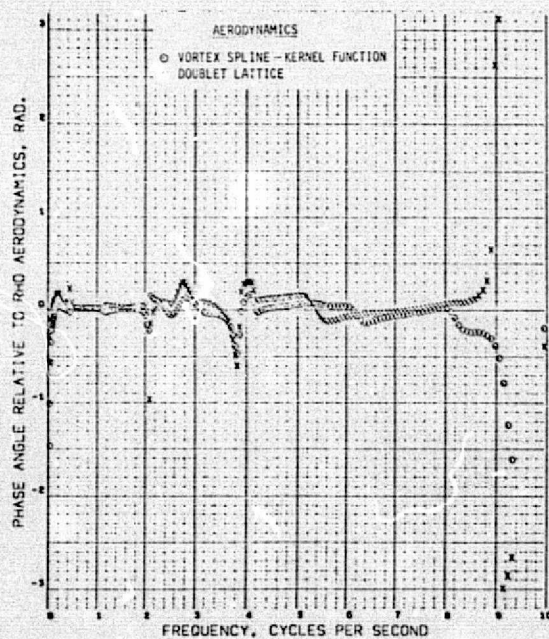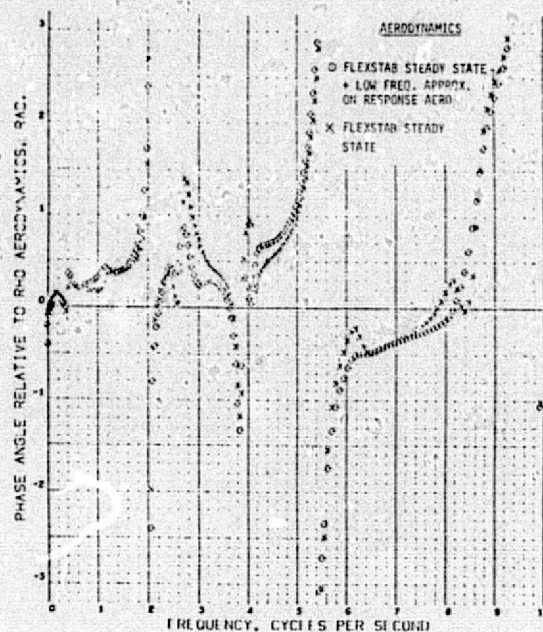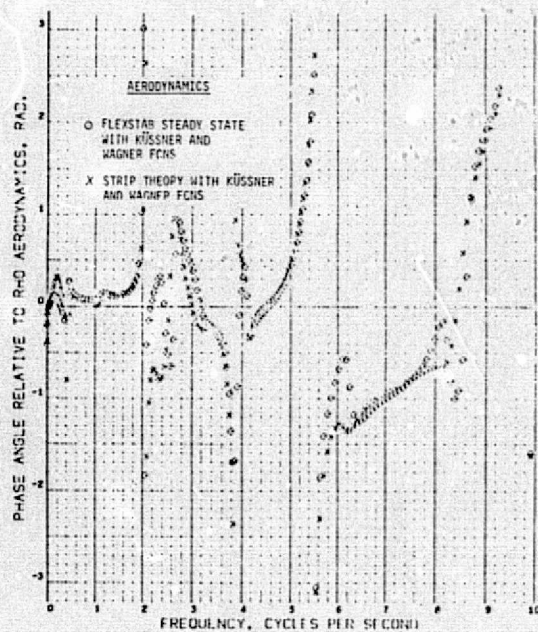
(b) Phase Angles

Figure 12.—(Concluded)

40
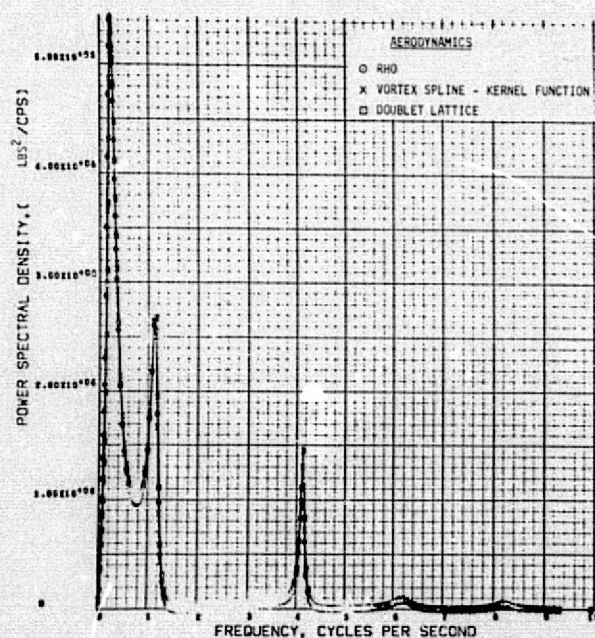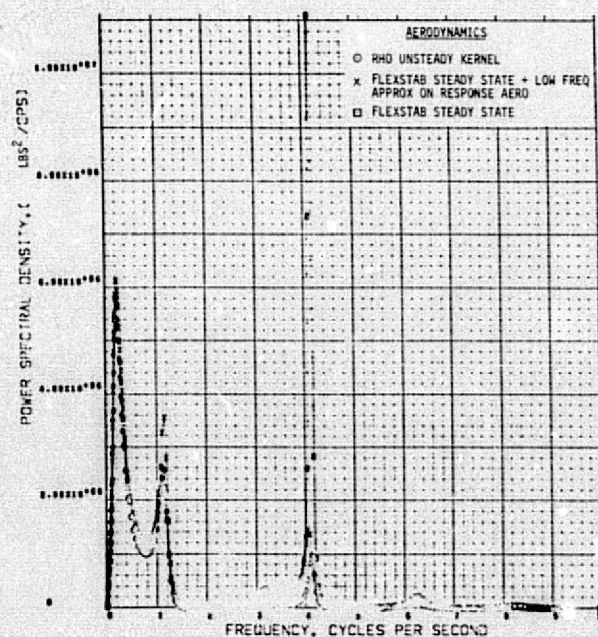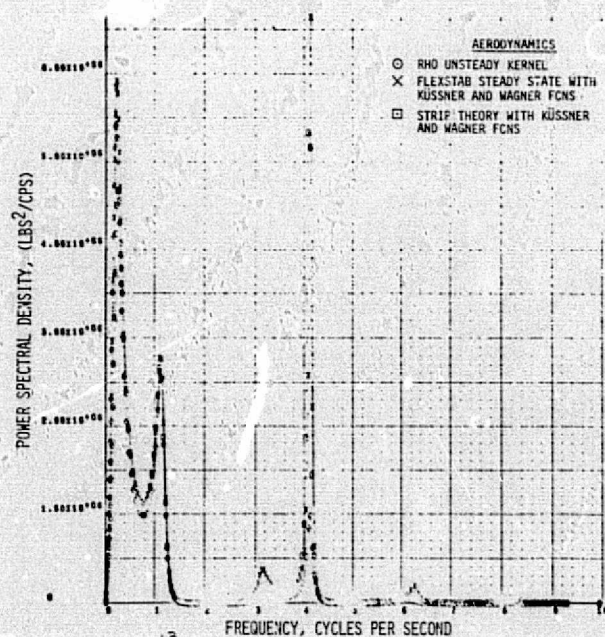
Figure 13.—Wing Root Shear Power Spectral Density
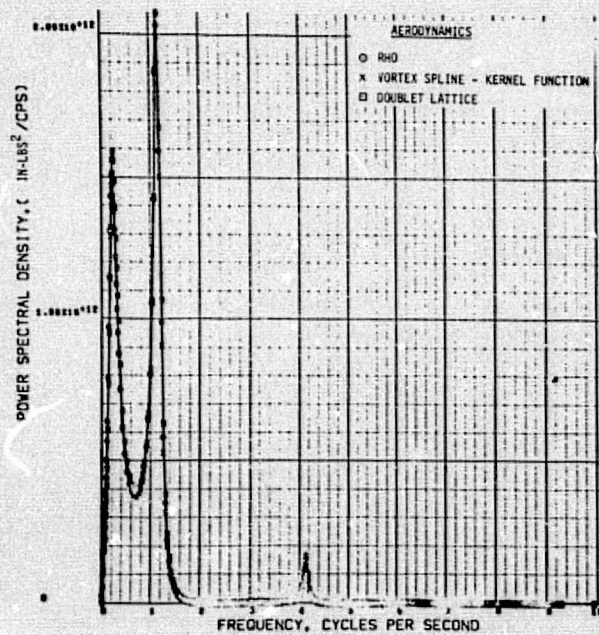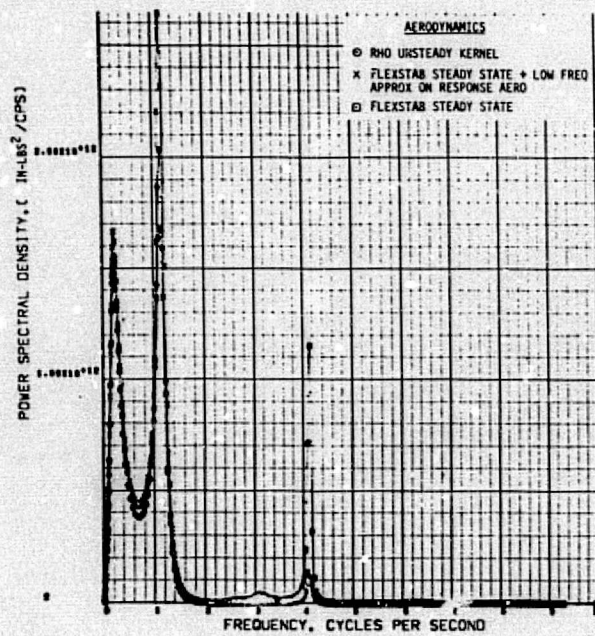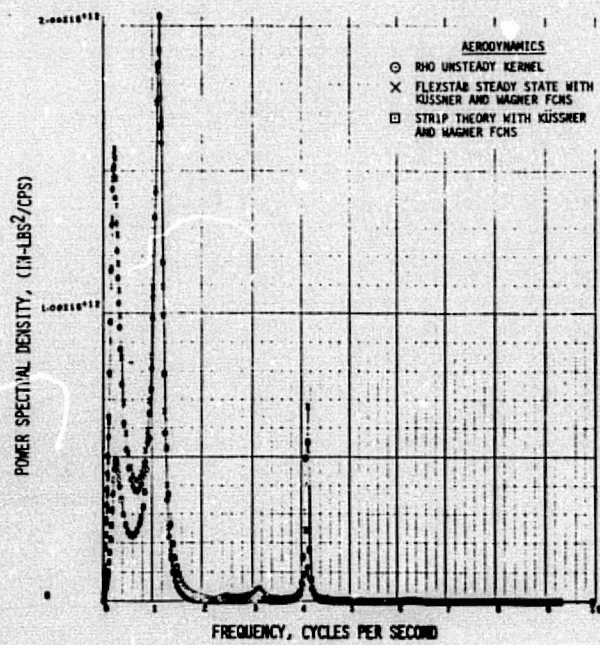
Figure 14.—Wing Root Bending Moment Power Spectral Density

42
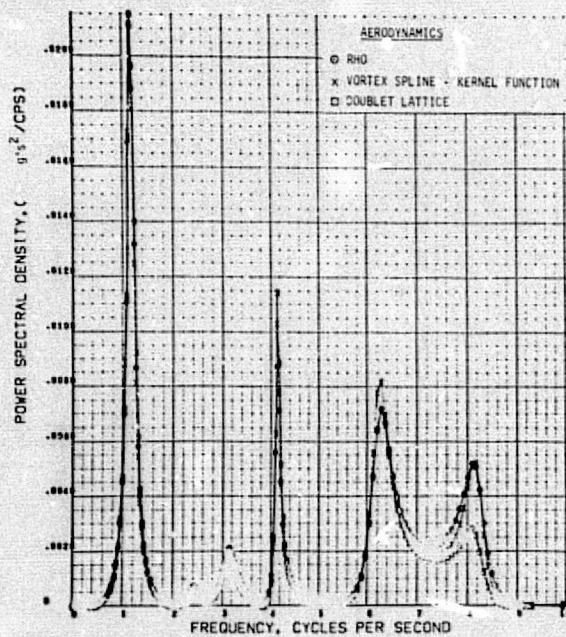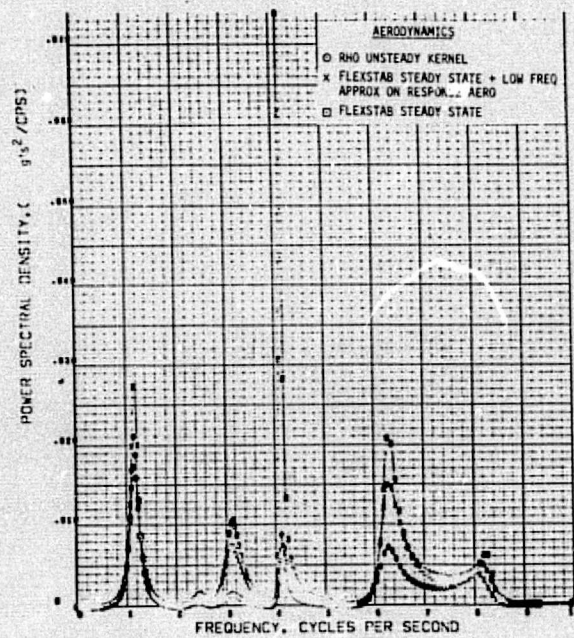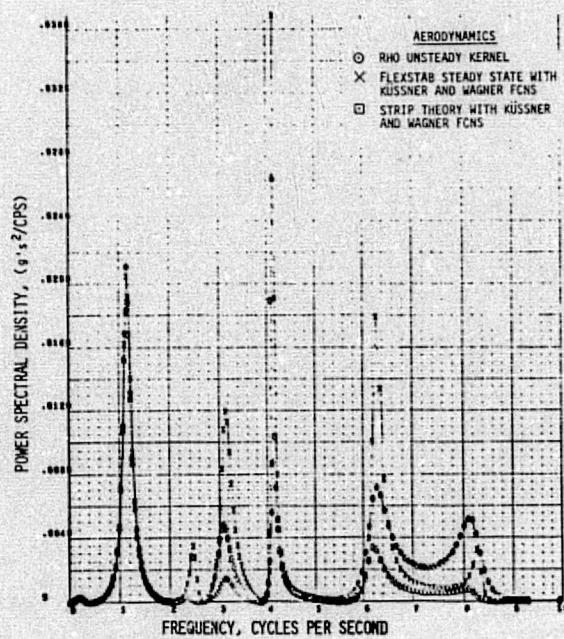
Figure 15.—Wingtip Acceleration Power Spectral Density

43
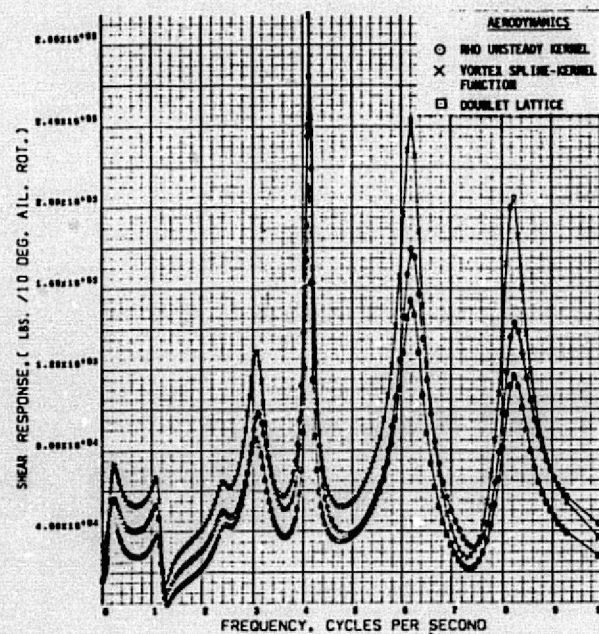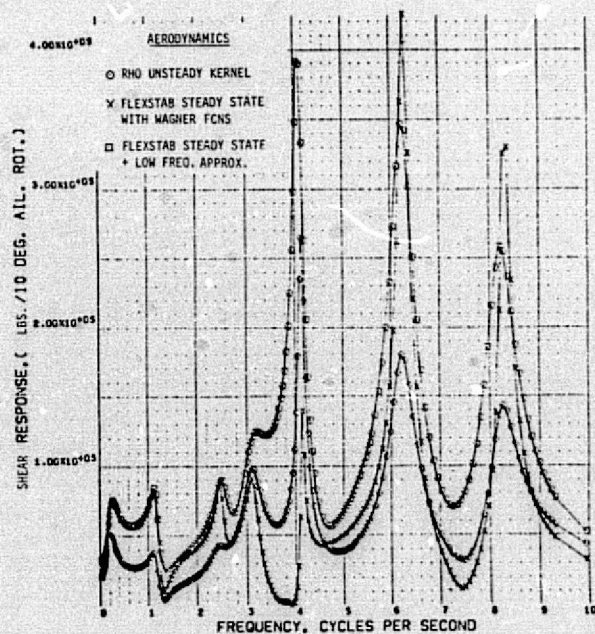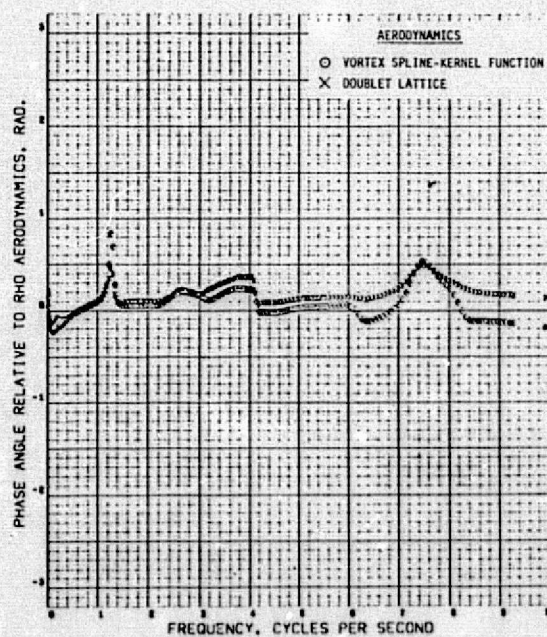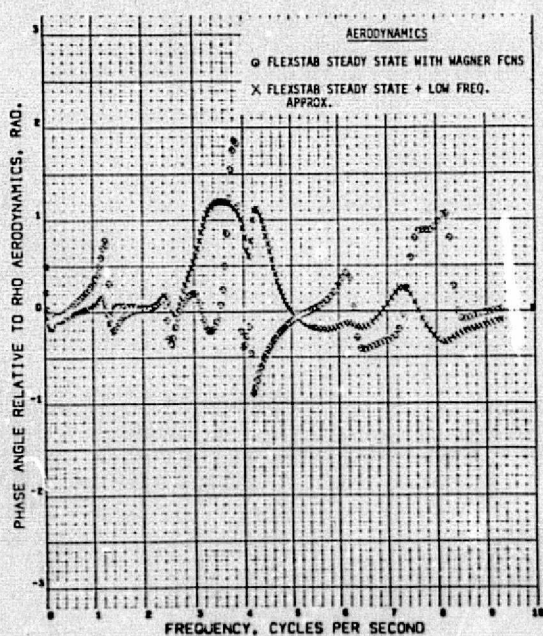
(a) Magnitudes

(b) Phase Angles

Figure 16.—Comparison of Wing Root Shear Frequency Response Function
Due to Aileron Excitation

44
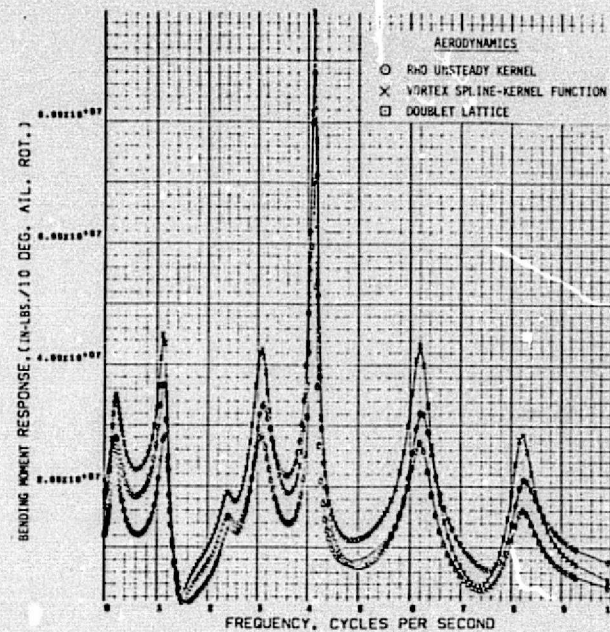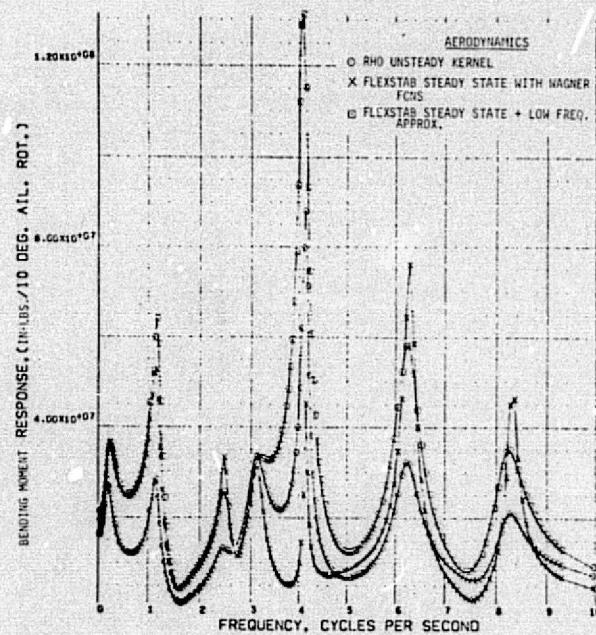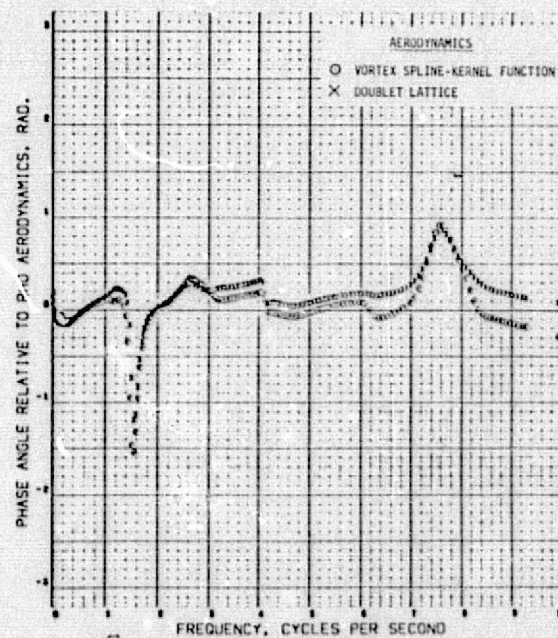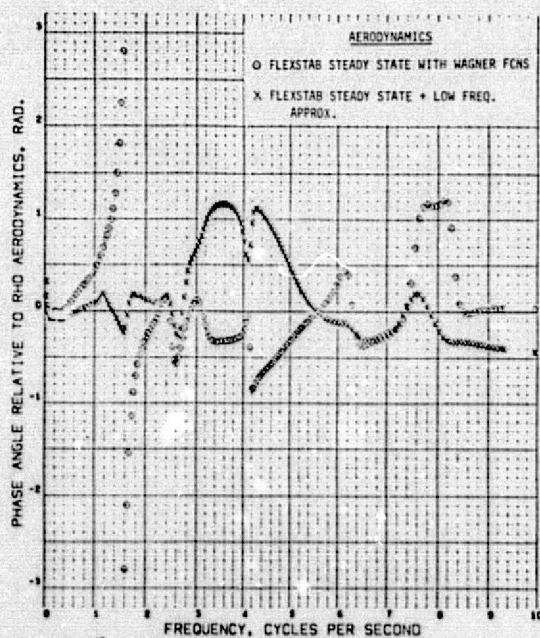
(a) Magnitudes

(b) Phase Angles

Figure 17.—Comparison of Wing Root Bending Moment Frequency Response Function
Due to Aileron Excitation

45
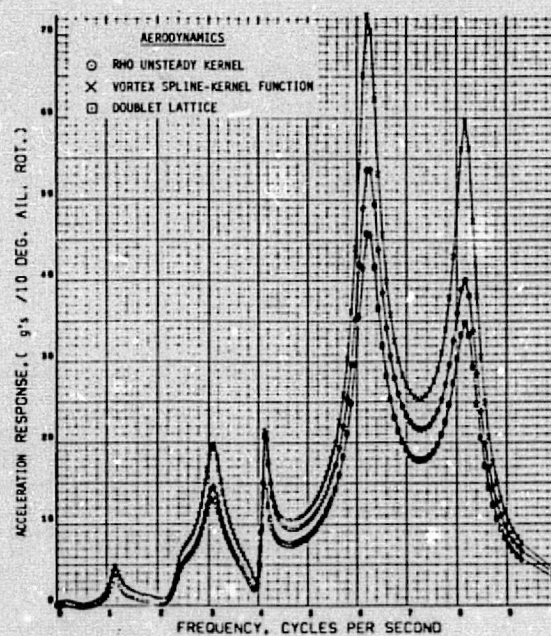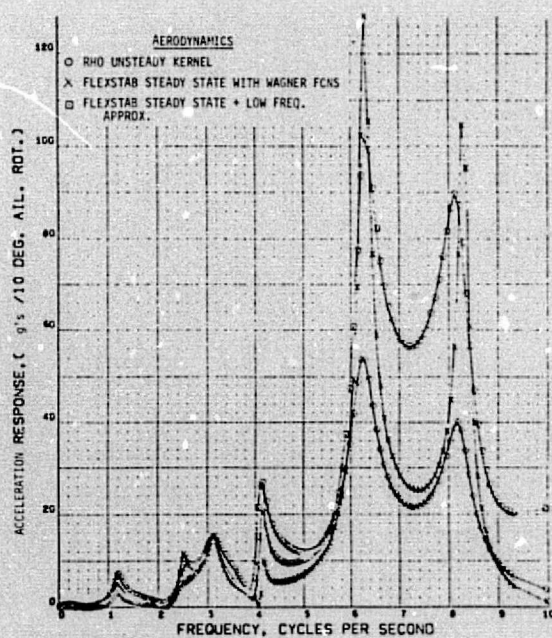
(a) Magnitudes
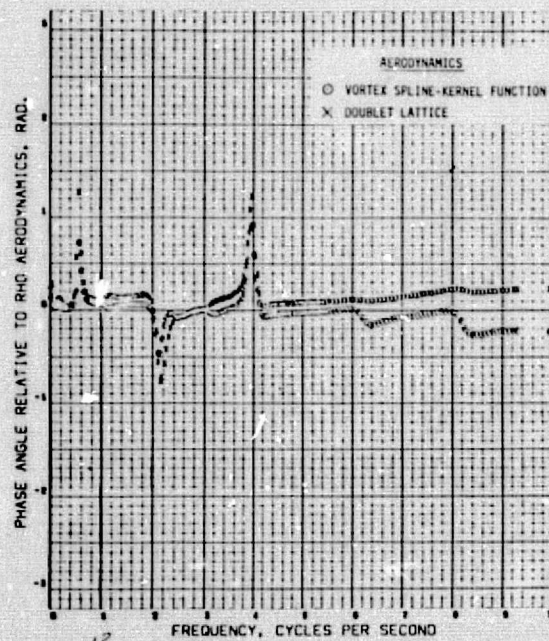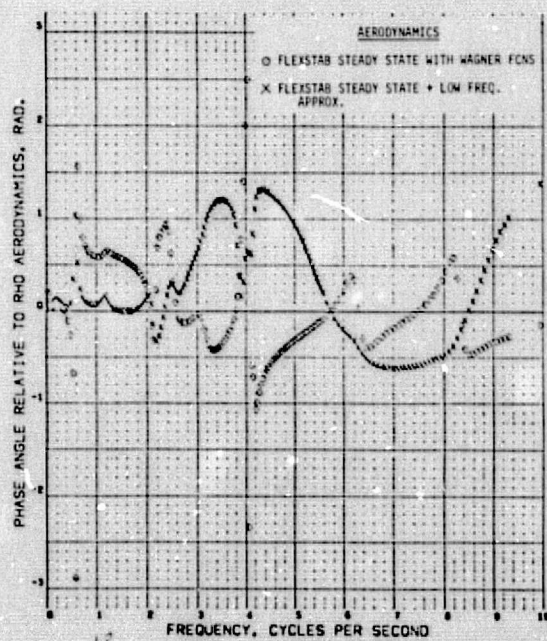
(b) Phase Angles

Figure 18.—Comparison of Wingtip Acceleration Frequency Response Function Due to Aileron Excitation

APPENDIX A

STRUCTURAL MODEL

In order to simplify the structural model but maintain a meaningful dynamic analysis, the airplane structural model was represented by only the wing elastic degrees of freedom. The body, empennage, and nacelles were considered to be rigid. The wing was modeled as a finite number of lumped masses, rotary inertias, and beam segments (fig. A-1). The lumped masses were considered to be attached to the elastic axis with rigid links perpendicular to the elastic axis. The flexibility matrix for this model was obtained and combined with the mass representation to form an eigenvalue problem. This problem was solved for free-free mode shapes and frequencies. The generalized mass and stiffness matrices were obtained for the first eight free-free modes which consisted of two rigid body modes (vertical translation and pitch) and six wing elastic modes. This representation of the generalized mass and stiffness was used for each aerodynamic method in formulating the equations of motion.

The elastic mode shapes obtained from the solution of the eigenvalue problem consisted of vertical bending displacement (ϕ_{Bdg}) and torsion (ϕ_{Tors}) and bending slopes at each point on the elastic axis where the mass was considered to be attached by rigid links (figs. A-2 through A-4).*

These mode shapes were then interpolated to the necessary aerodynamic reference points required by each aerodynamic method. Figures A-5 through A-11 show the grid used for the FLEXSTAB aerodynamics and the interpolated mode shapes at the associated aerodynamic reference points. The interpolation routine employed a cubic spline in arc lengths along a continuous planar curve (motion axis)** with mapping from the motion axis along defined reference lines which are assumed rigid with respect to displacement and rotations at the motion axis. In this case, the motion axis and elastic axis are the same. This interpolation routine was used to interpolate the mode shapes from the structural node points to the associated aerodynamic reference points of each aerodynamic method.

---

*In figures A-2 through A-4, the ordinate for torsional displacement is read as ϕ_{Tors} x 100, so that for a value of -0.4 read from the plots, the actual $\phi_{Tors} = -0.4/100$.

**A motion axis is a line along which the displacement due to rigid airplane and elastic motion is defined.
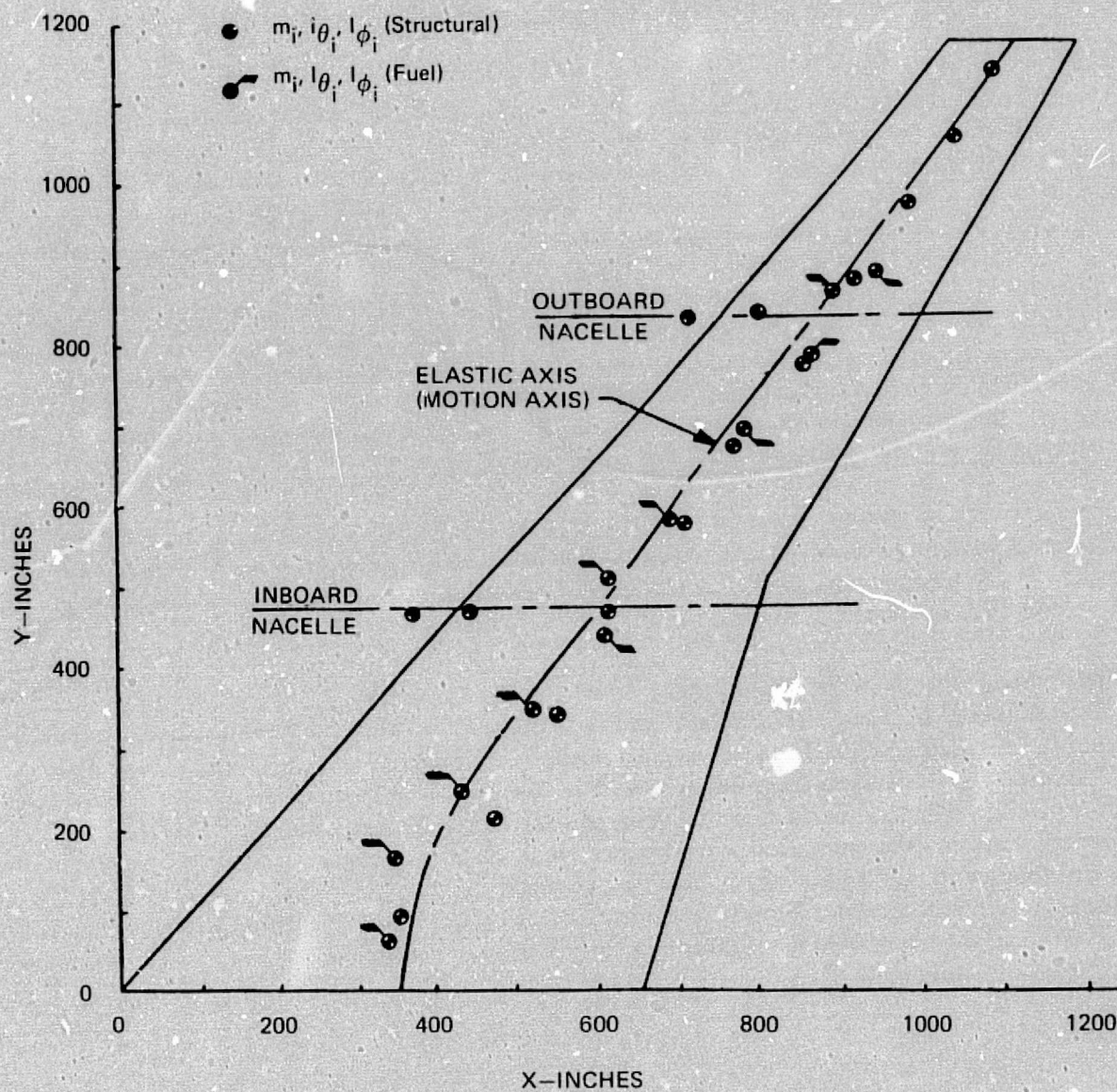
Figure A-1.—Model of Wing Mass, Inertia, and Elastic Axis (Motion Axis)

48

First Elastic Mode
Freq = 1.00 cps

ϕ_{Bdg}

ϕ_{Tors}

NORMALIZED MADE SHAPE $\phi_{Bdg}, \phi_{Tors} \times 100^b$

ELASTIC AXIS WING SPAN STATION, INCHES[a]
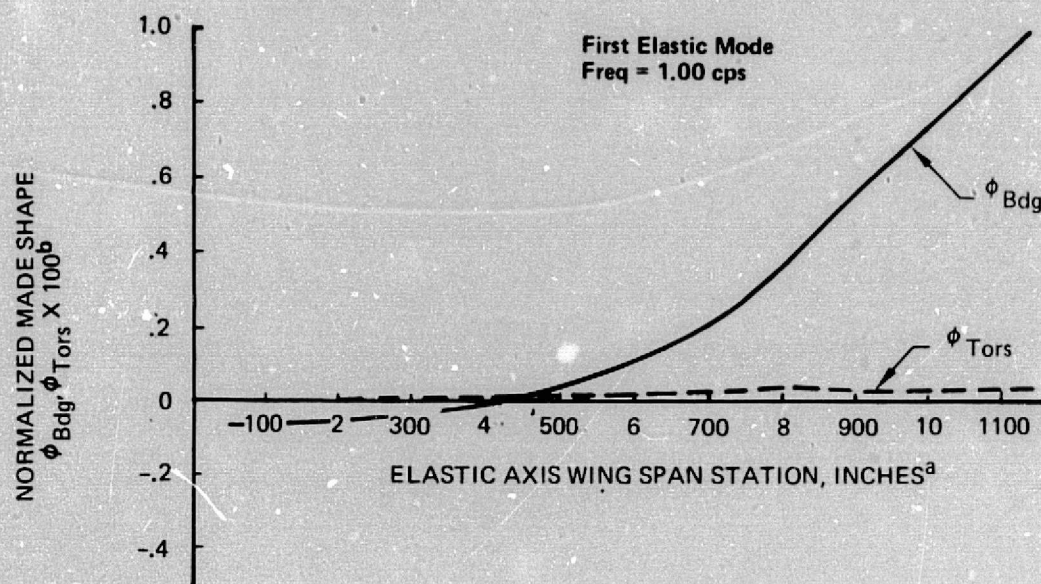
[a]Elastic axis wing span is the cummulative distance along the elastic axis starting at the wing root.

[b]All mode shapes normalized by tip deflections ϕ_{Bdg} are units of in./in. and ϕ_{Tors} are of units rad/in.

Second Elastic Mode
Freq = 2.15 cps

ϕ_{Bdg}

ϕ_{Tors}

NORMALIZED MADE SHAPE $\phi_{Bdg}, \phi_{Tors} \times 100$

ELASTIC AXIS WING SPAN STATION, INCHES
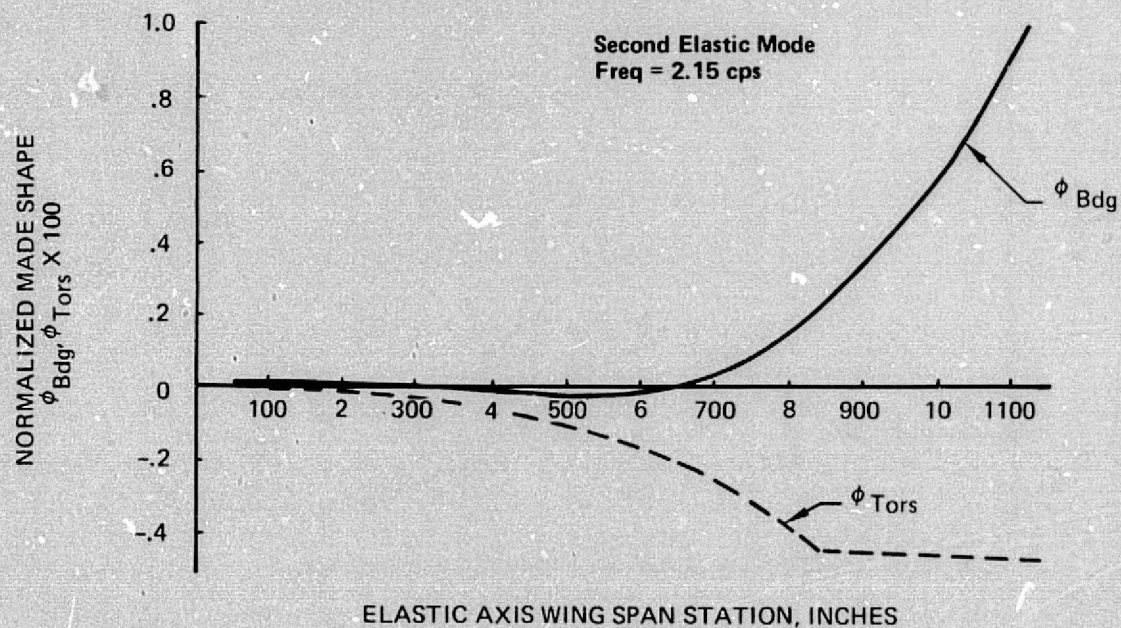
Figure A-2.—First and Second Elastic Mode Shapes on the Elastic Axis

49

Third Elastic Mode
Freq = 3.04 cps

ϕ_{Bdg}

ϕ_{Tors}

NORMALIZED MADE SHAPE
ϕ_{Bdg}, ϕ_{Tors} X 100

1.0
.8
.6
.4
.2
0
-.2

100   2   300   4   500   6   700   8   900   10   1100

ELASTIC AXIS WING SPAN STATION, INCHES

Fourth Elastic Mode
Freq = 4.16 cps

ϕ_{Bdg}

ϕ_{Tors}

NORMALIZED MADE SHAPE
ϕ_{Bdg}, ϕ_{Tors} X 100

1.0
.8
.6
.4
.2
0
-.2

100   2   300   4   500   6   700   8   900   10   1100

ELASTIC AXIS WING SPAN STATION, INCHES
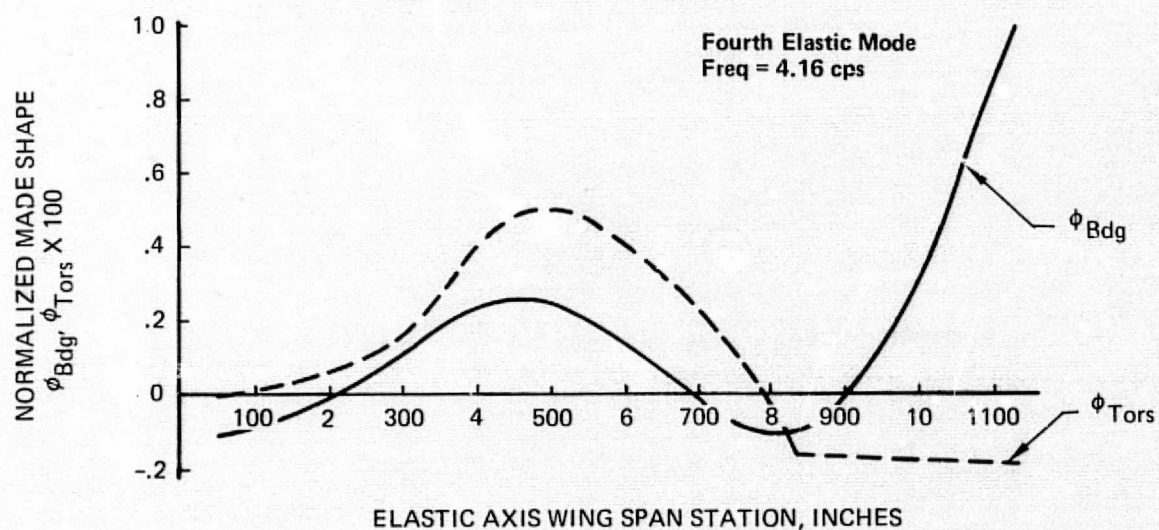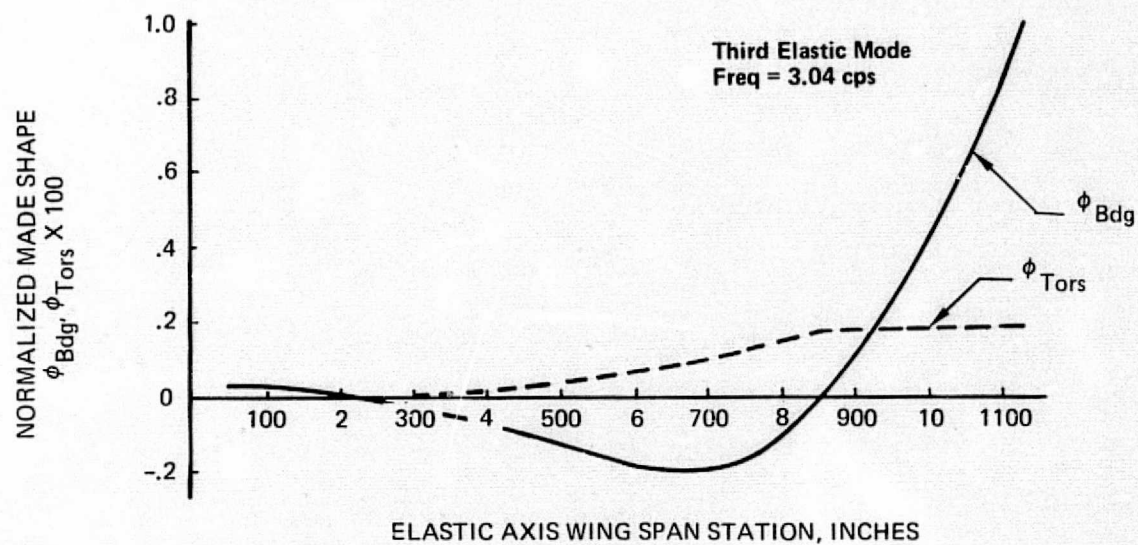
Figure A-3.—Third and Fourth Elastic Mode Shapes on the Elastic Axis
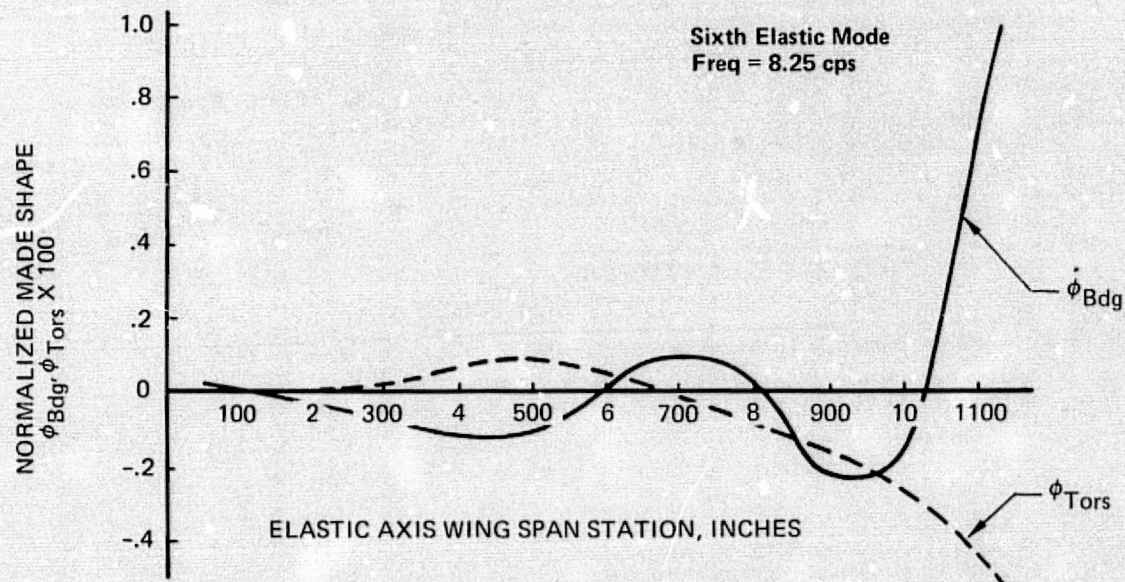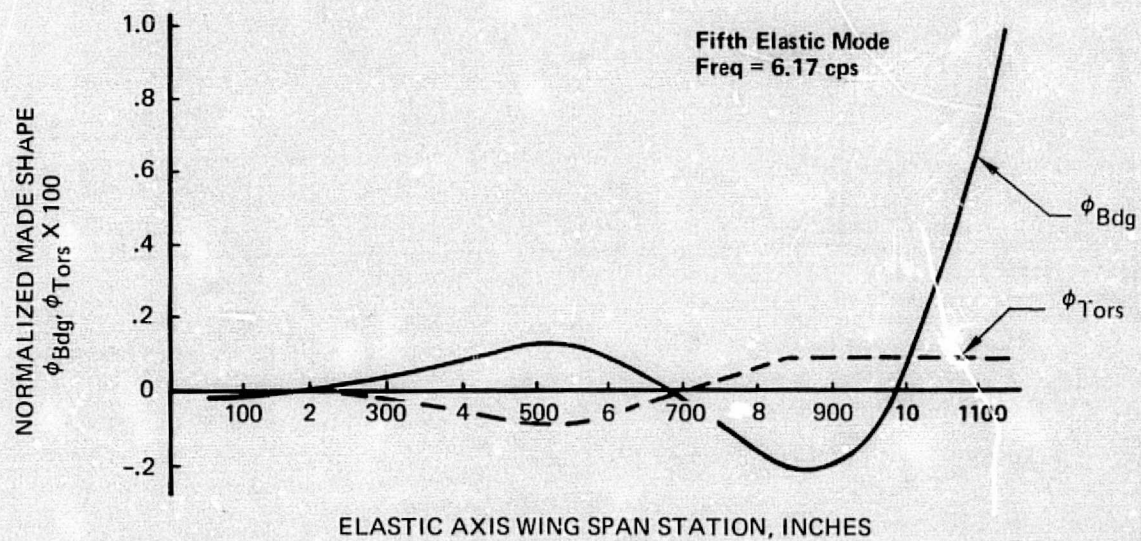
Figure A-4.—Fifth and Sixth Elastic Mode Shapes on the Elastic Axis

51
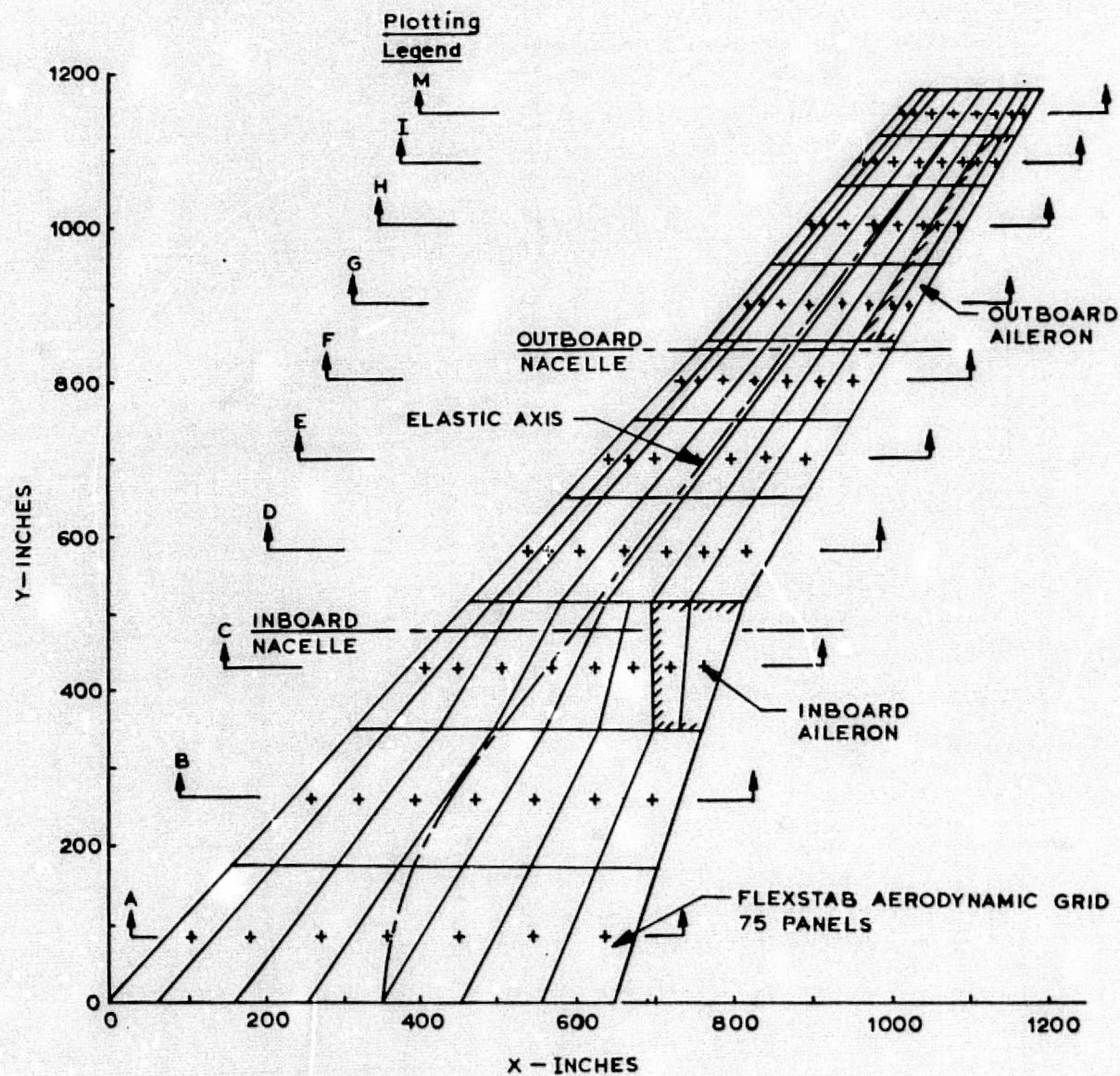
Figure A-5.—Modal Geometry Definition Used With FLEXSTAB Aerodynamic Grid
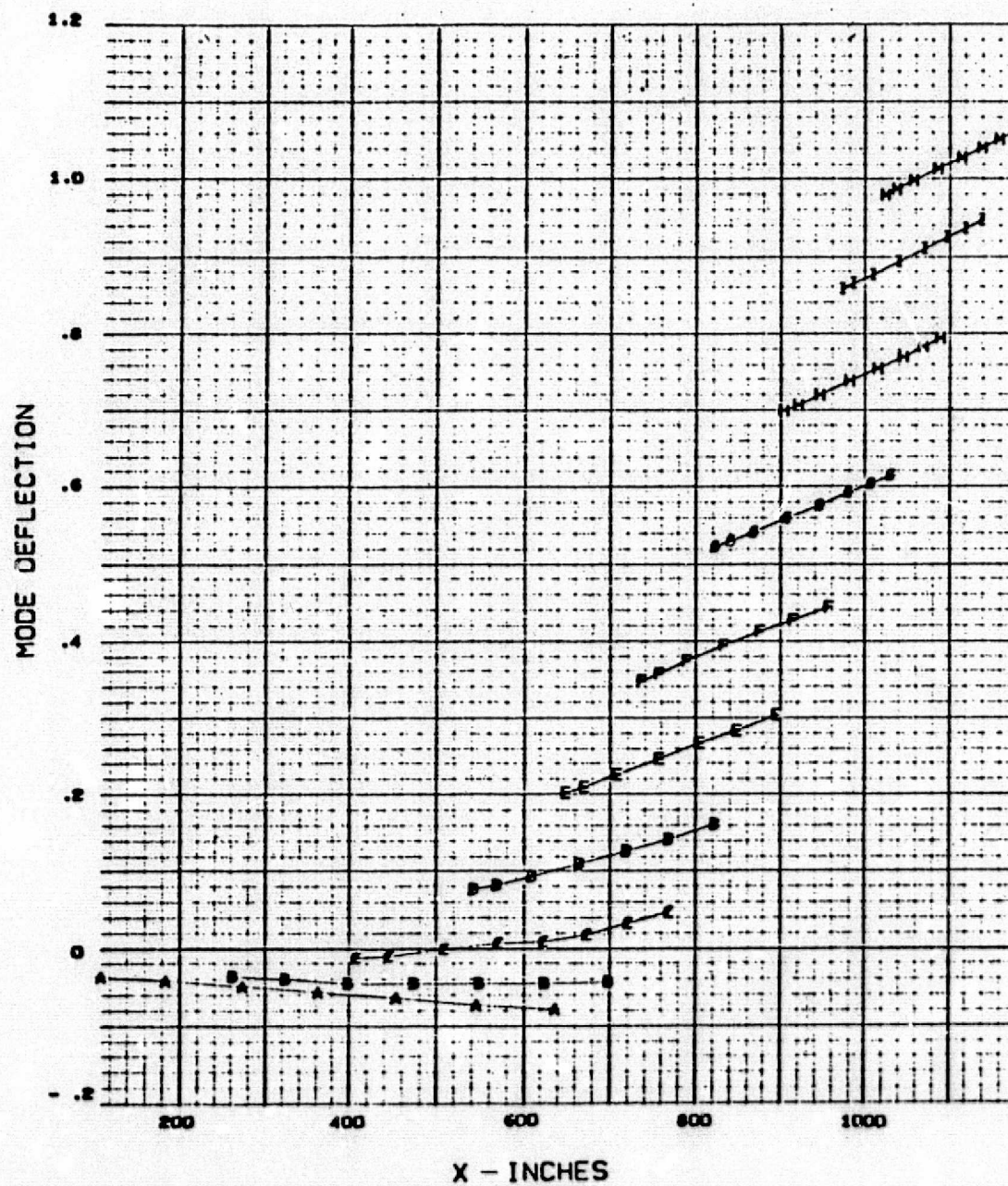
Figure A-6.—First Elastic Mode Shape at FLEXSTAB Aerodynamic Nodes
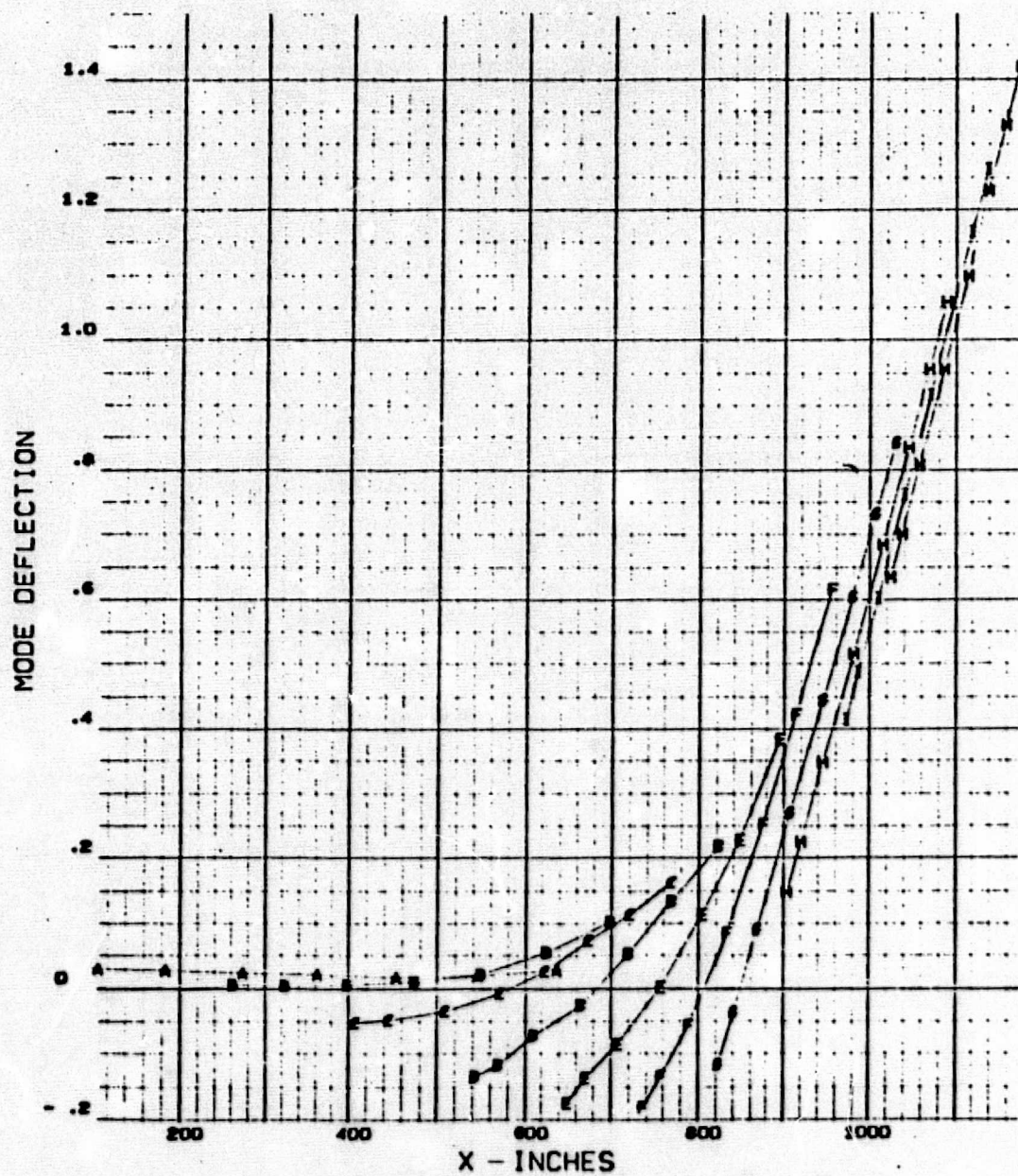
Figure A-7.—Second Elastic Mode Shape at FLEXSTAB Aerodynamic Nodes
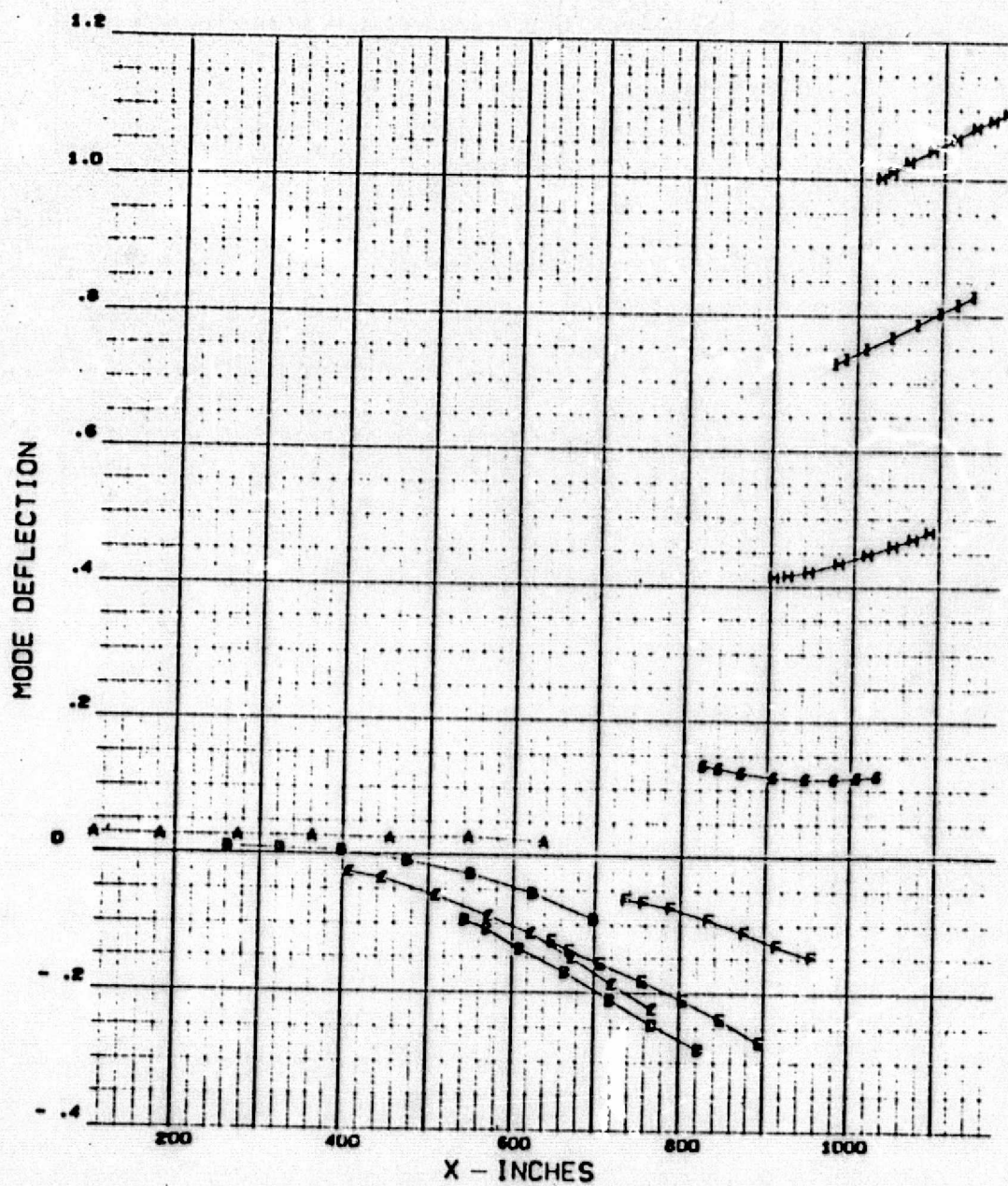
Figure A-8.—Third Elastic Mode Shape at FLEXSTAB Aerodynamic Nodes
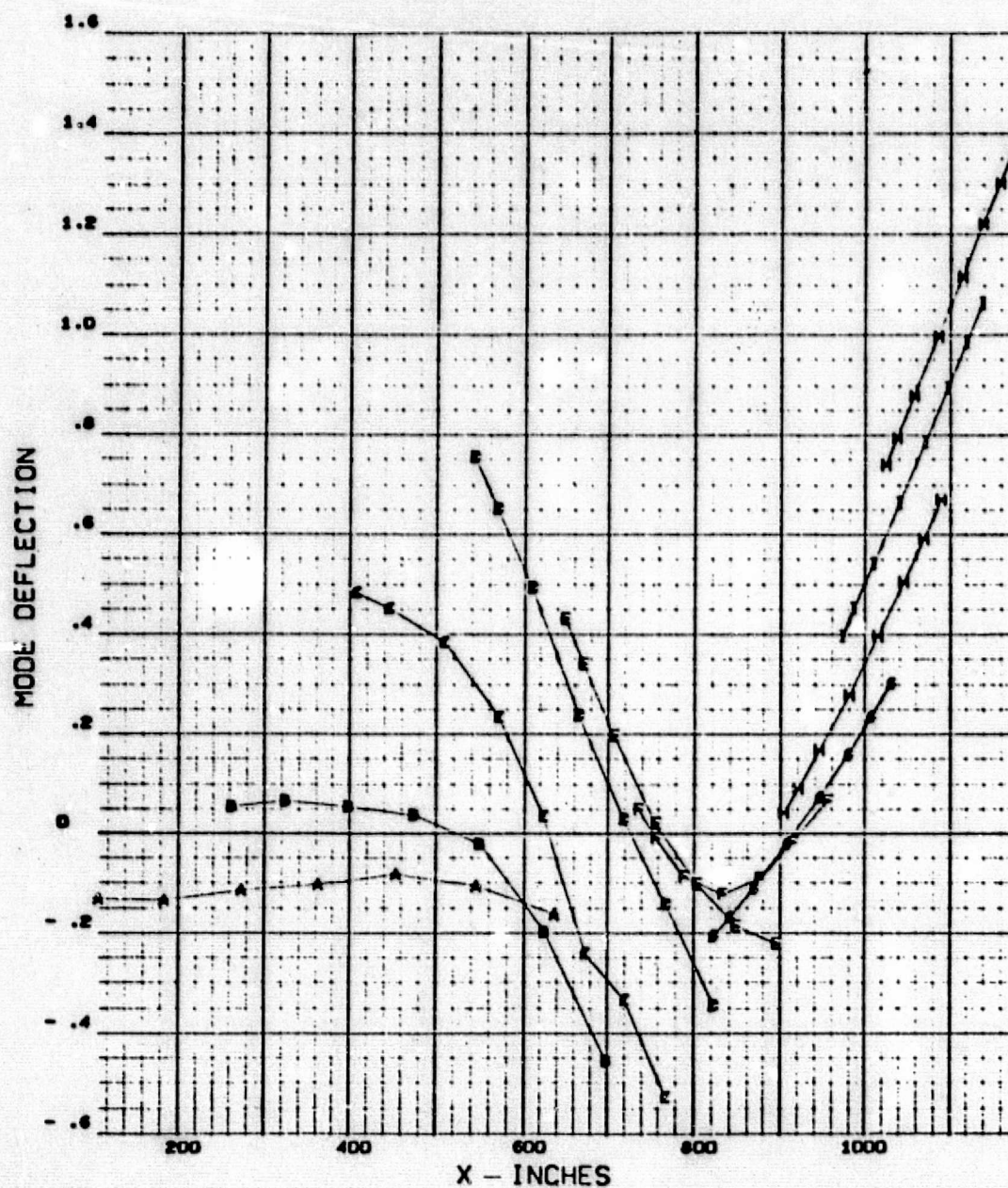
Figure A-9.—Fourth Elastic Mode Shape at FLEXSTAB Aerodynamic Nodes
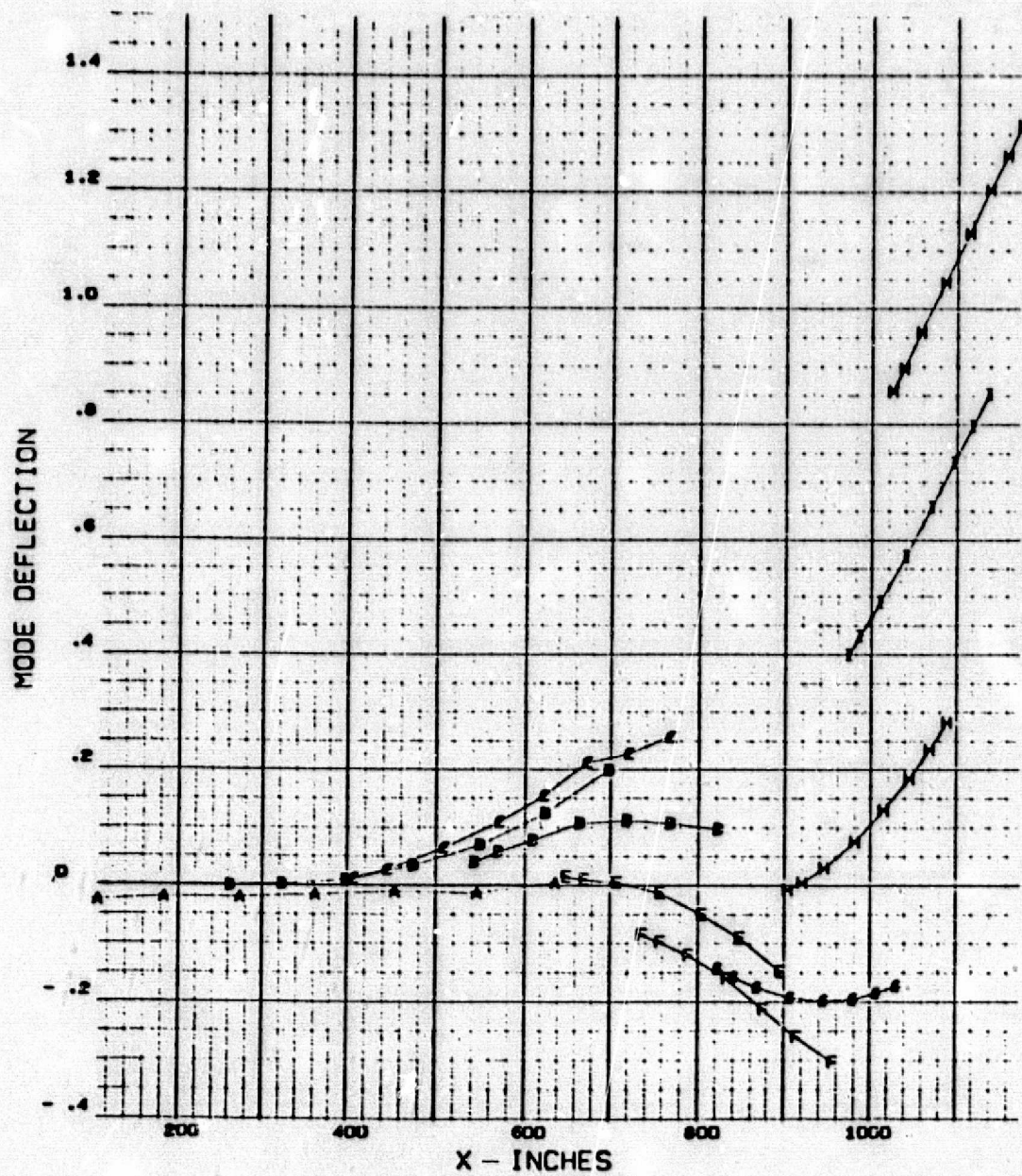
Figure A-10.—Fifth Elastic Mode Shape at FLEXSTAB Aerodynamic Nodes
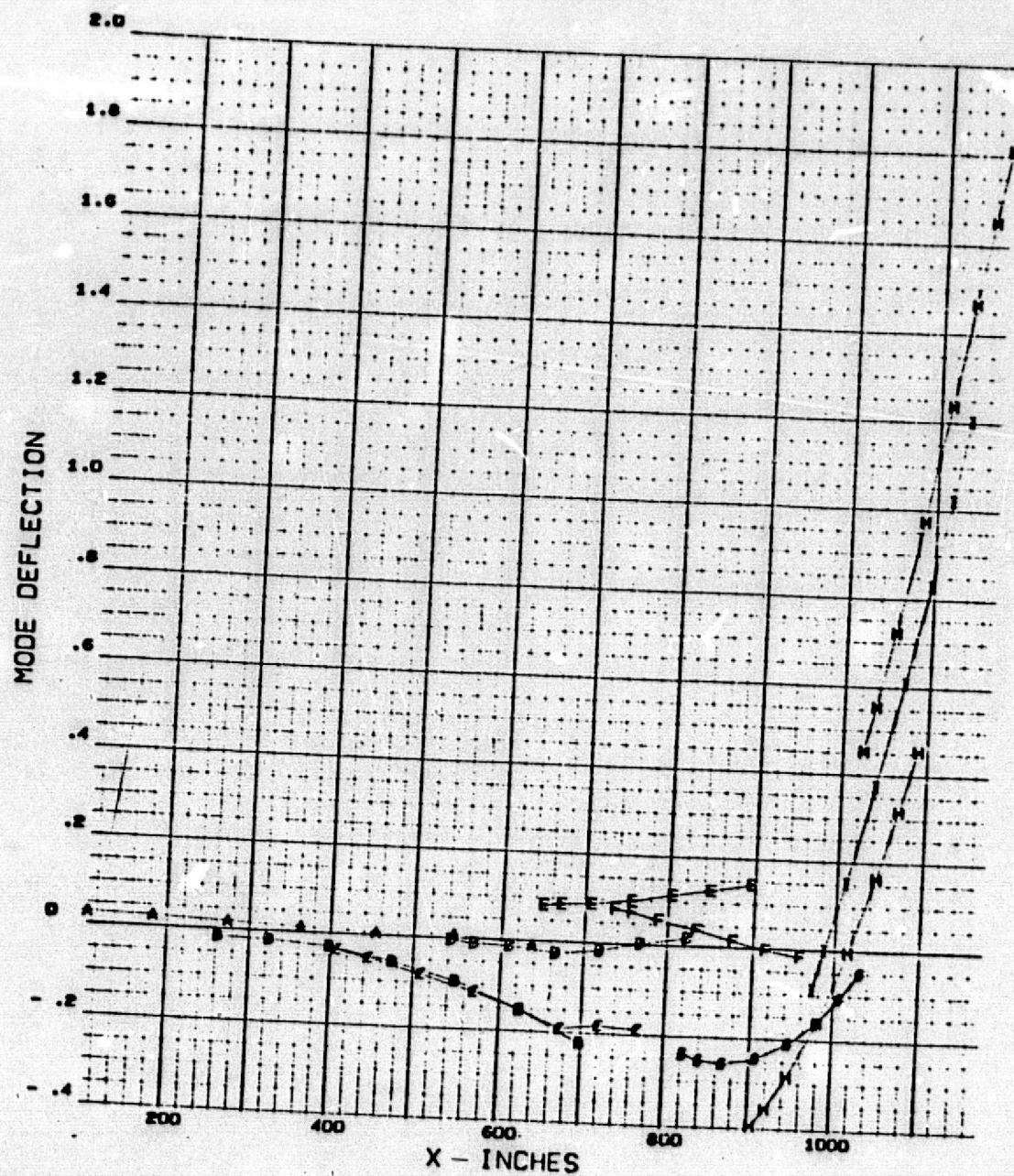
Figure A-11.—Sixth Elastic Mode Shape at FLEXSTAB Aerodynamic Nodes

APPENDIX B

EQUATIONS OF MOTION
AND LOAD EQUATIONS FORMULATION

The equations of motion were formulated by using the Lagrangean approach. Two basic forms were developed depending on the aerodynamic representation: (1) constant coefficient equations formed by utilizing steady state aerodynamic methods and approximating unsteady aerodynamics with either Küssner and Wagner indicial lift growth functions or the FLEXSTAB low frequency representation and (2) nonconstant coefficient equation with respect to frequency formed utilizing the more exact unsteady aerodynamic methods.

The generalized structural inertia and stiffness coefficients were obtained from the structural representation defined in appendix A. Although these coefficients are constant with respect to frequency, they were used in conjunction with both of the basic forms defined above.

The aerodynamic methods which produced constant coefficient equations for the generalized aerodynamic forces were:*

1.   Quasi-steady formulation of the FLEXSTAB steady state aerodynamics

2.   Quasi-steady formulation of the FLEXSTAB steady state aerodynamics and the instantaneous angle of incidence modified with Küssner and Wagner indicial lift growth functions

3.   Quasi-steady formulation of the FLEXSTAB steady state and low frequency approximation aerodynamics used both for response and gust aerodynamic forces

4.   Quasi-steady formulation of the FLEXSTAB steady state aerodynamics used for gust aerodynamic forces, and both FLEXSTAB steady state and low frequency approximation aerodynamics used for response aerodynamic forces

Note: This method is the aerodynamics developed in FLEXSTAB and used in method 3 but with only the low frequency approximation aerodynamics on the response forces included. With the aerodynamic gust forces due to the flow incidence time rate of change eliminated, this method is theoretically incomplete. However, it is useful for some stability and control analyses when evaluating the stability of the system. Thus, it was included as an aerodynamic method for use in comparison.

---

*Note: These methods are numbered in the same order as in table 1 and as in section 5.0.

59

5. Quasi-steady formulation of strip theory aerodynamics corrected to match wind tunnel steady state data, and the instantaneous angle of incidence modified with Küssner and Wagner indicial lift growth functions

The other basic form of equations, nonconstant coefficients formulated using the exact unsteady aerodynamic methods, consisted of the:

6. Rho unsteady kernel function aerodynamics

7. Vortex spline-kernel function unsteady aerodynamics

8. Doublet Lattice unsteady aerodynamics

The equations of motion* have the following form for the constant coefficient equations (refs. 8 and 13):

$$[M_1]\{q\} + [M_3]\{\ddot{q}\} + [M_4]\{\dot{q}\} * \Phi + [M_5]\{\ddot{q}\} * \Phi = \{C_1\}\dot{F} * \psi \qquad \text{(B-1)}$$

A variation of equation (B-1) for the frequency dependent coefficients from the unsteady aerodynamic methods (refs. 14 and 15) is shown in equation (B-2).

$$[M_3]\{\ddot{q}\} + [M_4 + M_1]\{q\} + [M_5]\{\dot{q}\} = \{C_2\}F \qquad \text{(B-2)}$$

where:

$[M_1]$ = generalized structural stiffness matrix

$[M_3]$ = generalized structural inertia matrix

$[M_4]$ = generalized aerodynamic stiffness matrix

$[M_5]$ = generalized aerodynamic damping matrix

$\{C_1\}$ = generalized forcing function coefficients (real)

$\{C_2\}$ = generalized forcing function coefficients (complex)

F = forcing function

Φ = Wagner indicial lift function

ψ = Küssner indicial lift function

---

*The equations are formulated in the inertial axis system for the initial condition of straight and level flight.

$*$ = indicial convolution

q = generalized coordinates

The equation of motion formulation for aerodynamic methods 1 through 4 used the "s" plane formulation as given in reference 7 with the exception of the low frequency approximation aerodynamics, which requires the rate of change of the downwash (W), given by:

$$\{\dot{W}\} = [\phi']\{\dot{q}\} + \frac{1}{V}[\phi]\{\ddot{q}\}$$ (B-3)

as well as the downwash (W) which is required when using the FLEXSTAB steady state aerodynamic force formulation (ref. 1).

The strip theory aerodynamics (method 5) also used the "s" plane formulation. The aerodynamic lift was formulated using two-dimensional incompressible flow. Steady state three-dimensional lift was then obtained by modifying the two-dimensional lift coefficients with compressibility factors (F_c), wind tunnel test data, and a static induction matrix based on the method developed in reference 6. From this, the generalized aerodynamic force coefficient matrices were formed.

The vortex spline-kernel function aerodynamics produced an AIC matrix which relates panel downwash to panel pressure, which was used as in the method presented in reference 7. The Rho unsteady kernel function and the Doublet Lattice unsteady aerodynamic representations could not be used in this manner, as explained in the following paragraph.

The output from the Rho kernel function and Doublet Lattice aerodynamic program consisted of complex matrix coefficients which yielded generalized forces and surface pressures when multiplied by the generalized coordinates (q).

$$\{Q\} = \left([Q_{Re}] + i[Q_{Im}]\right)\{q\}$$ (B-4)
$$\{P\} = \left([P_{Re}] + i[P_{Im}]\right)\{q\}$$

where:

$\{Q\}, \{P\}$ = complex generalized forces and surface pressures, respectively

$[Q_{Re}], [Q_{Im}]$ = real and imaginary parts of the generalized force coefficients obtained from the aerodynamic programs

$[P_{Re}], [P_{Im}]$ = real and imaginary parts of the pressure coefficients obtained from the aerodynamic programs

$\{q\}$ = generalized coordinate

The solution program required that the generalized force coefficients be coefficients of q and $\dot{q}$. Therefore, using the sinusoidal relationship

$$\dot{q} = i\omega q \qquad \text{(B-5)}$$

the generalized forces and surface pressures were written as:

$$\{Q\} = [Q_{Re}]\{q\} + 1/\omega[Q_{Im}]\{\dot{q}\}$$
$$\{P\} = [P_{Re}]\{q\} + 1/\omega[P_{Im}]\{\dot{q}\} \qquad \text{(B-6)}$$

Further modification was made to the generalized force and surface pressure coefficient matricies to account for nondimensionalizing.

In addition, because of the computer time required to calculate the unsteady aerodynamic generalized forces and pressures at each frequency, only a limited number of base frequencies were calculated (20), and the matrices were then linearly interpolated to a larger number of frequencies (210) so as to adequately define the transfer functions once the equations were solved.

The load equations have a form similar to the equations of motion:

$$\text{load} = [\overline{M}_3]\{\ddot{q}\} + [\overline{M}_4]\{\dot{q}\}*\Phi + [\overline{M}_5]\{\ddot{q}\}*\Phi + \{\overline{C}_1\}\dot{F}*\psi \qquad \text{(B-7)}$$

A variation of equation (B-7) for the frequency dependent coefficients from the unsteady aerodynamic methods is shown in equation (B-8).

$$\text{load} = [\overline{M}_3]\{\ddot{q}\} + [\overline{M}_4]\{q\} + [\overline{M}_5]\{\dot{q}\} + \{\overline{C}_2\}F \qquad \text{(B-8)}$$

where:

$\overline{M}_3$ = inertia force coefficients

$\overline{M}_4$ = aerodynamic stiffness force coefficients

$\overline{M}_5$ = aerodynamic damping force coefficients

$\overline{C}_1$ = real matrix coefficients of loads due to the forcing function

$\overline{C}_2$ = complex matrix coefficients of loads due to the forcing function

F = forcing function

Although the computer program used to solve the constant coefficient equations differed from that used to solve the frequency dependent coefficient equations, there existed commonality between the two programs in the solution and output routines. Only the input routines were different. The computer program used for the frequency dependent coefficient equations allowed input of matrices at various base frequencies and then

linearly interpolated the matrices for a larger number of solution frequencies. In addition, complex matrices for the forcing functions could be used as input.

The acceleration load equation matrix coefficients for all of the aerodynamic methods were formulated and generated as defined in reference 7. The shear and bending moment load equation matrix coefficients were also formulated and generated as defined in reference 7 for the aerodynamic methods 1 through 4, 7, and 8, and for the coefficients representing the inertia forces used with all of the aerodynamic methods. The strip theory (method 5) represented aerodynamic forces and moments at a point on the elastic axis and at the midspan point of each strip. These forces and moments were summed to calculate the shear and bending moment matrix coefficients at the specific load stations.

In order to calculate the shear and bending moment matrix coefficients using the Rho unsteady kernel (method 6), it was necessary to perform a chordwise integration of the chordwise pressure distributions reported by Rho, since this aerodynamic method is a collocation point method and not a panel-type method. This procedure, using a trapezoidal integration scheme, produced lifts and moments at the quarter point of each chord where pressures were reported. These lifts and moments were then integrated to the required load stations to produce the appropriate shear and bending moment matrix coefficients.

Parameters used in the equations of motion, load equations, and solution routines for the Küssner and Wagner indicial lift growth functions and gust parameters were:

Gust spectrum	Von Karman
Gust velocity	1 fps
Scale of turbulence	2500 ft

Küssner indicial lift growth coefficients (where applicable):

$$\psi(t) = 1.0 - 0.488\, e^{-0.58\frac{V}{c}t} - 0.272\, e^{-1.45\frac{V}{c}t} - 0.193\, e^{-6.0\frac{V}{c}t} \tag{B-9}$$

Wagner indicial lift growth coefficients (where applicable):

$$\phi(t) = 1.0 - 0.361\, e^{-0.762\frac{V}{c}t} \tag{B-10}$$

APPENDIX C

GENERALIZED COORDINATES
AND LOAD FREQUENCY RESPONSE FUNCTIONS

The generalized coordinates and load magnitude frequency response plots for the solutions of the equations identified in appendixes A and B are shown in figures C-1a through C-36a. The corresponding phase angle difference $(\phi_{method_j} - \phi_{Rho})$ frequency response plots are shown in figures C-1b through C-36b.

The solutions of the equations were separated into two types of analysis consisting of: (1) dynamic gust loads analysis with controls fixed and (2) dynamic loads analysis performed with the excitation function defined by an oscillatory control surface (inboard aileron). The transfer functions for the dynamic gust loads analysis with controls fixed are shown in figures C-1a through C-18a for magnitudes and figures C-1b through C-18b for phase angles. The transfer functions for the dynamic loads analysis performed with an oscillatory control surface excitation function are shown in figures C-19a though C-36a for magnitudes and figures C-19b through C-36b for phase angles. A content summary of figures C-1 through C-36 is given in table C-1.

The Rho unsteady kernel function aerodynamic method is presently the theoretically most exact unsteady aerodynamic representation. Consequently, it was used as a basis for comparing the accuracy of the other aerodynamic methods, and its transfer functions are presented in each figure for comparison purposes.

Table C-1.—Content of Comparison Plots in Appendix C Figures

| Figure	Rigid body modes		Elastic modes	Sinusoidal[a] gust		Oscillating inboard control surface	
	Vertical translation	Pitch	1 2 3 4 5 6	Magnitude	Phase angle	Magnitude[b]	Phase angle[b]
C-1 C-2 C-3 • • • C-8	✓	✓	✓ − − − − ✓	✓ ✓ ✓ • • • ✓	✓ ✓ ✓ • • • ✓		
C-19 C-20 C-21 • • • C-26	✓	✓	✓ − − − − ✓			✓ ✓ ✓ • • • ✓	✓ ✓ ✓ • • • ✓
	V_{root} V_{in} V_{out}	M_{root} M_{in} M_{out}	A_{tip} A_{out} A_{in} A_{root}				
C-9 • • • C-18	✓ − − −	− − − −	− − − ✓	✓ • • • ✓	✓ • • • ✓		
C-27 • • • C-36	✓ − − −	− − −	− − − ✓			✓ • • • ✓	✓ • • • ✓

[a]All eight aerodynamic methods.

[b]Aerodynamic methods 2, 4, 6, 7, and 8.
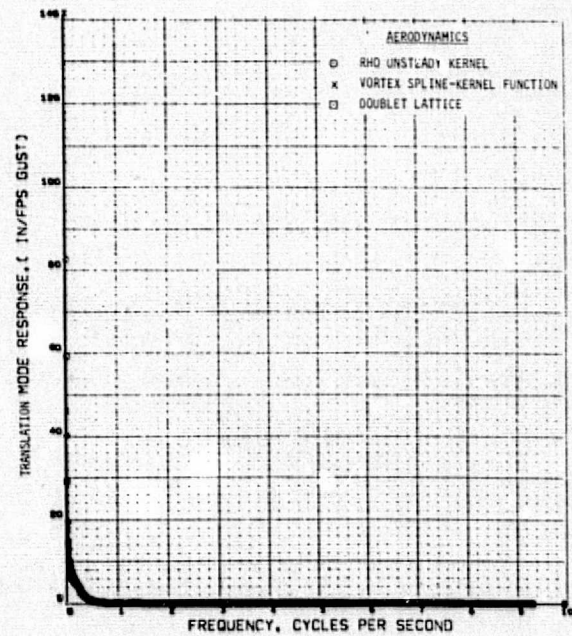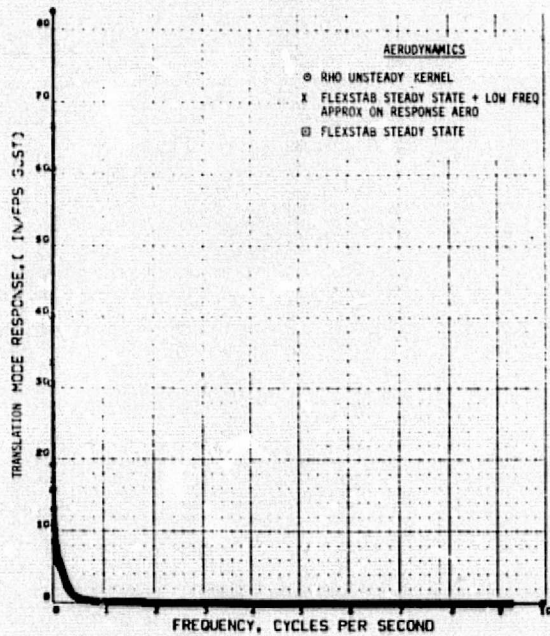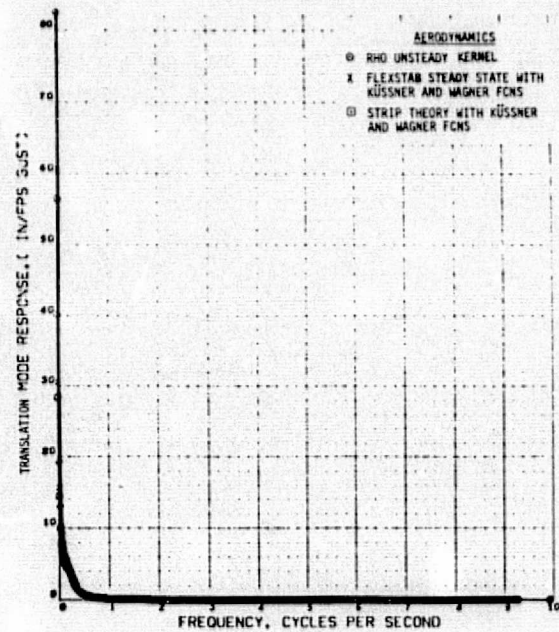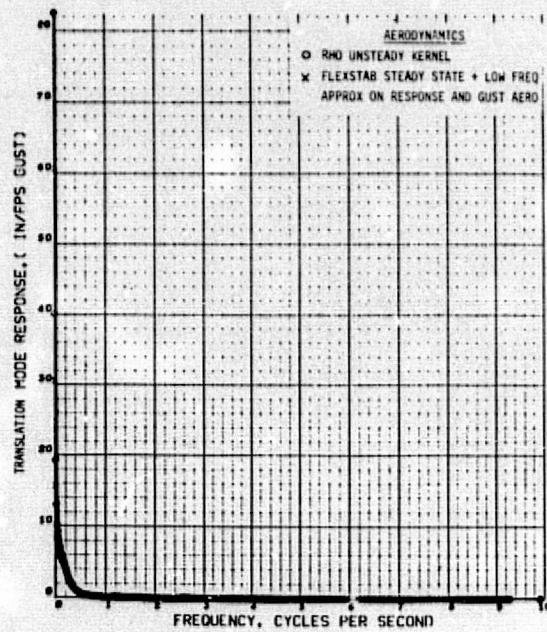
(a) Magnitudes
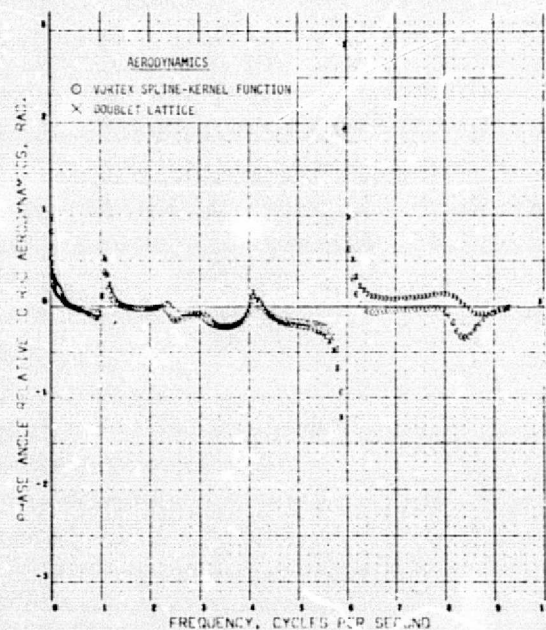
Figure C-1.—Comparison of Generalized Coordinate Frequency Response Function
Due to Gust Excitation

67
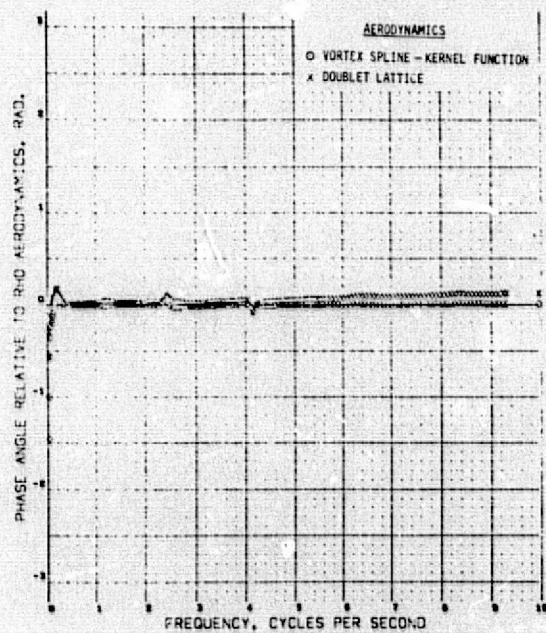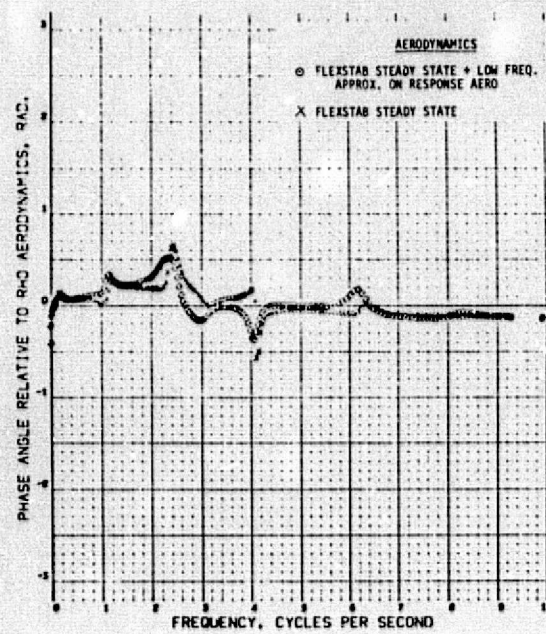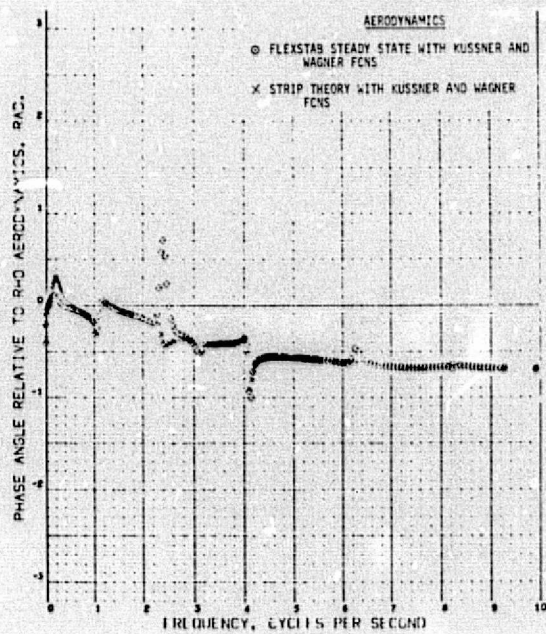
(b) Phase Angles

Figure C-1.—(Concluded)
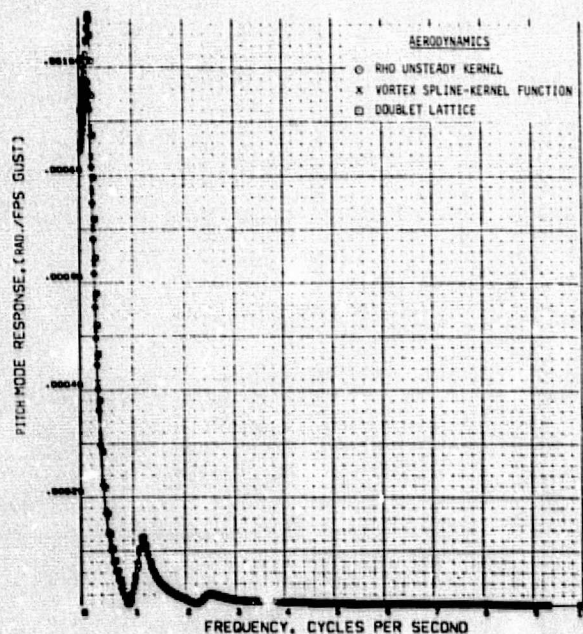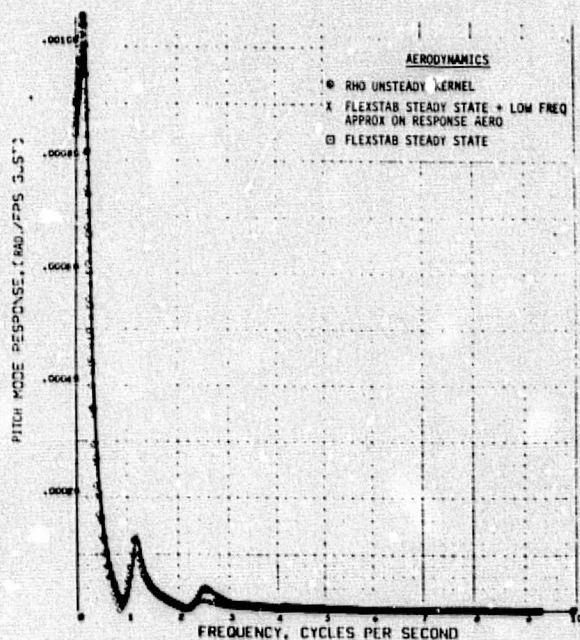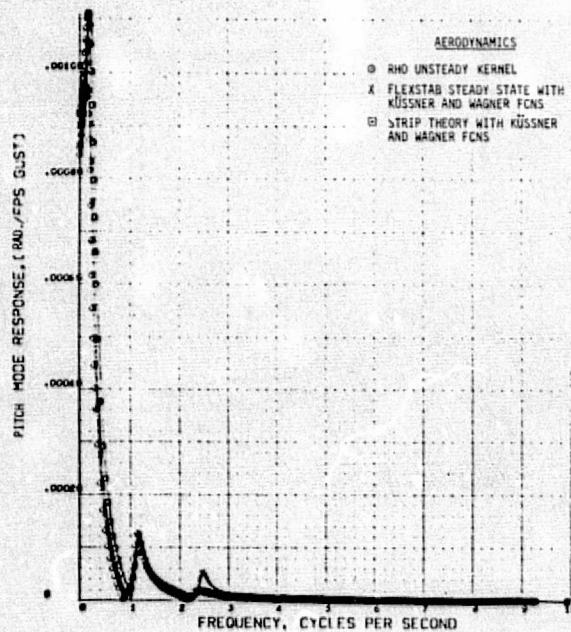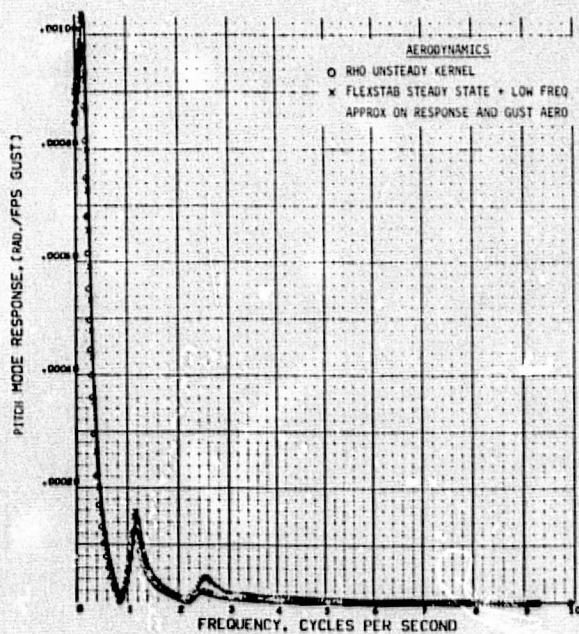
(a) Magnitudes

Figure C 2.—Comparison of Generalized Coordinate Frequency Response Function
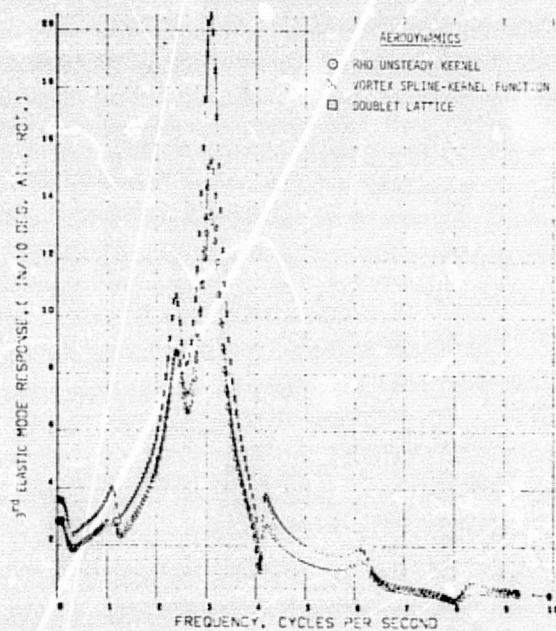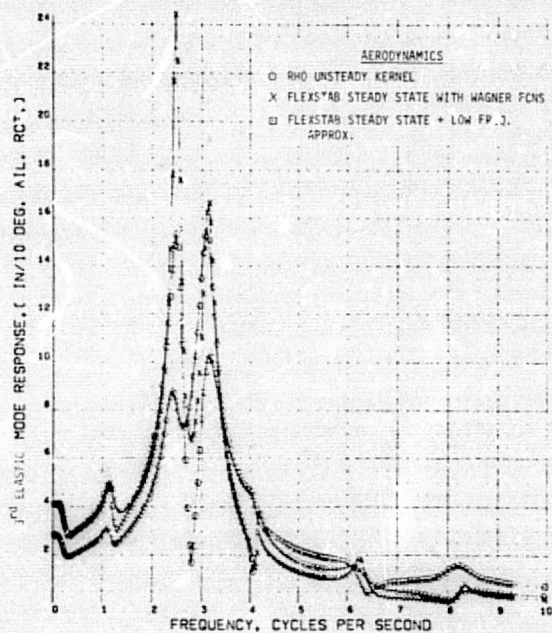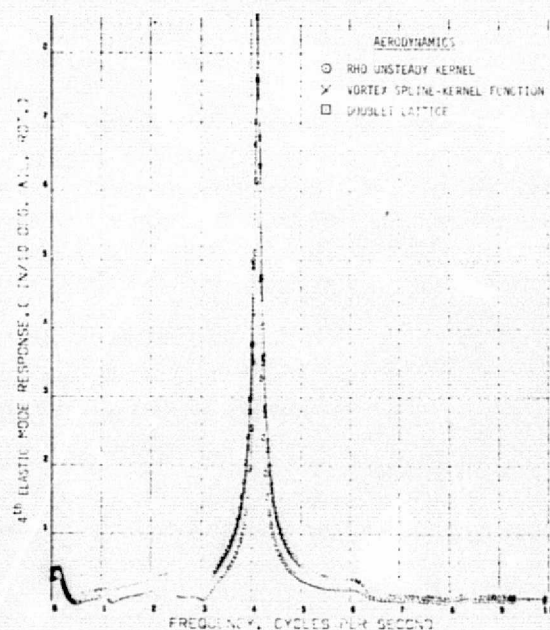Due to Gust Excitation
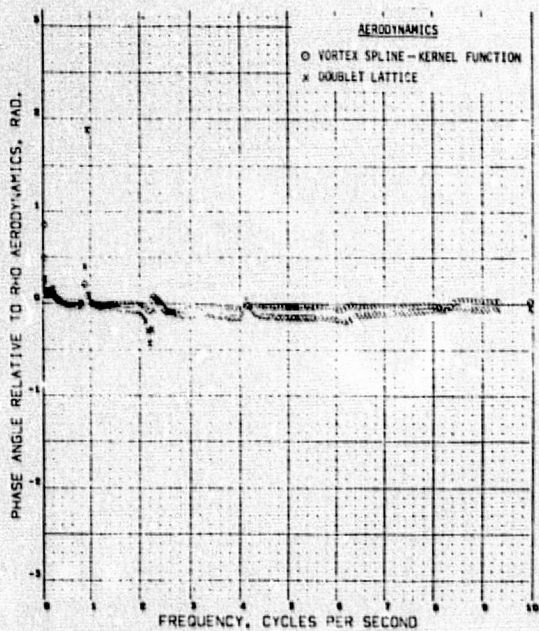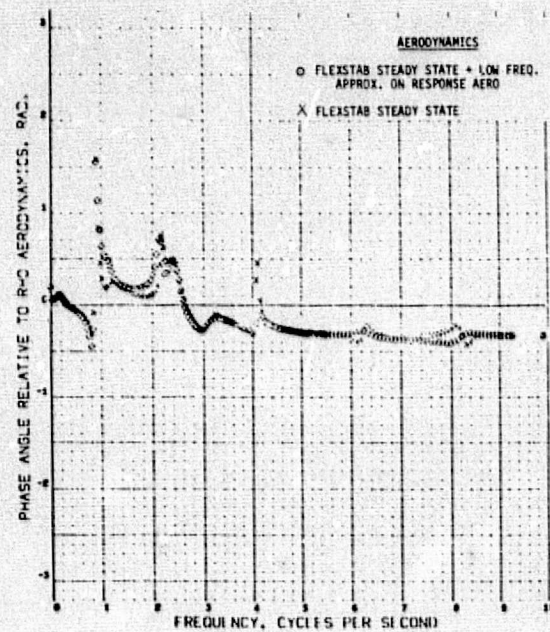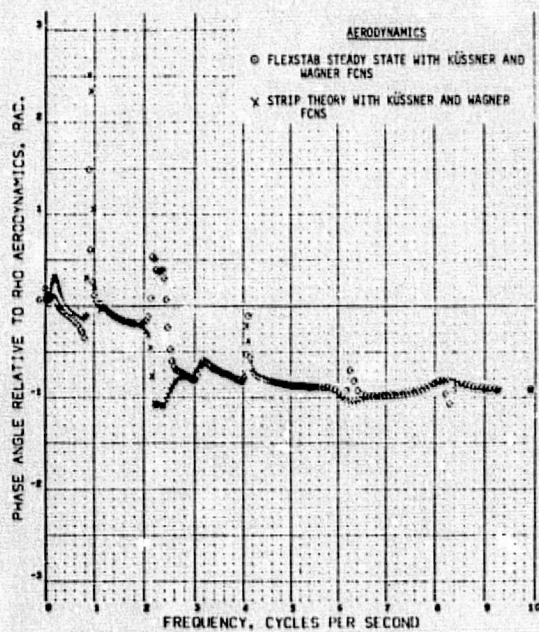
(b) Phase Angles

Figure C-2.—(Concluded)

70
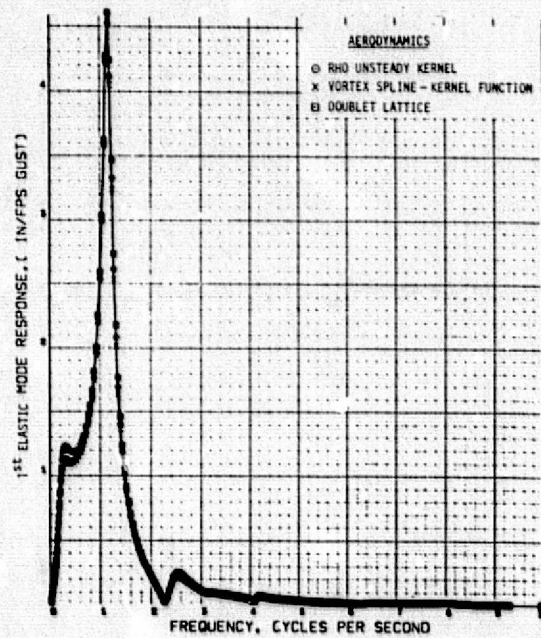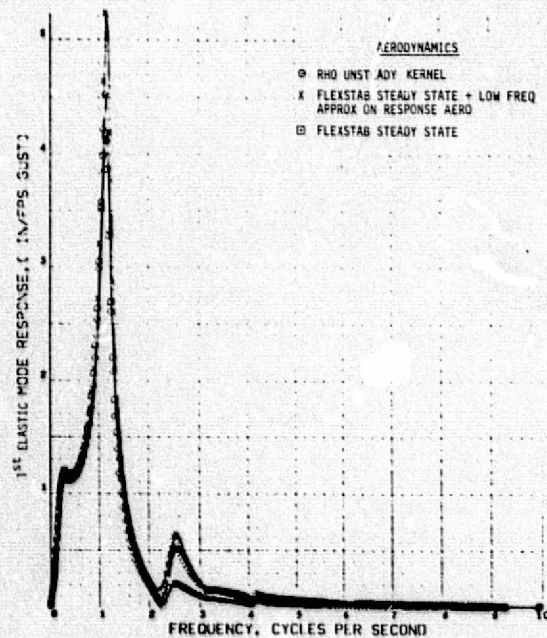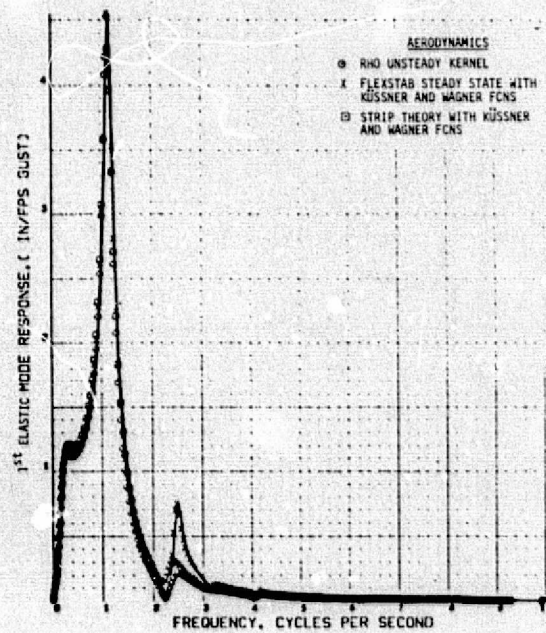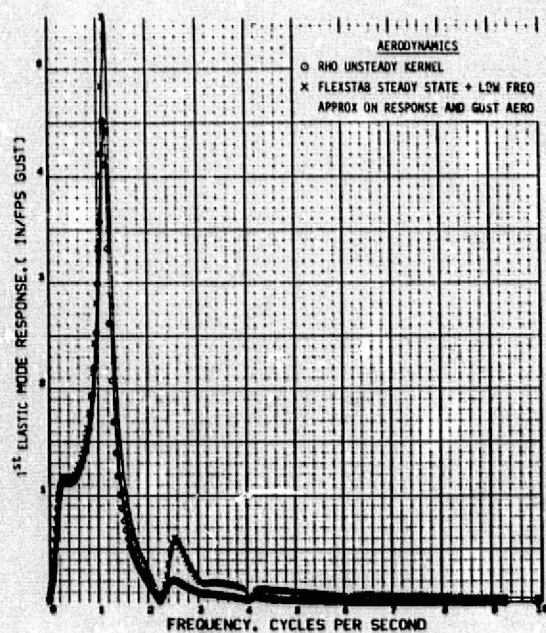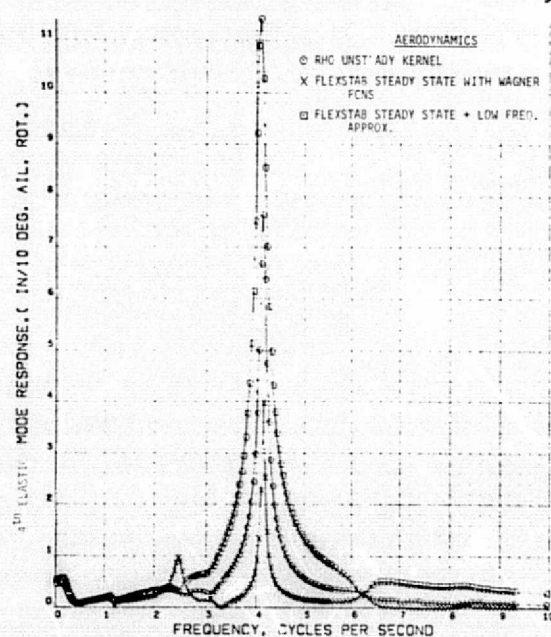
(a) Magnitudes
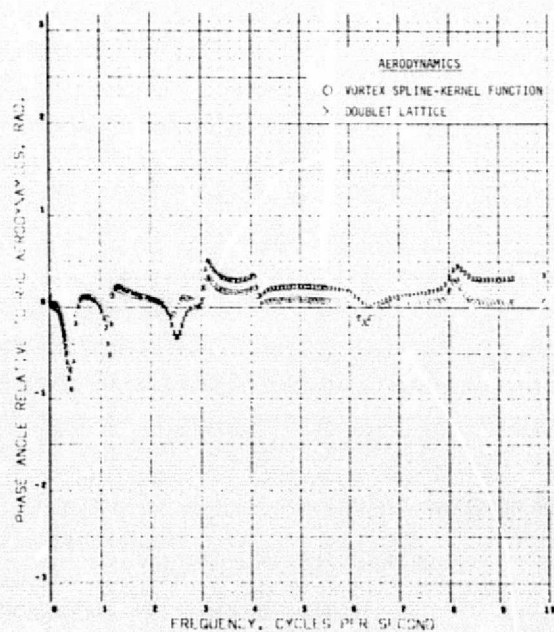
Figure C-3.—Comparison of Generalized Coordinate Frequency Response Function
Due to Gust Excitation
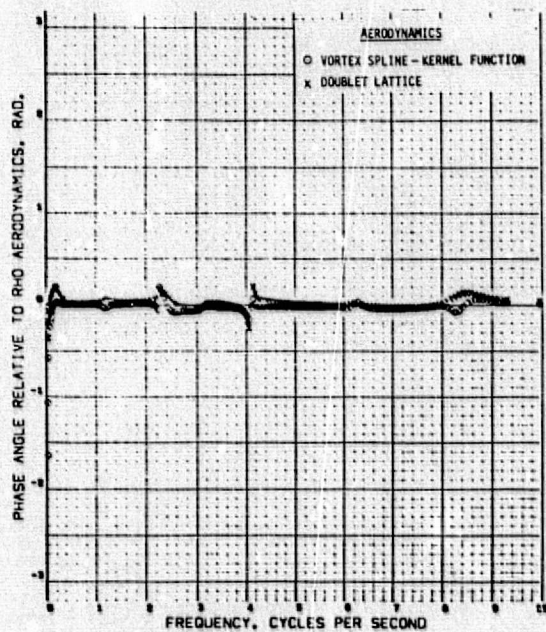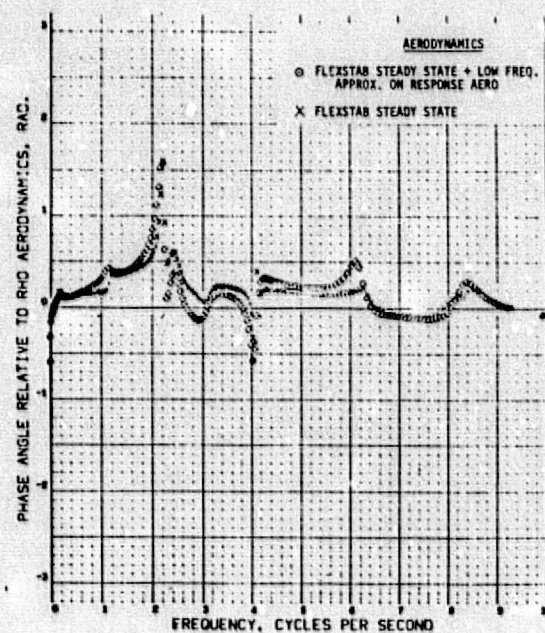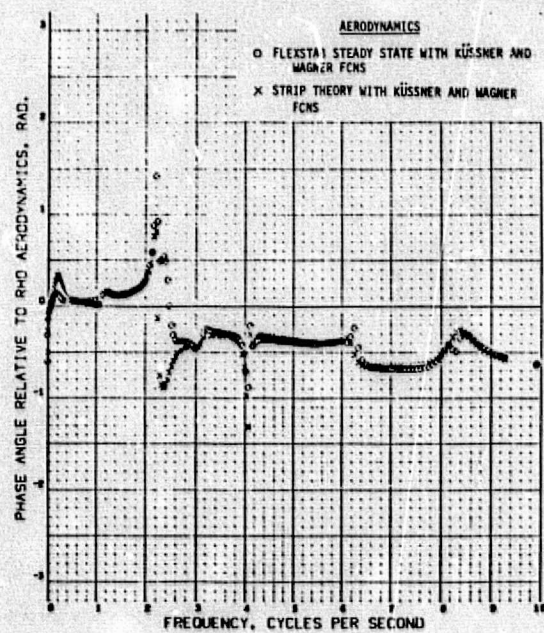
(b) Phase Angles

Figure C-3.—(Concluded)

72
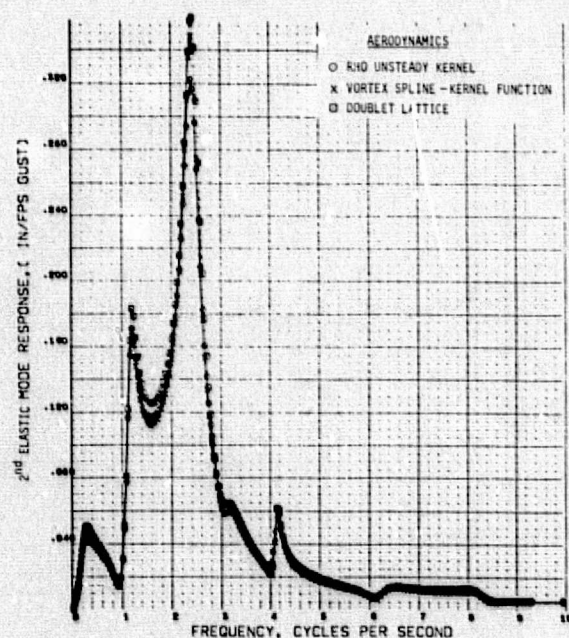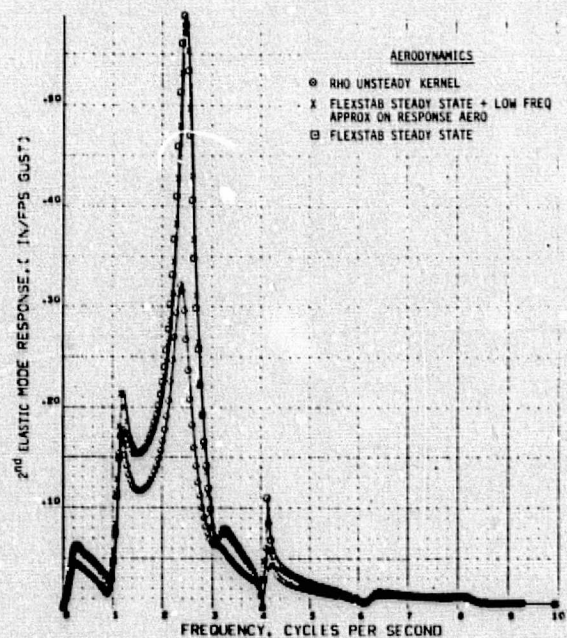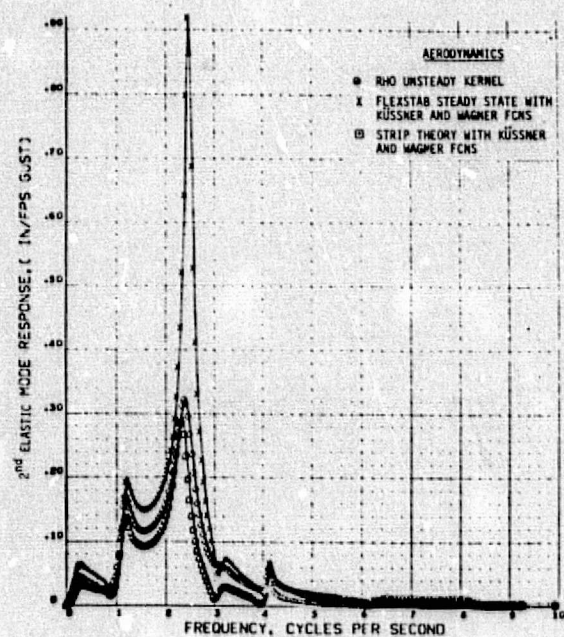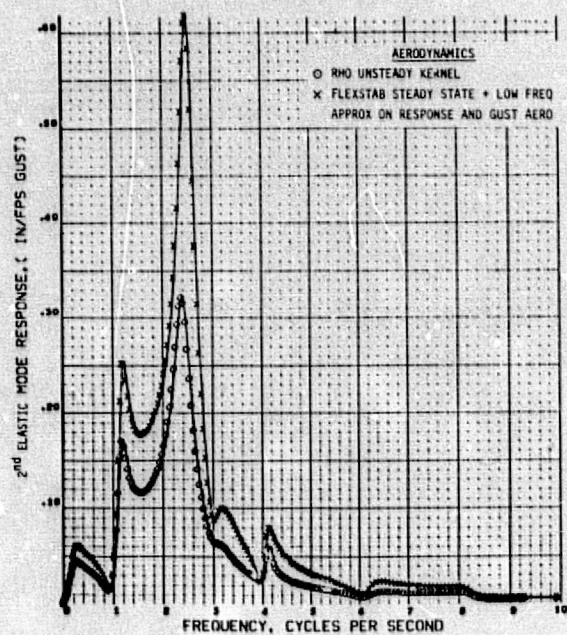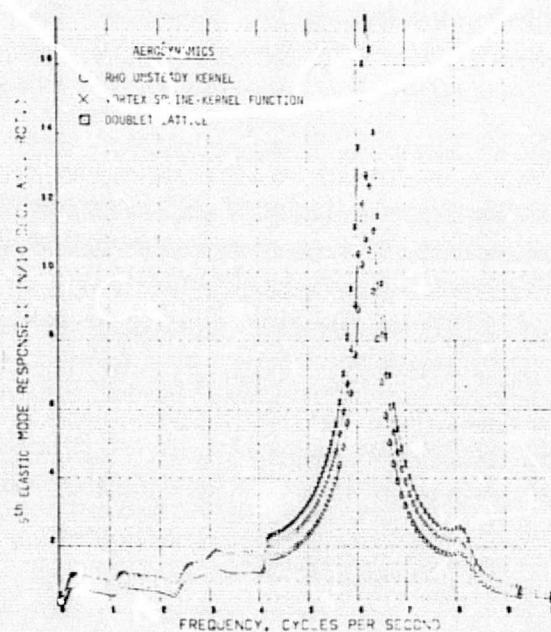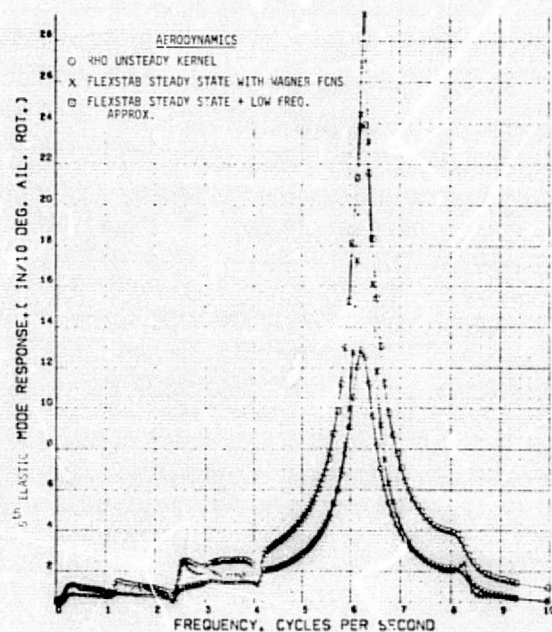
(a) Magnitudes
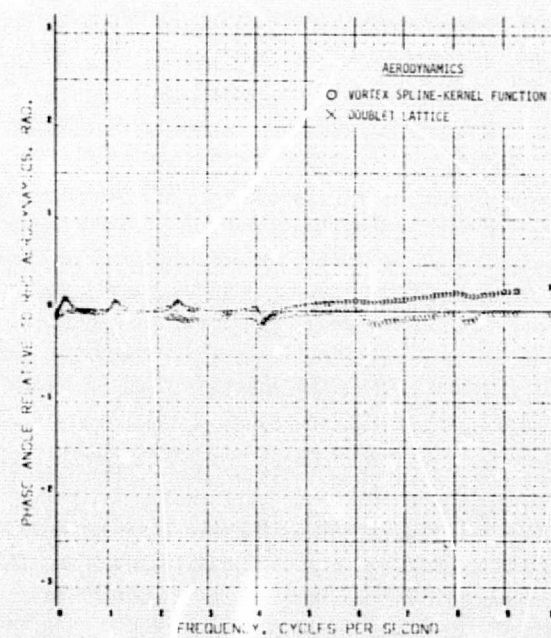
Figure C-4.—Comparison of Generalized Coordinate Frequency Response Function
Due to Gust Excitation

73
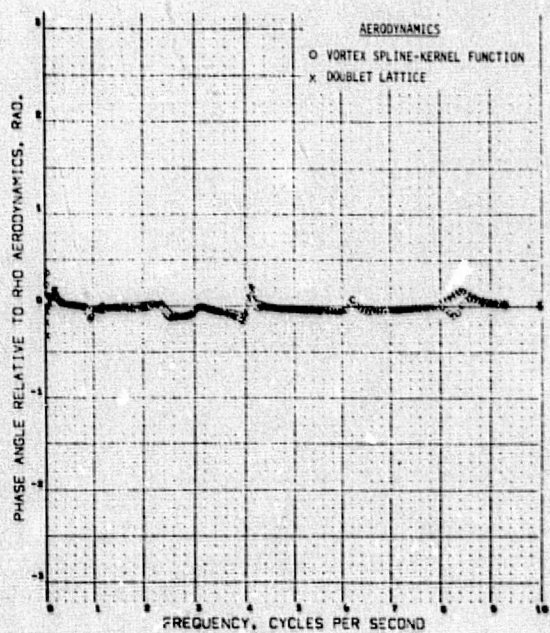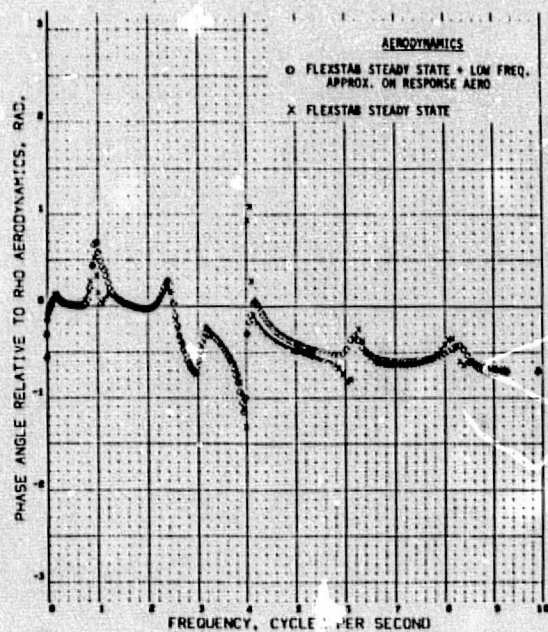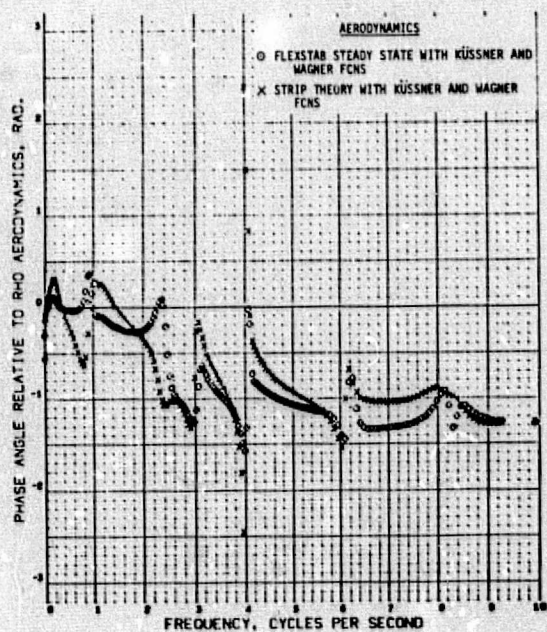
(b) Phase Angles

Figure C-4.—(Concluded)
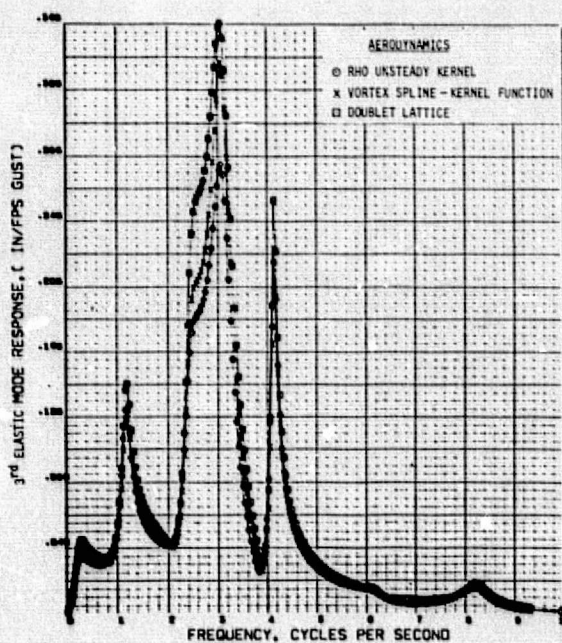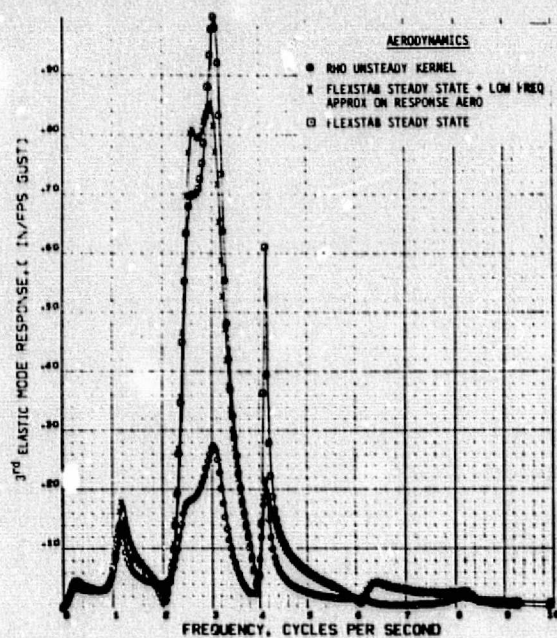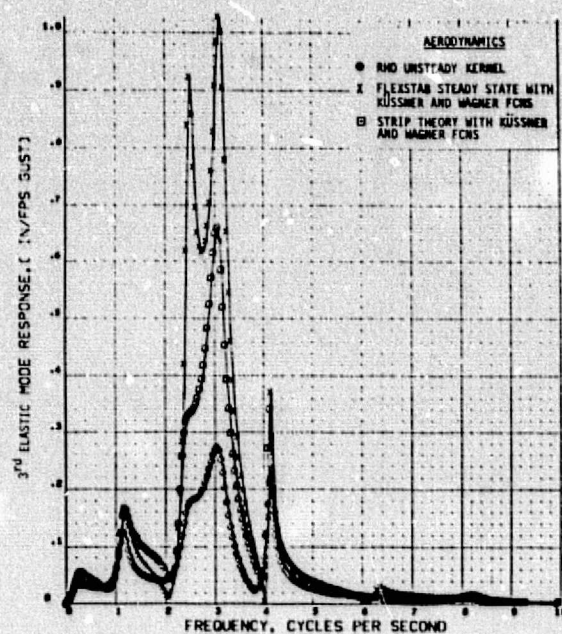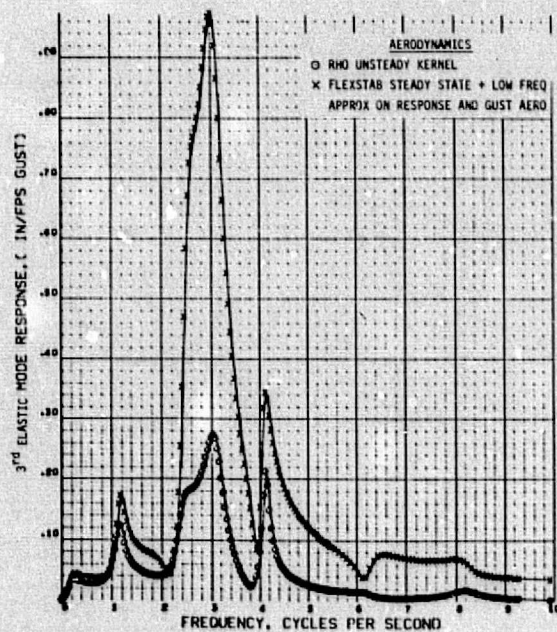
(a) Magnitudes

Figure C-5.—Comparison of Generalized Coordinate Frequency Response Function
Due to Gust Excitation

75
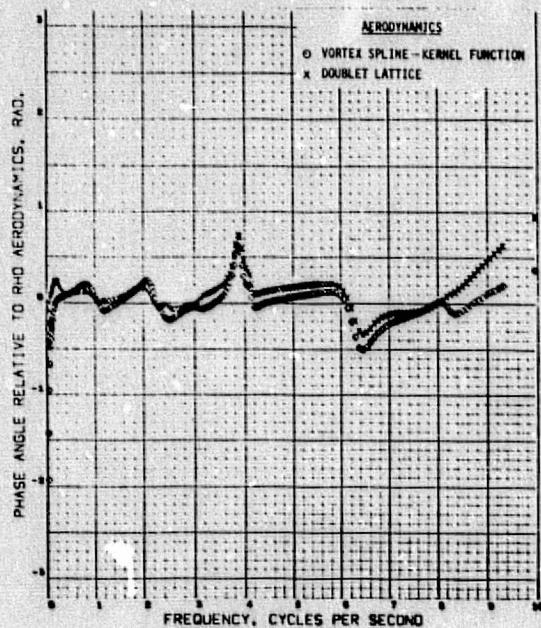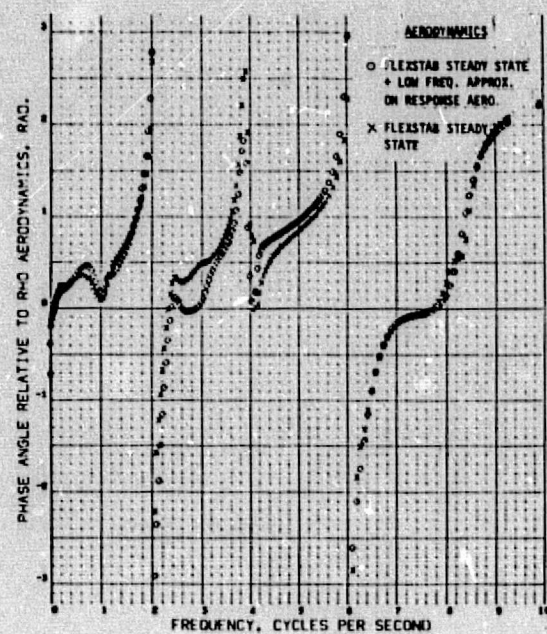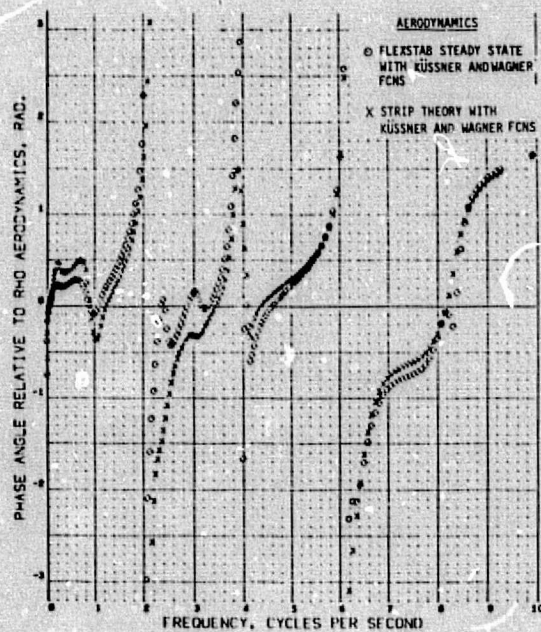
(b) Phase Angles

Figure C-5.—(Concluded)
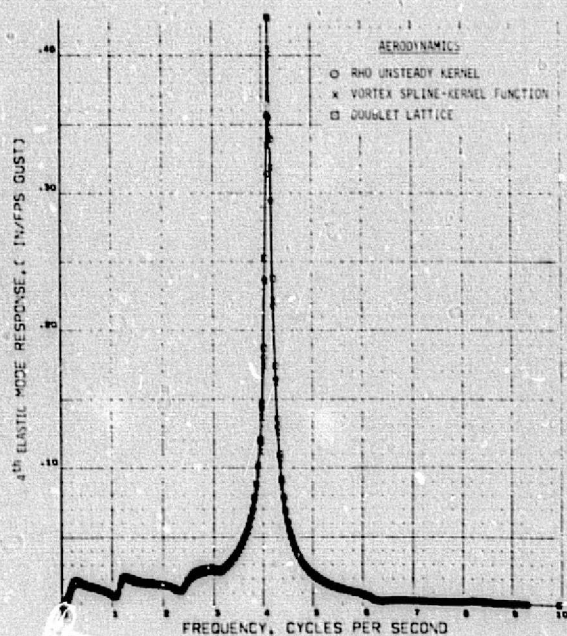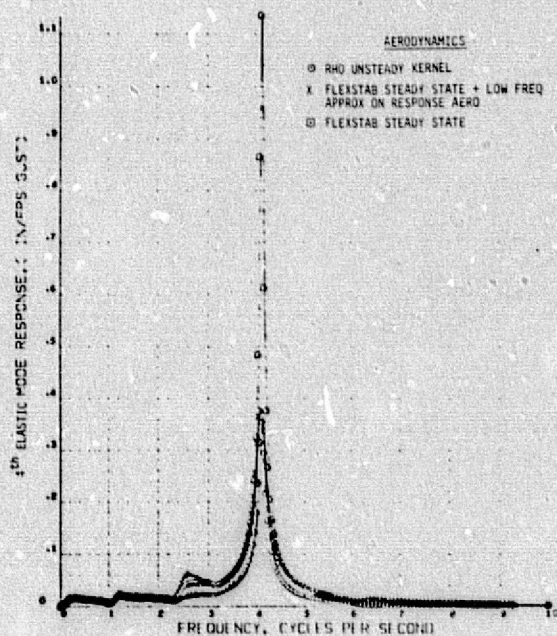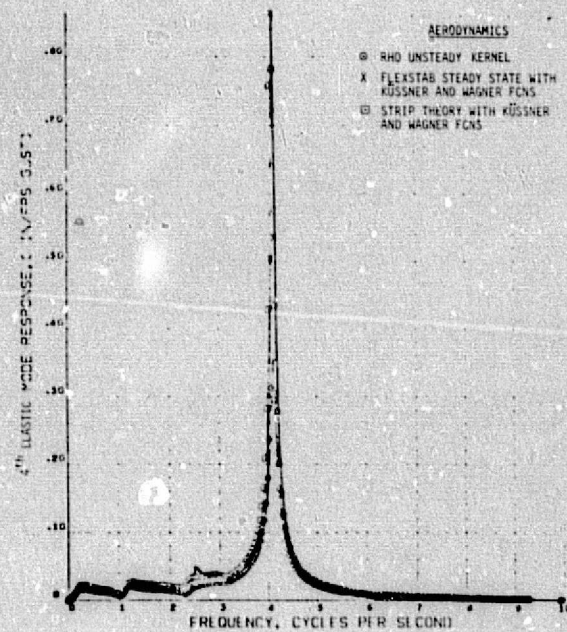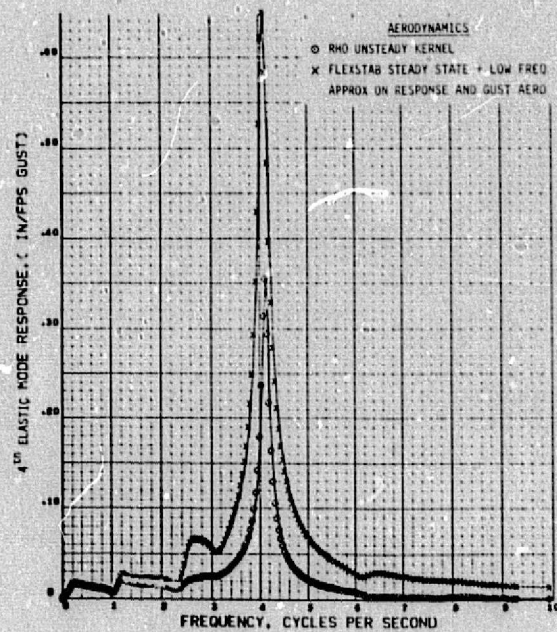
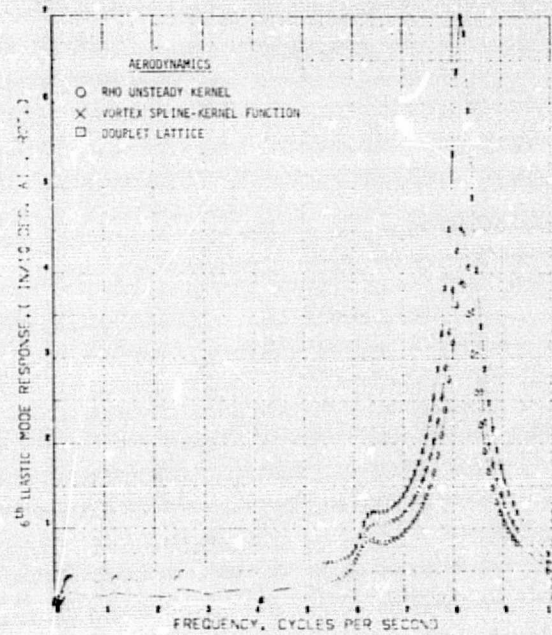(a) Magnitudes

Figure C-6.—Comparison of Generalized Coordinate Frequency Response Function
Due to Gust Excitation
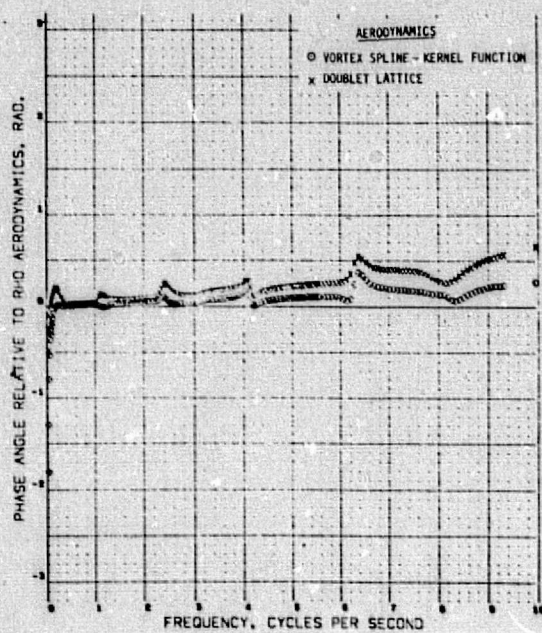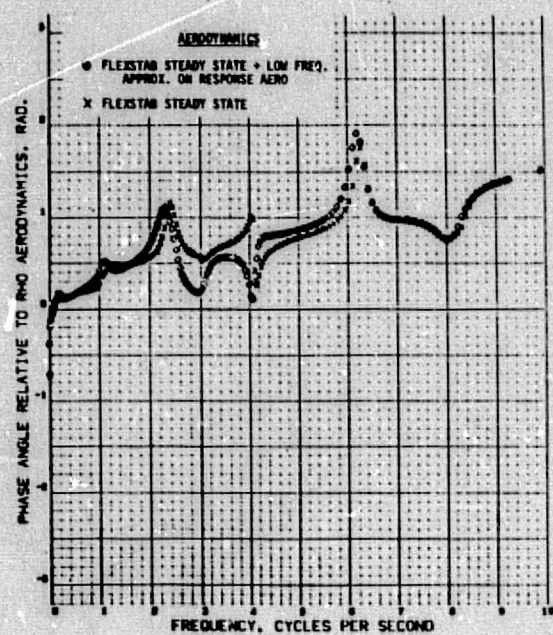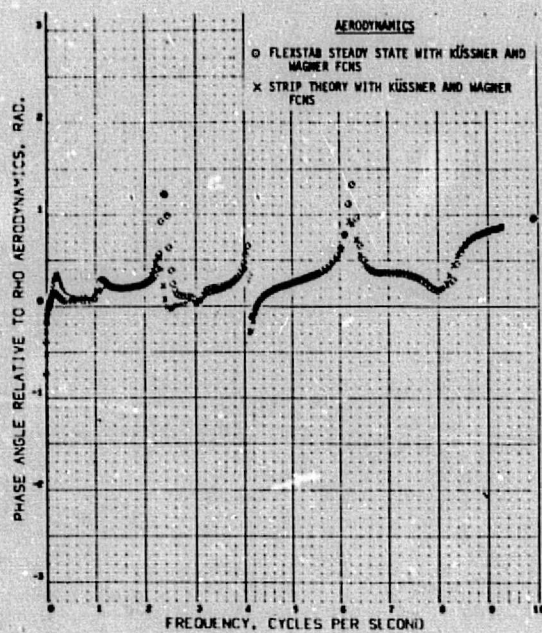
(b) Phase Angles

Figure C-6.—(Concluded)
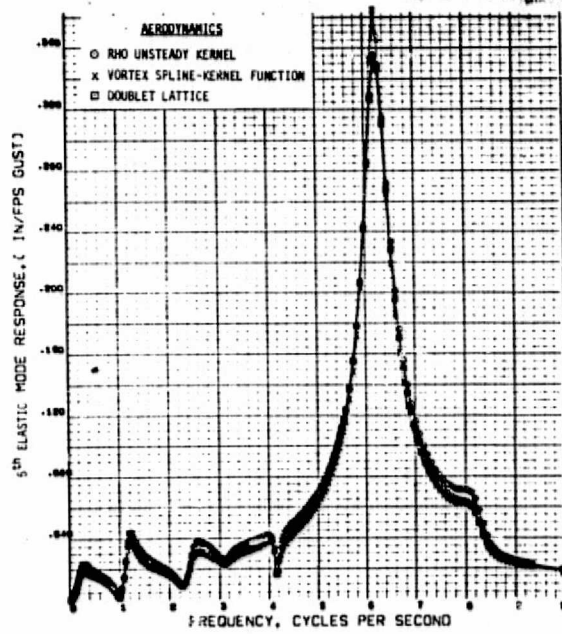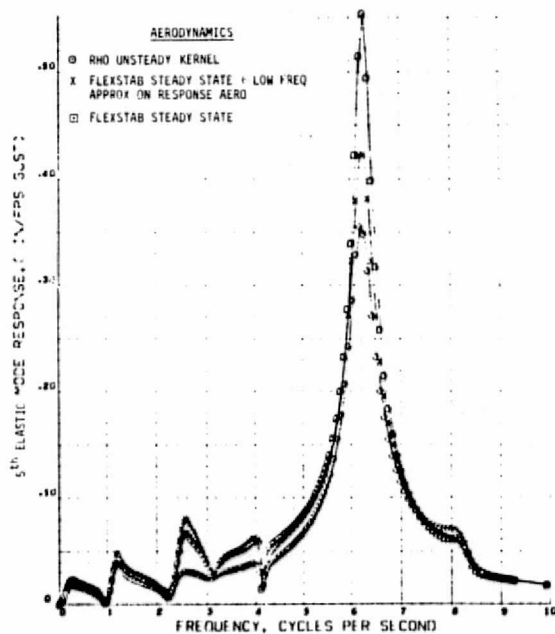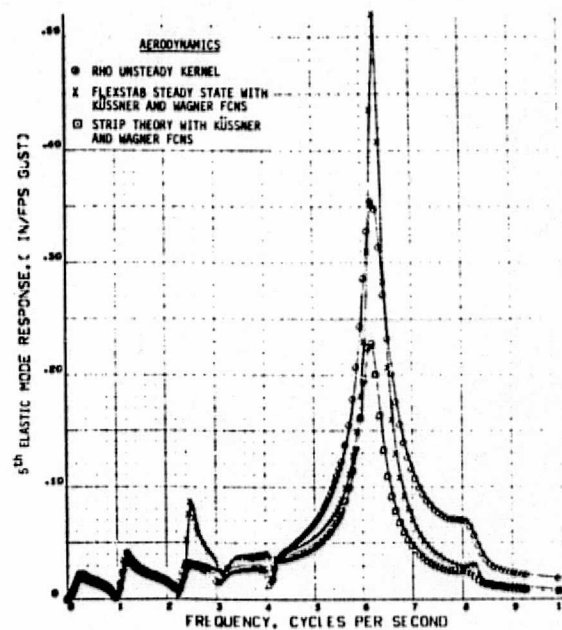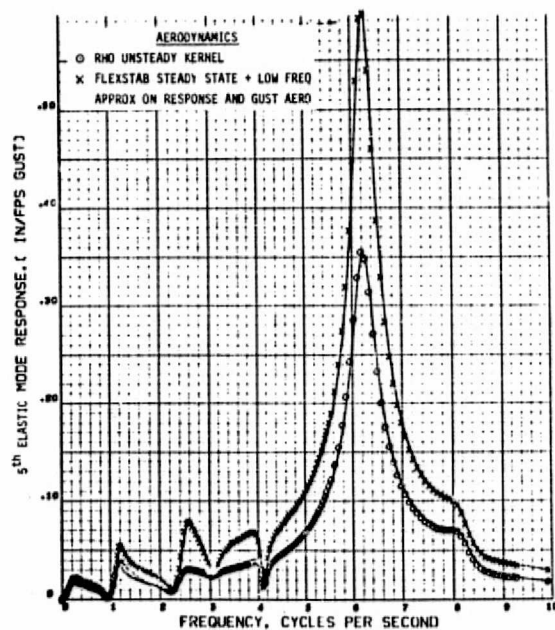
(a) Magnitudes

Figure C-7.—Comparison of Generalized Coordinate Frequency Response Function
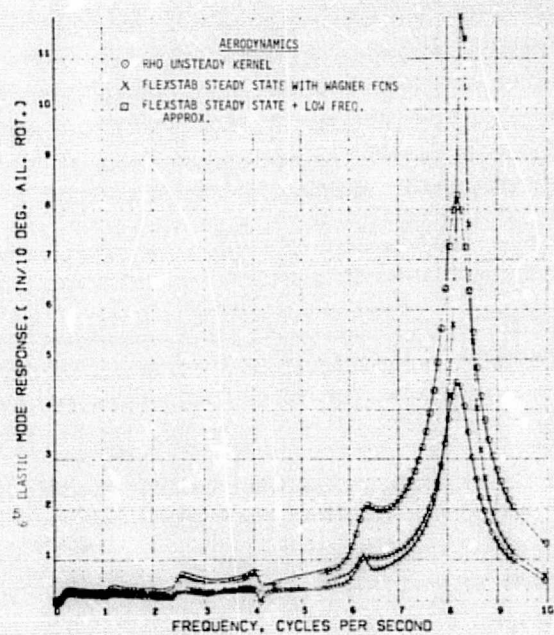Due to Gust Excitation

79
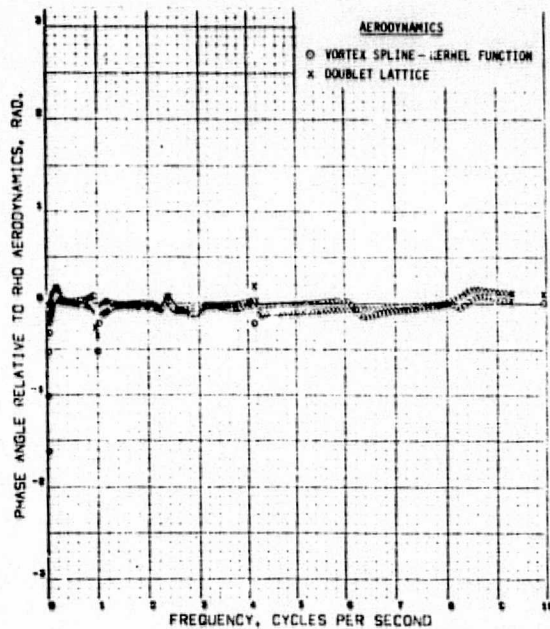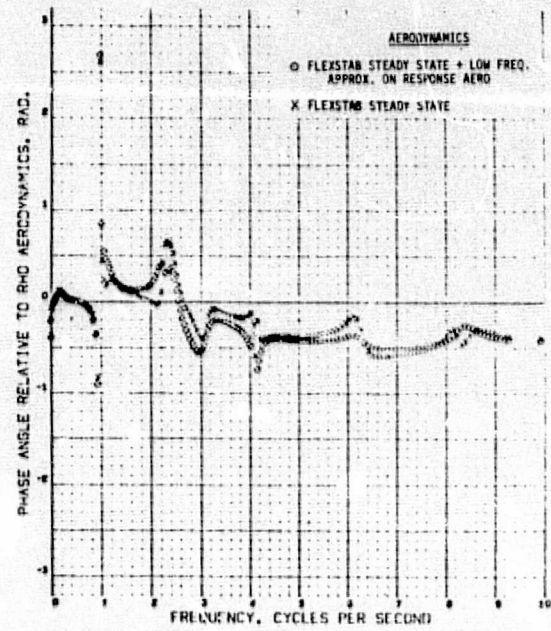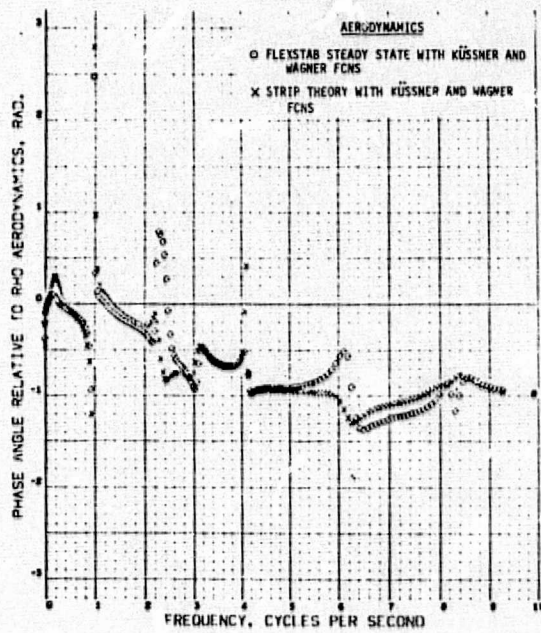
(b) Phase Angles

Figure C-7.—(Concluded)
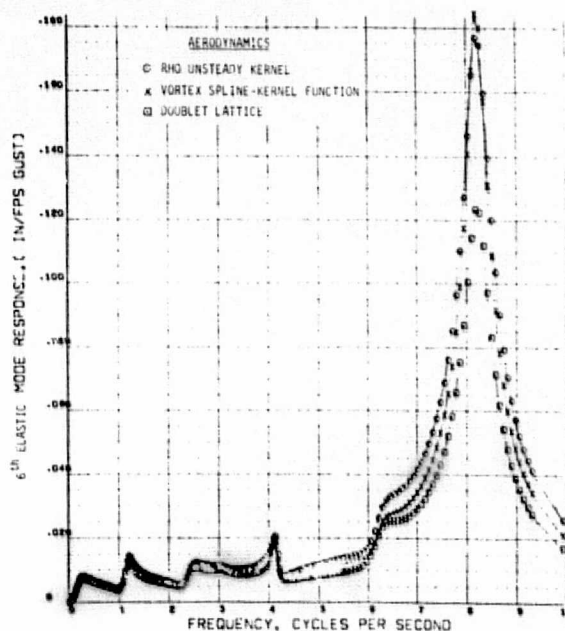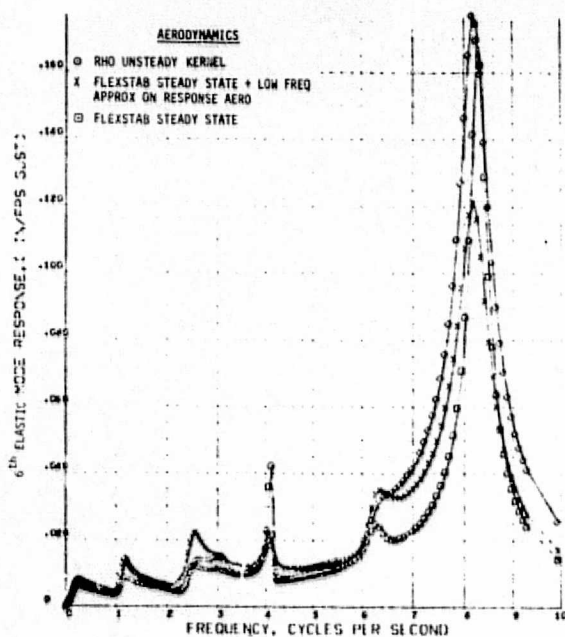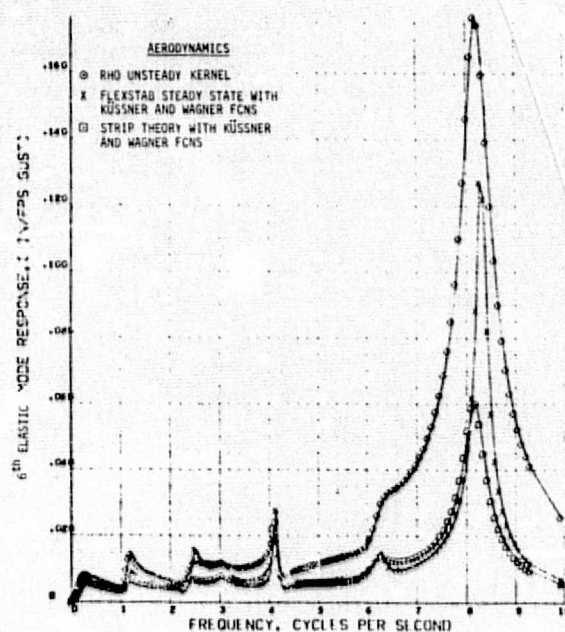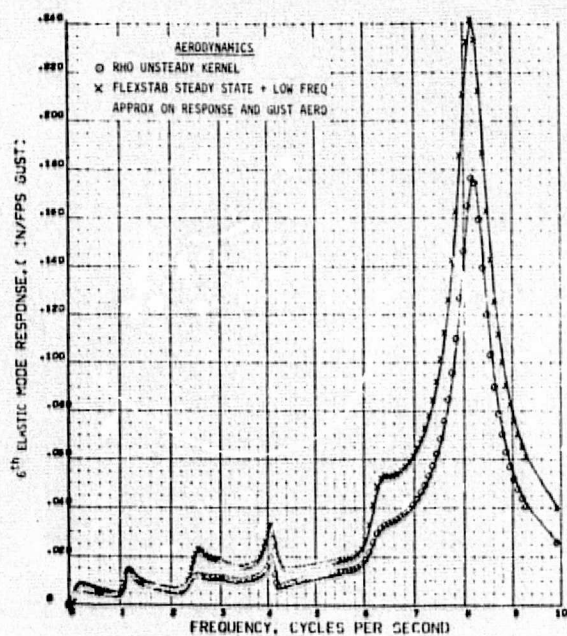
(a) Magnitudes

Figure C-8.—Comparison of Generalized Coordinate Frequency Response Function Due to Gust Excitation
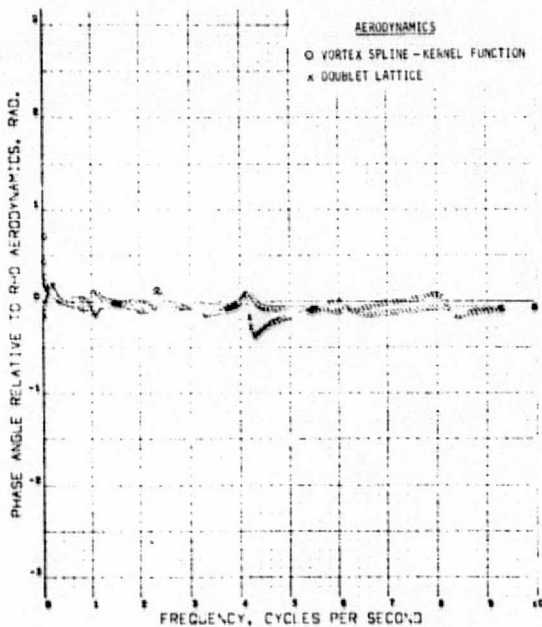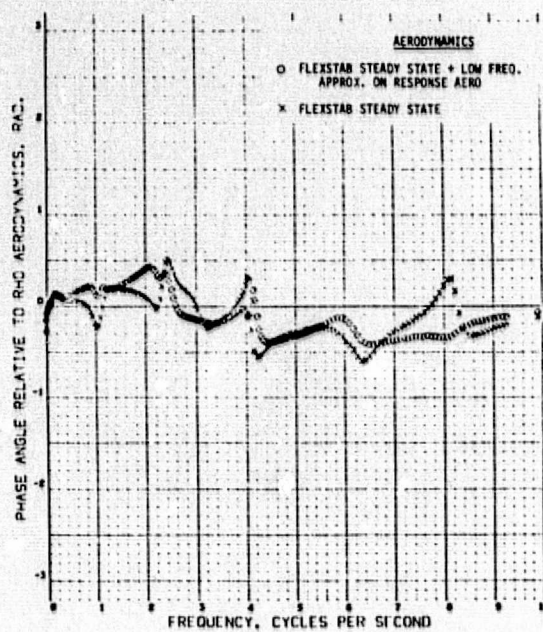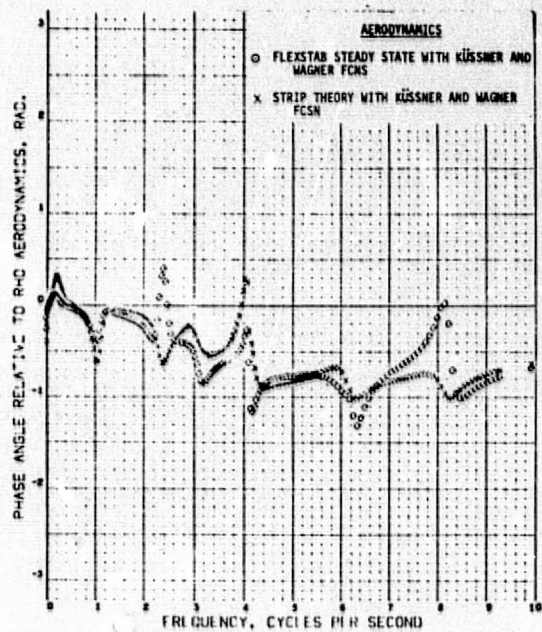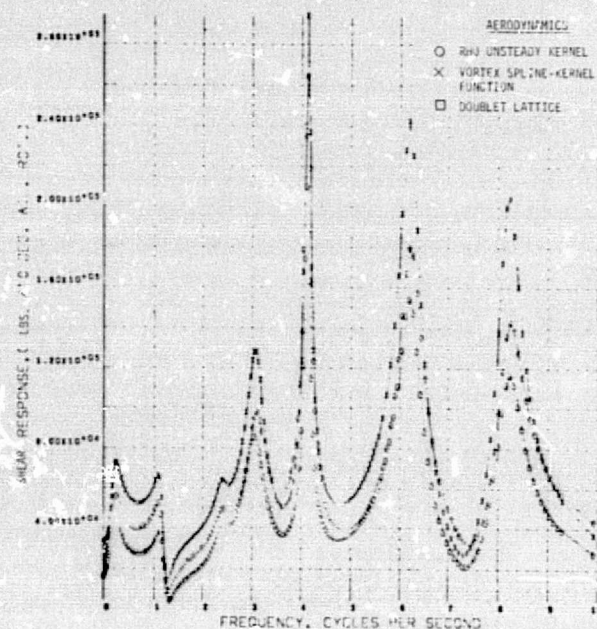
(b) Phase Angles

Figure C-8.—(Concluded)

82
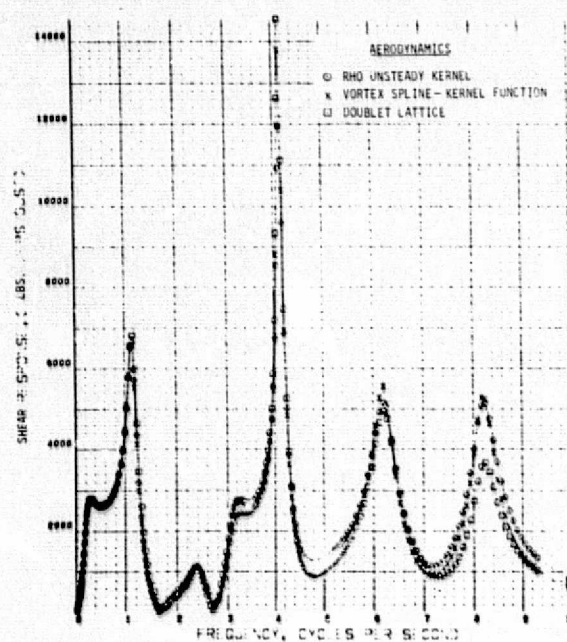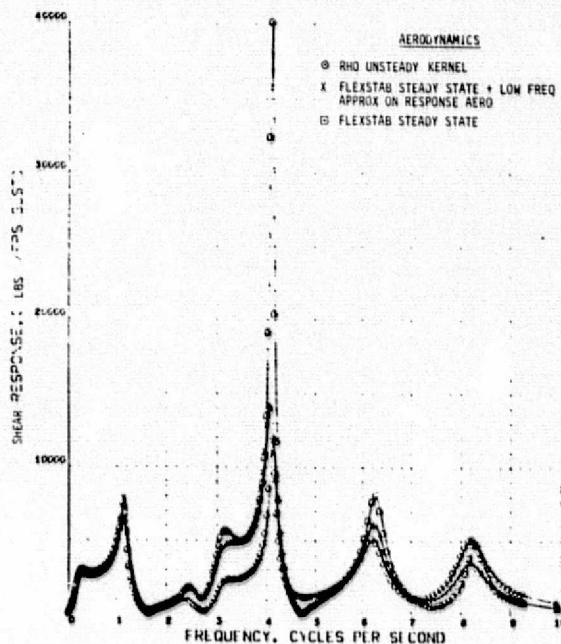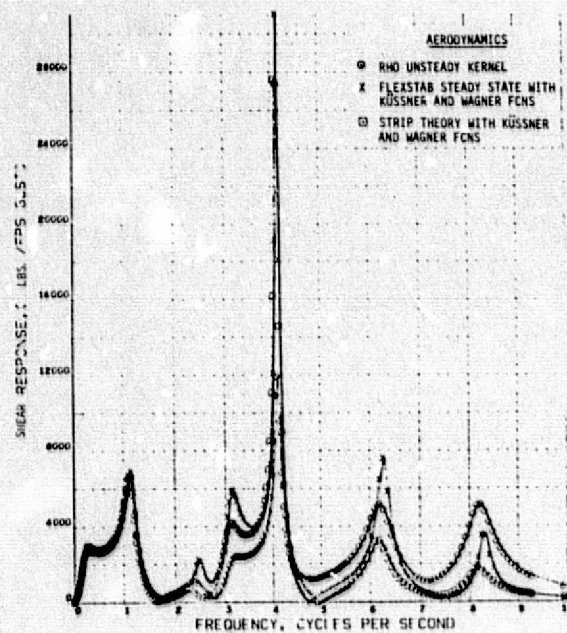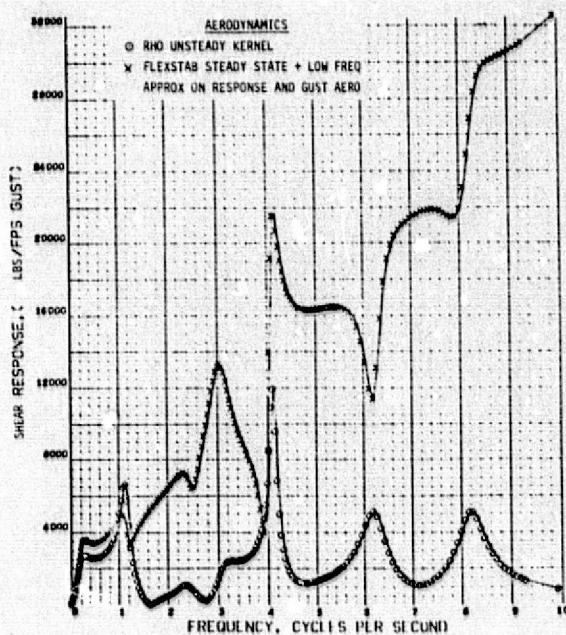
(a) Magnitudes

Figure C-9.—Comparison of Wing Shear Frequency Response Function at Wing
Root Due to Gust Excitation

83
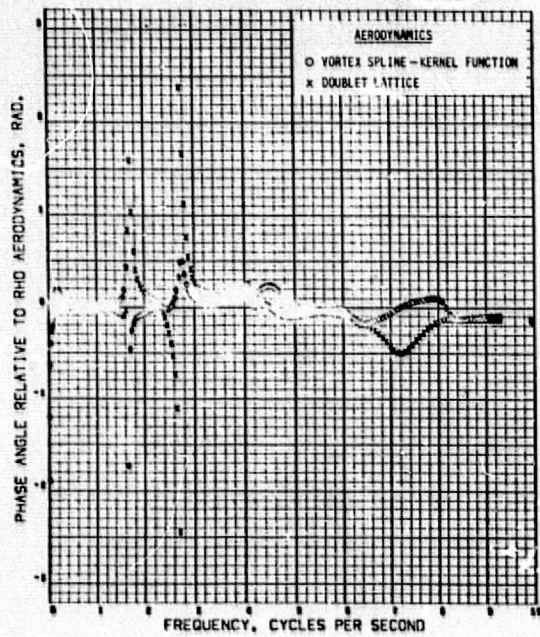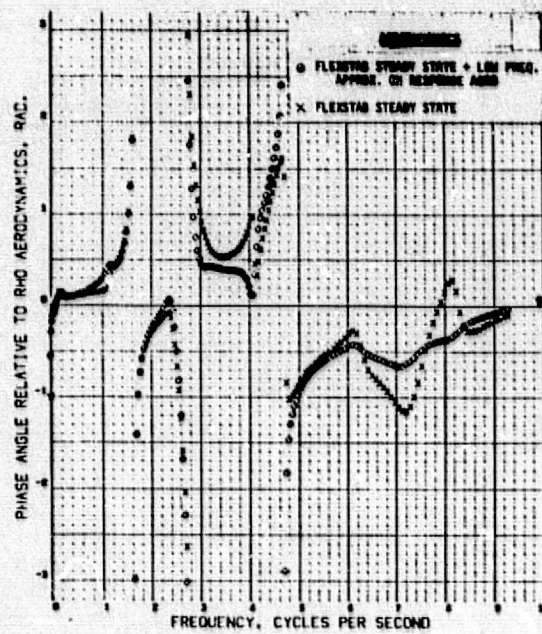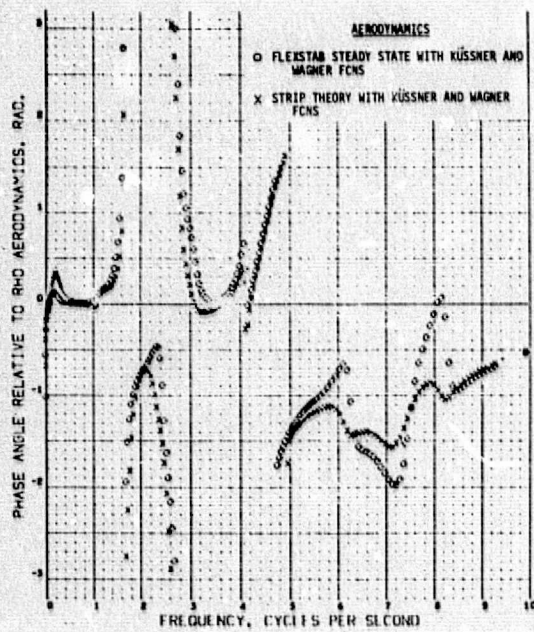
(b) Phase Angles

Figure C-9.—(Concluded)

84
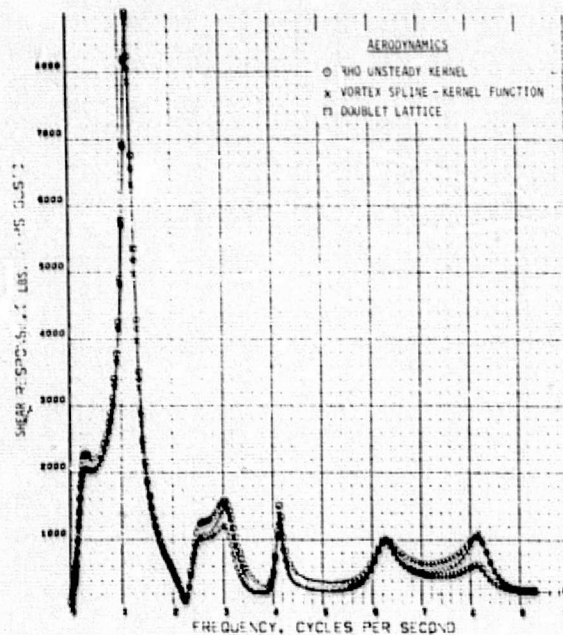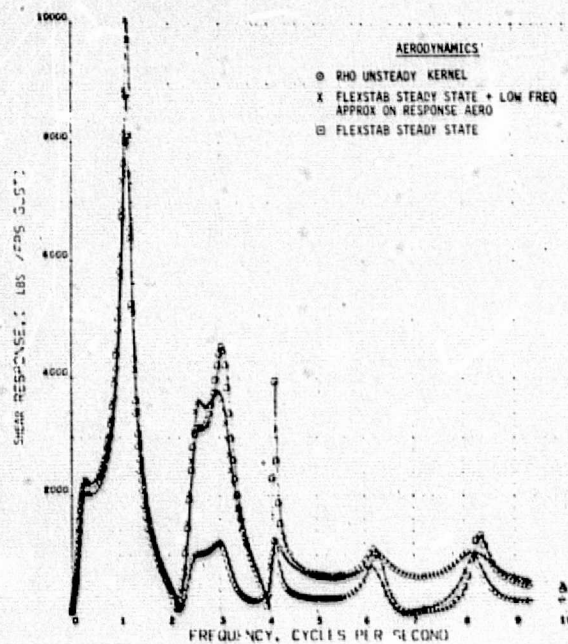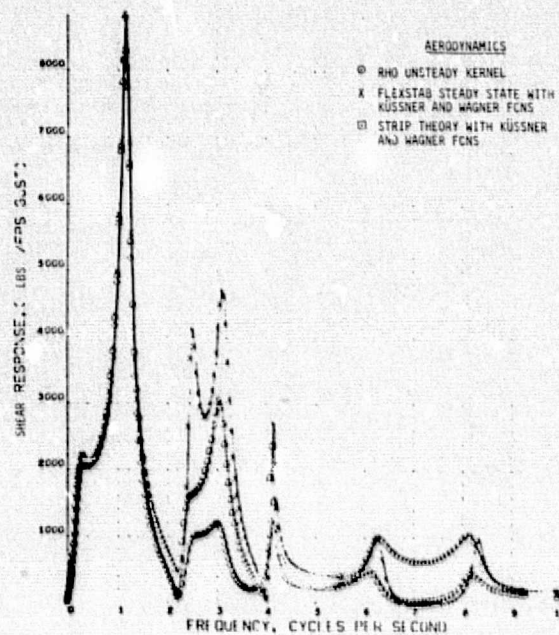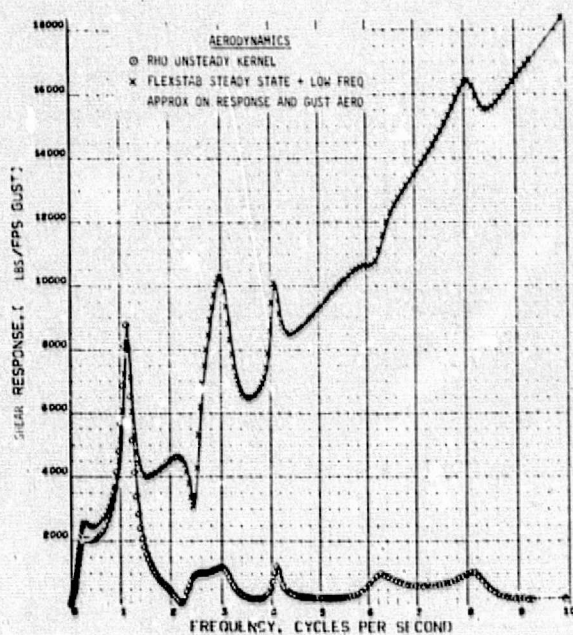
(a) Magnitudes

Figure C-10.—Comparison of Wing Shear Frequency Response Function at
Inboard Nacelle Due to Gust Excitation

85
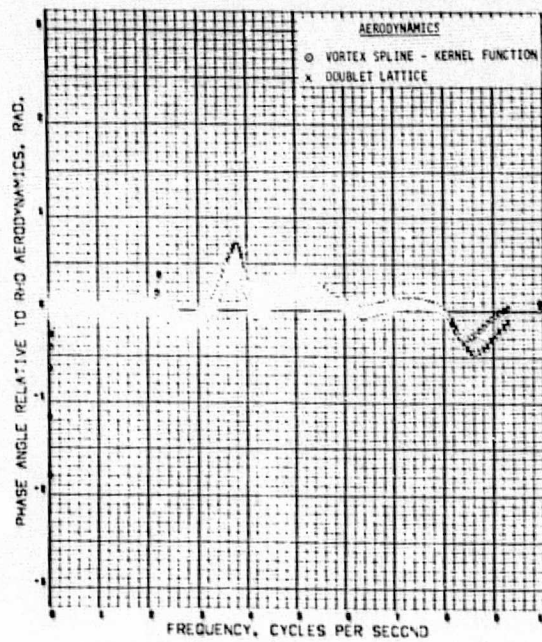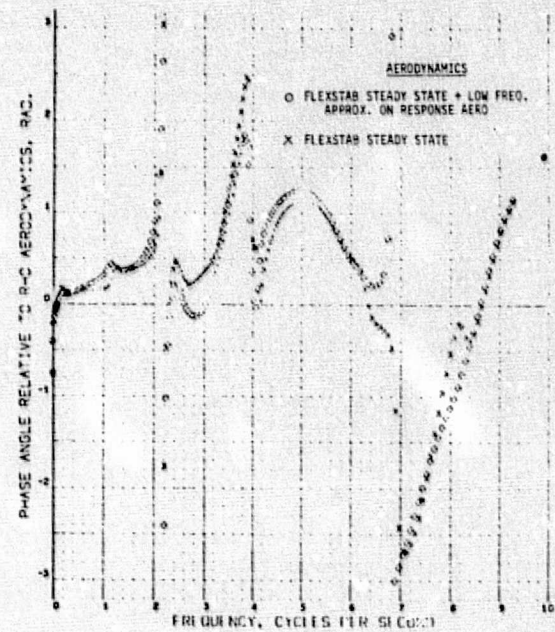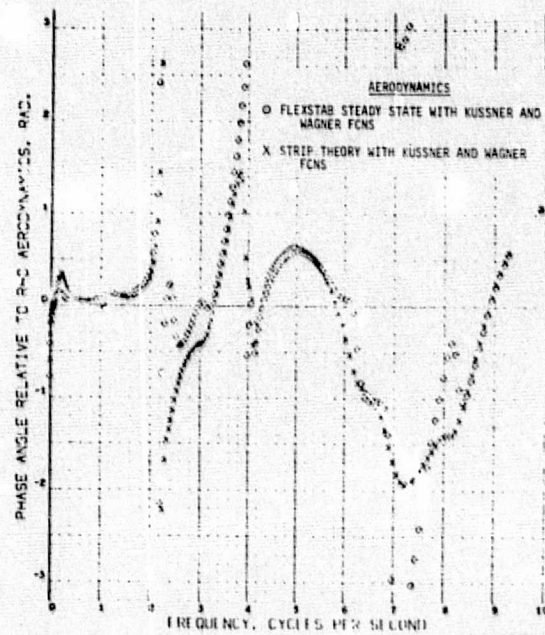
(b) Phase Angles

Figure C-10.—(Concluded)

86
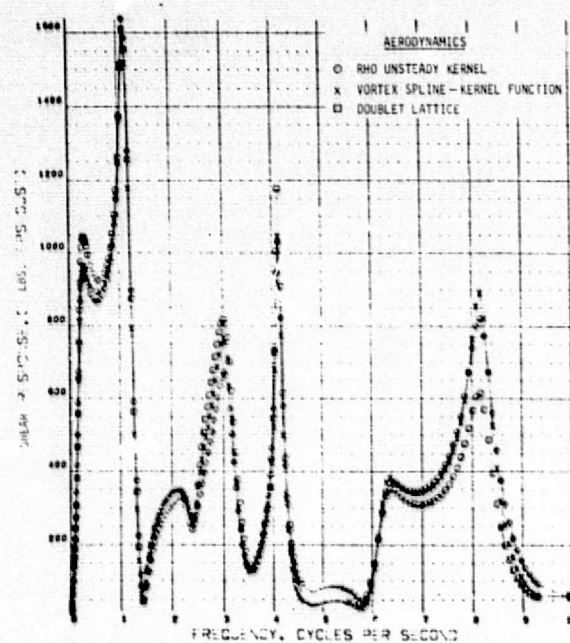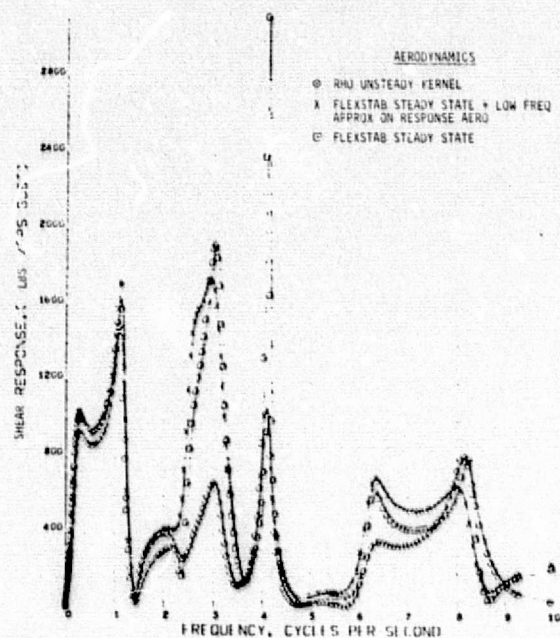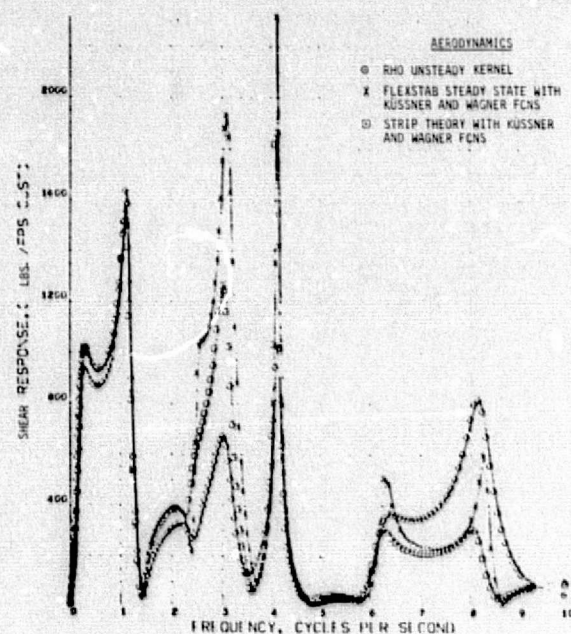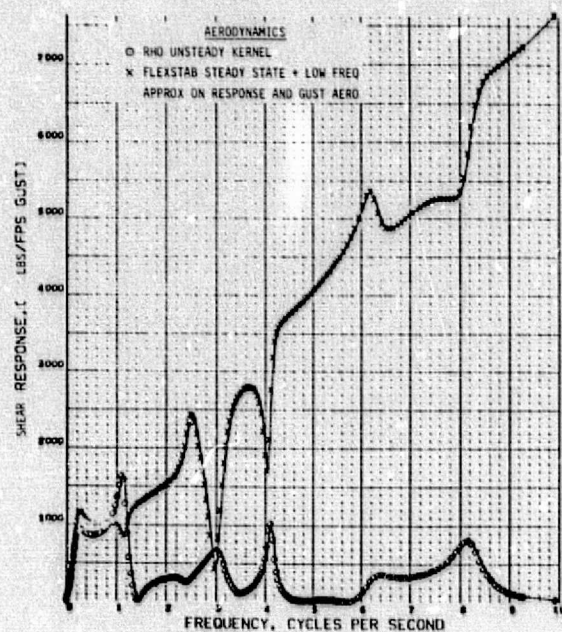
(a) Magnitudes

Figure C-11.—Comparison of Wing Shear Frequency Response Function at
Outboard Nacelle Due to Gust Excitation

87
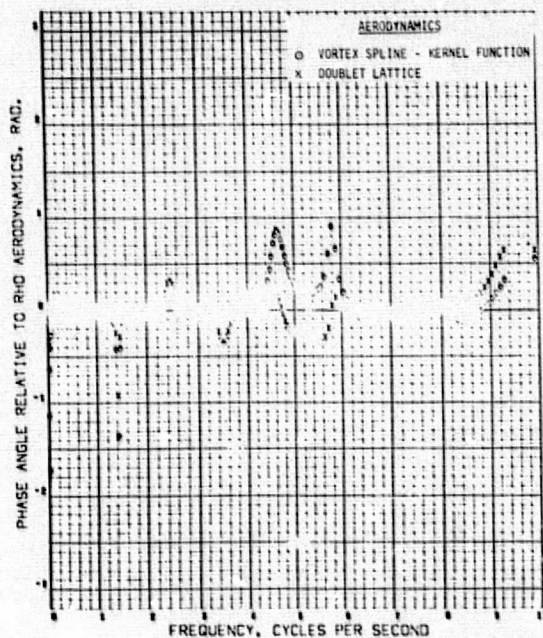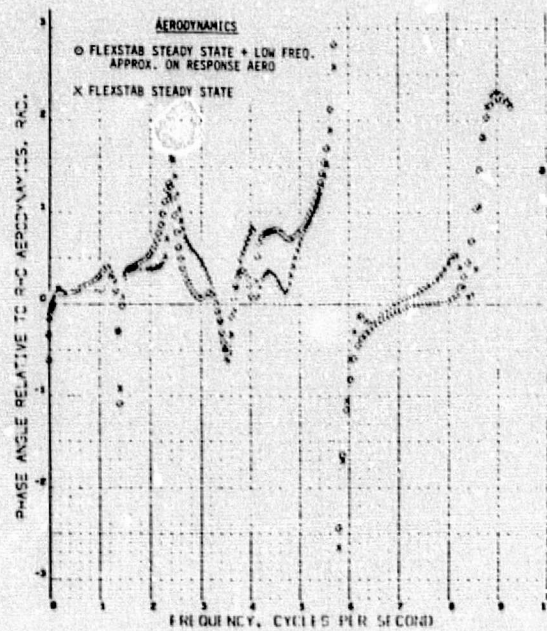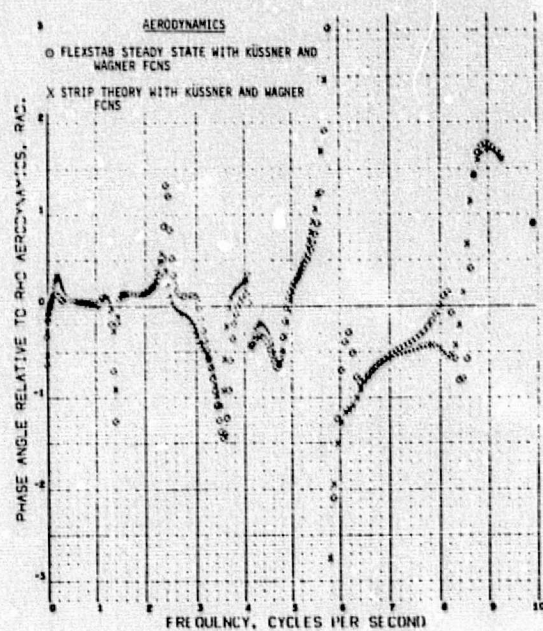
(b) Phase Angles

Figure C-11.—(Concluded)
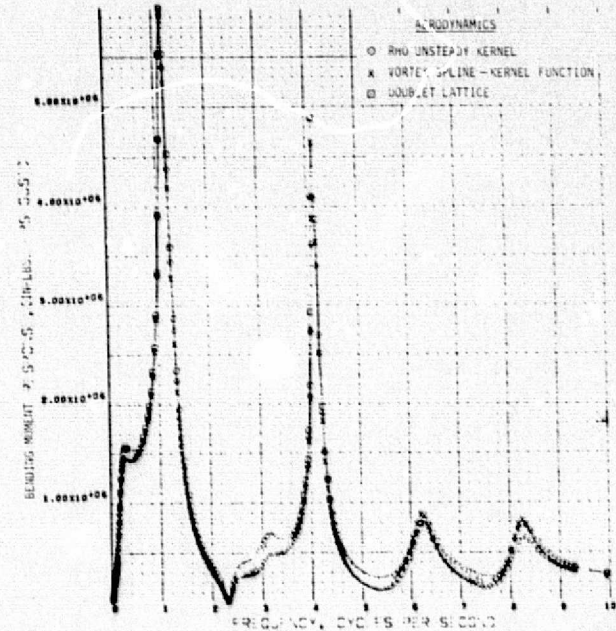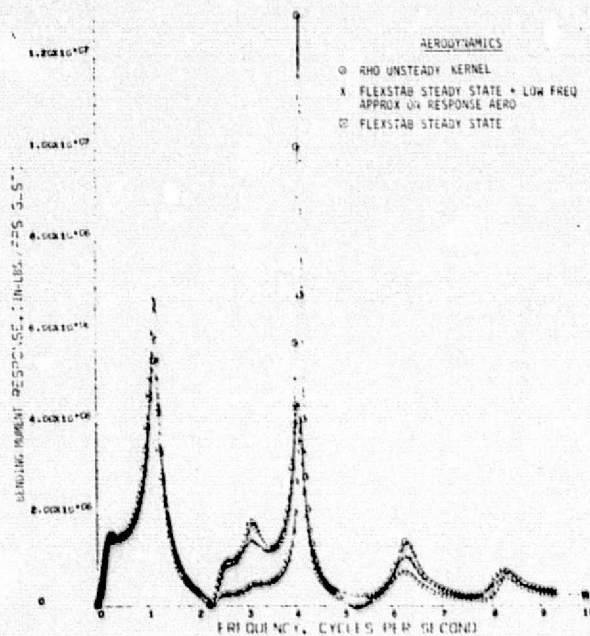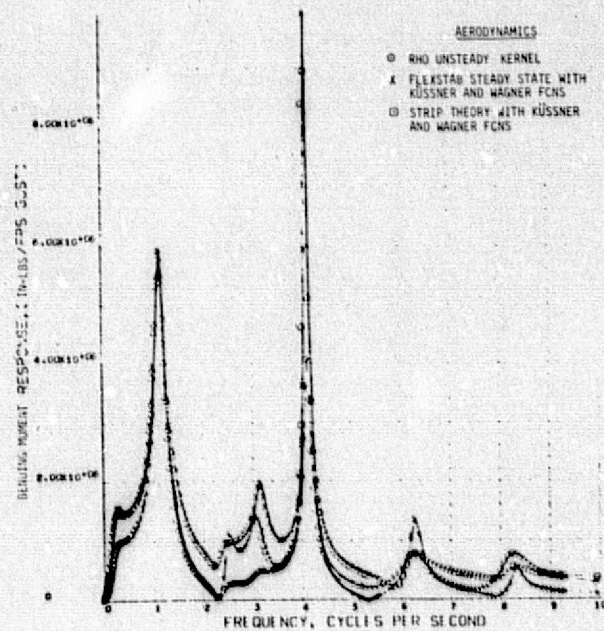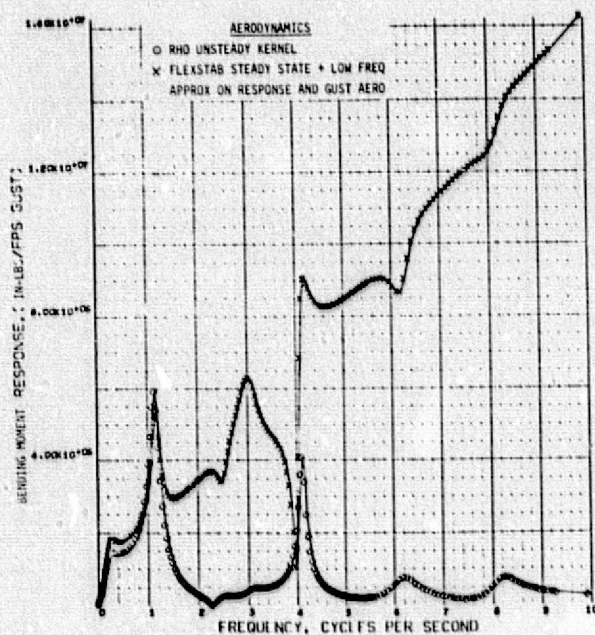
(a) Magnitudes
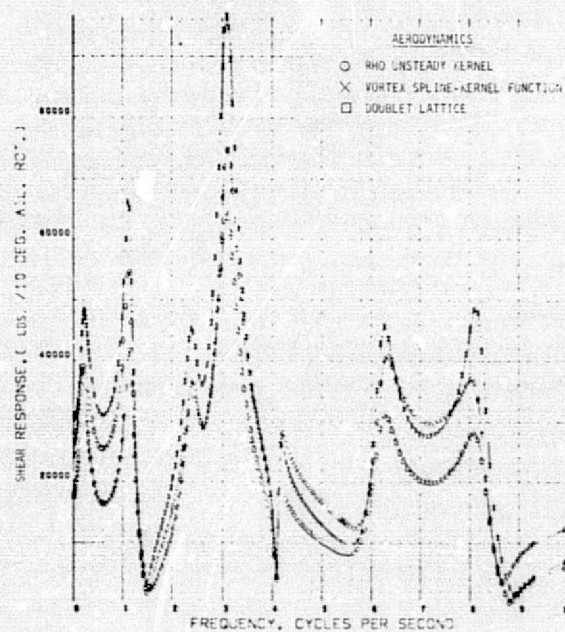
Figure C-12.—Comparison of Wing Bending Moment Frequency Response Function at Wing Root Due to Gust Excitation

89
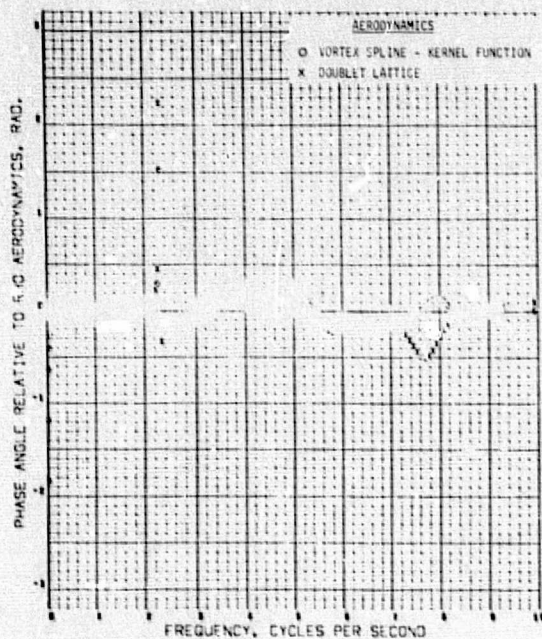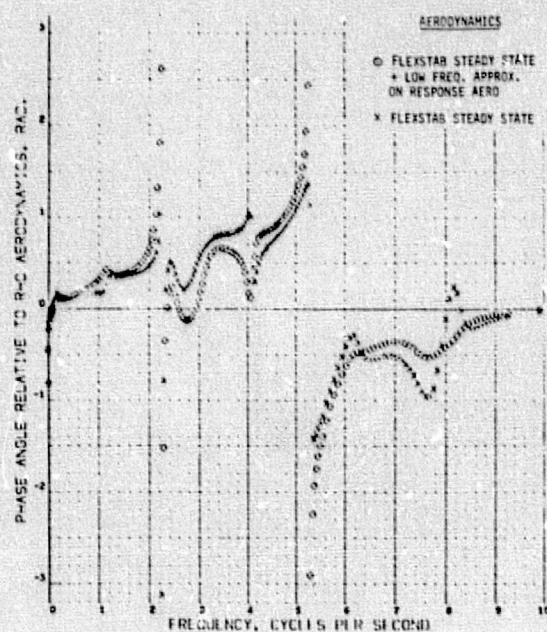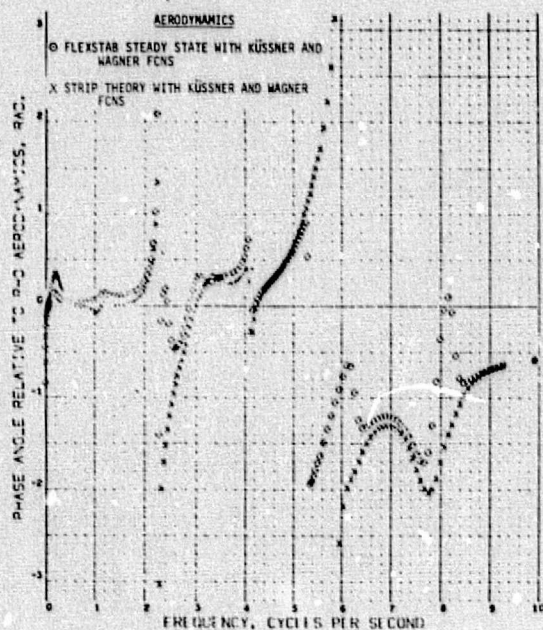
(b) Phase Angles

Figure C-12.—(Concluded)
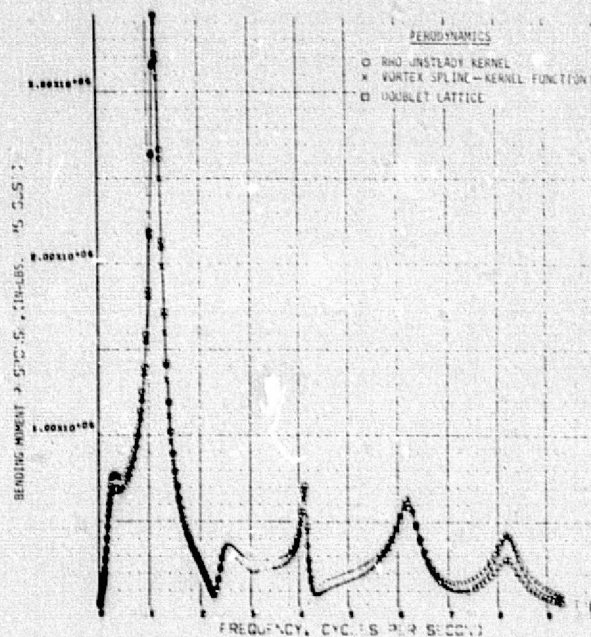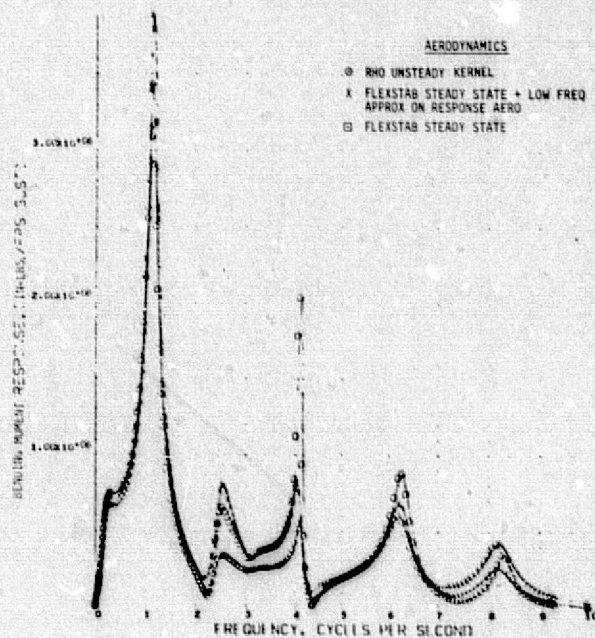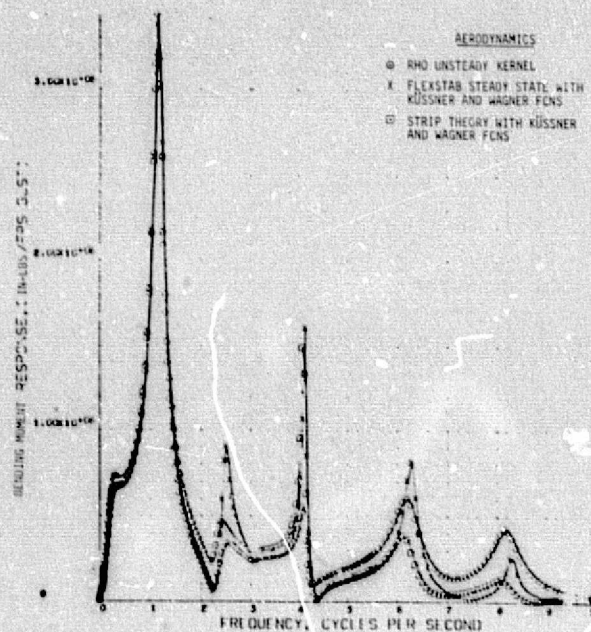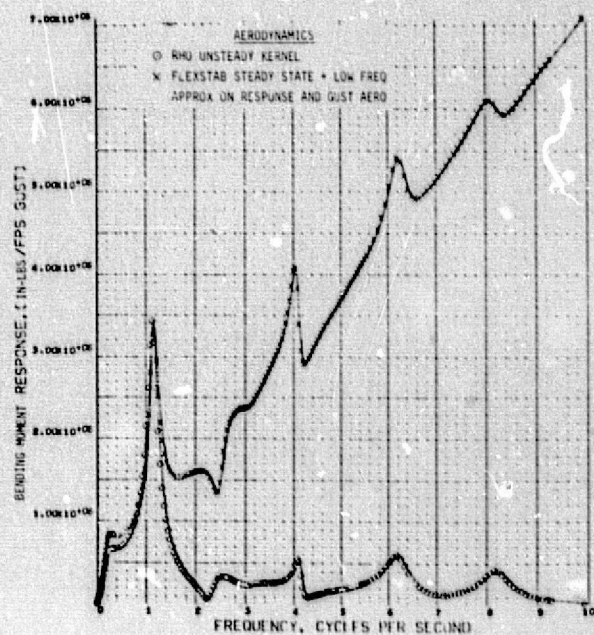
(a) Magnitudes

Figure C-13.—Comparison of Wing Bending Moment Frequency Response Function
at Inboard Nacelle Due to Gust Excitation
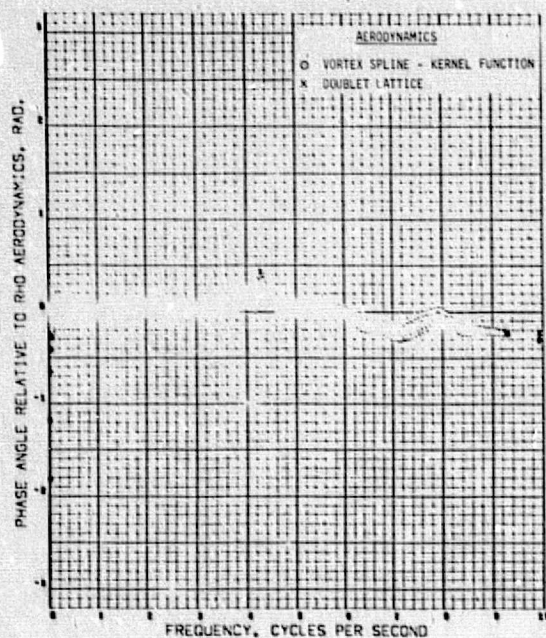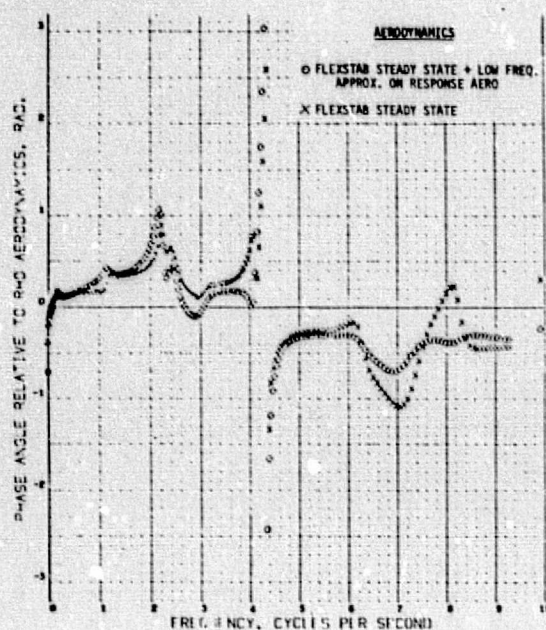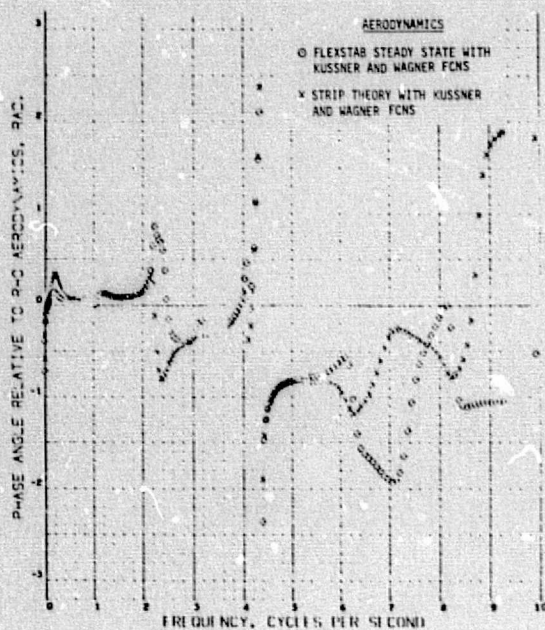
(b) Phase Angles

Figure C-13.—(Concluded)
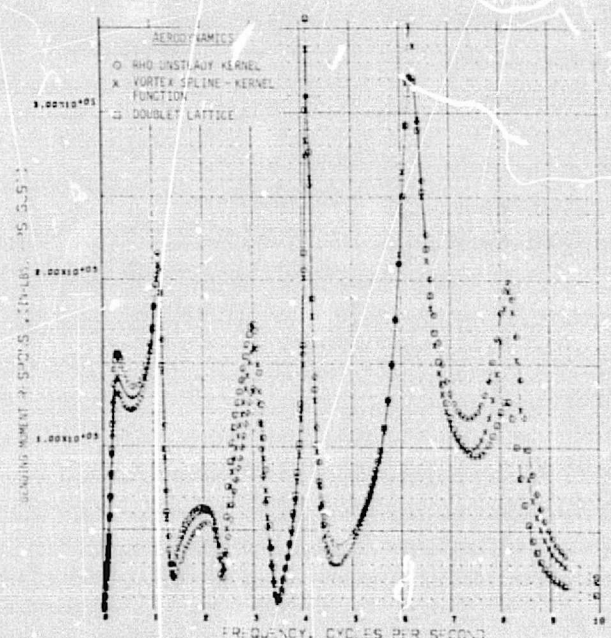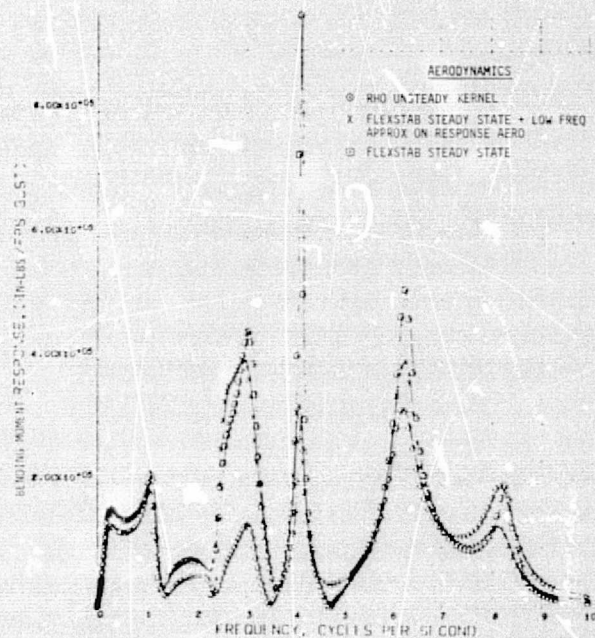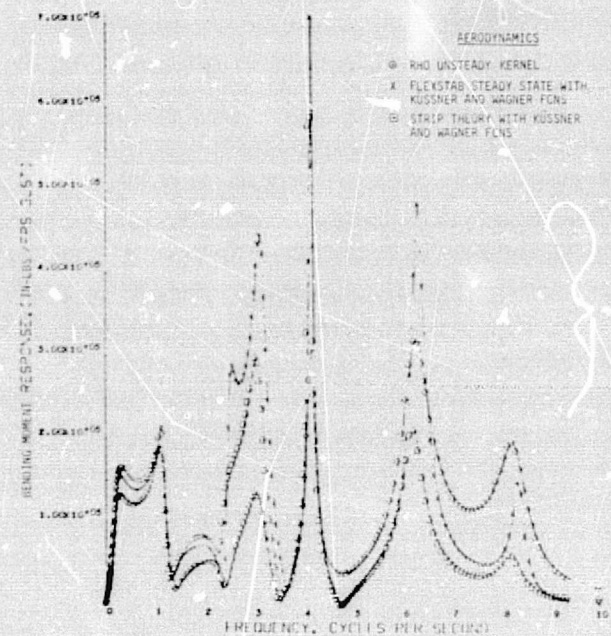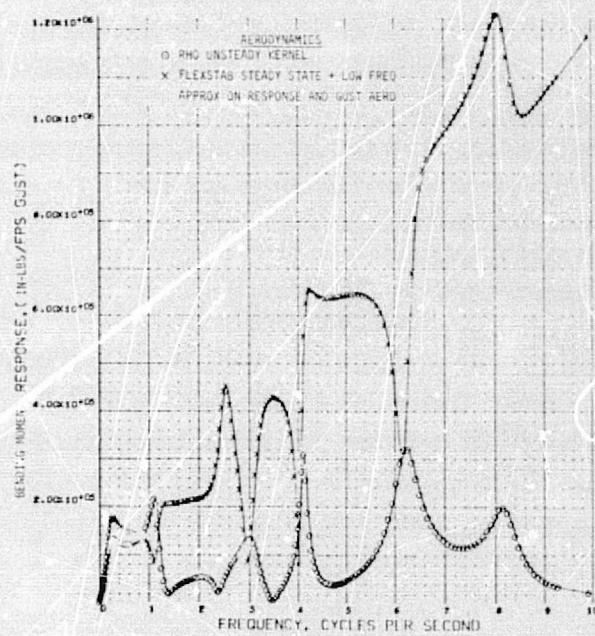
(a) Magnitude

Figure C-14.—Comparison of Wing Bending Moment Frequency Response Function
at Outboard Nacelle Due to Gust Excitation

C-2
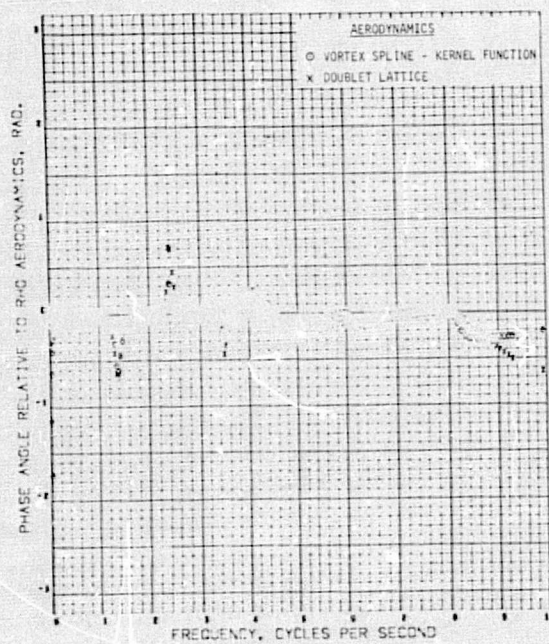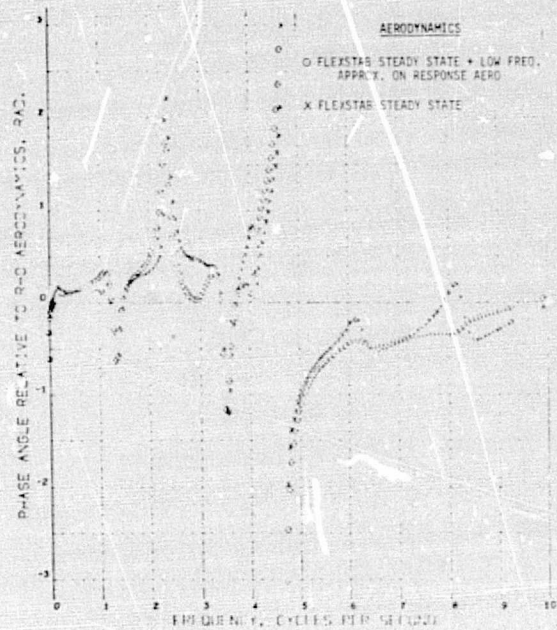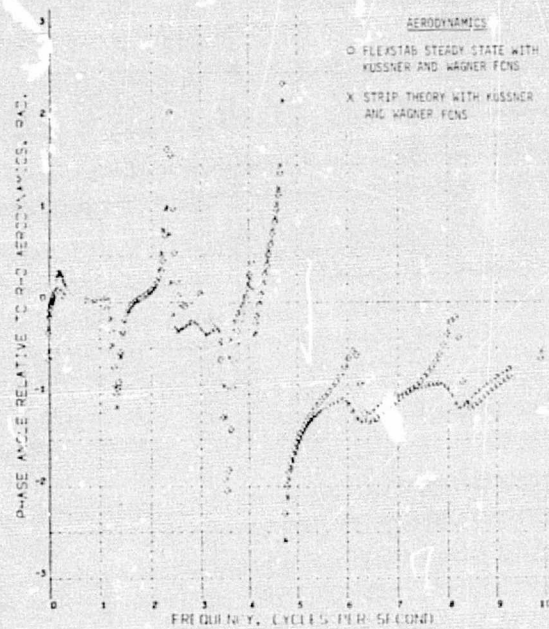
(b) Phase Angles

Figure C-14.—(Concluded)
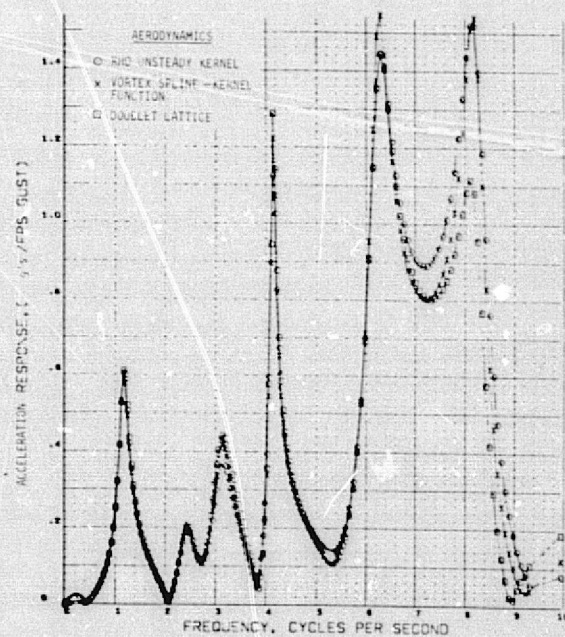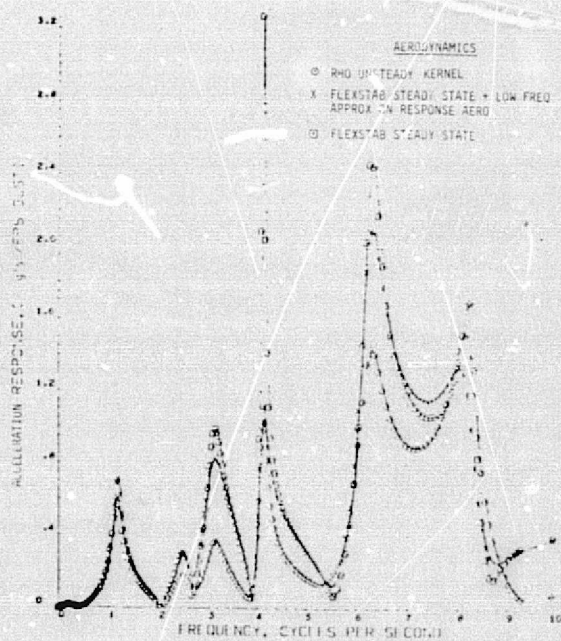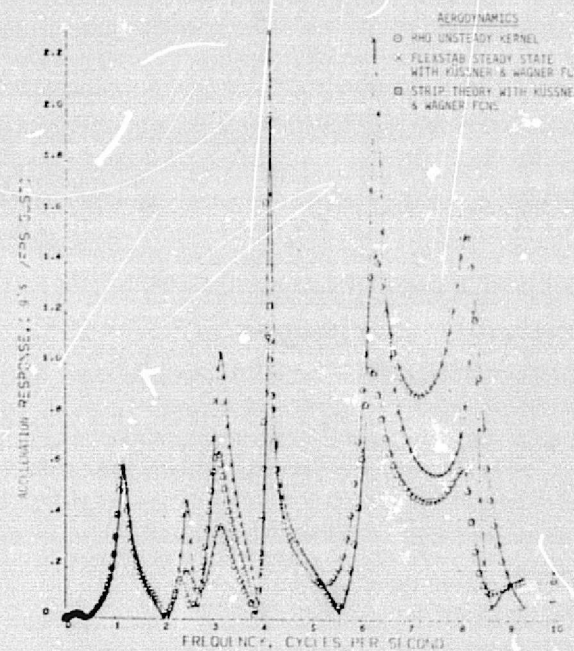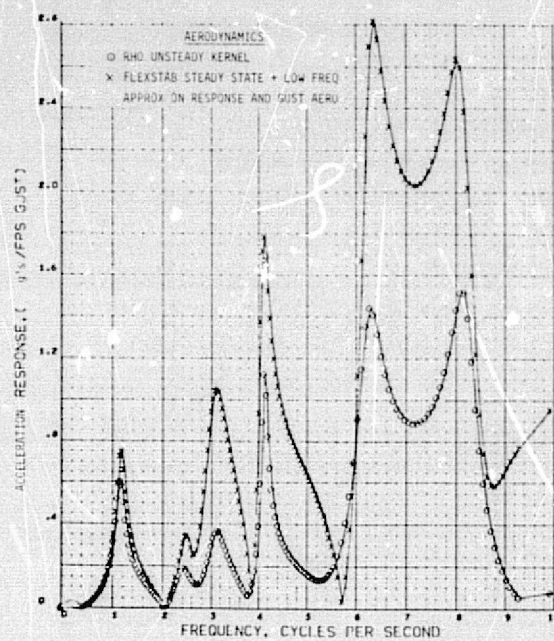
(a) Magnitudes

Figure C-15.—Comparison of Wing Acceleration Frequency Response Function at Wingtip Due to Gust Excitation
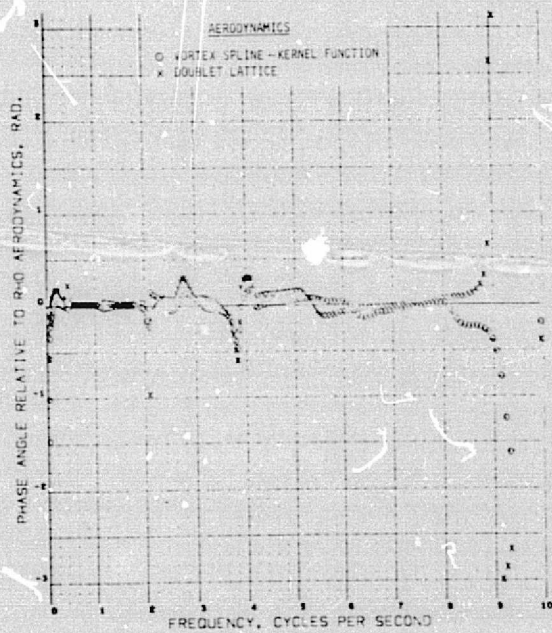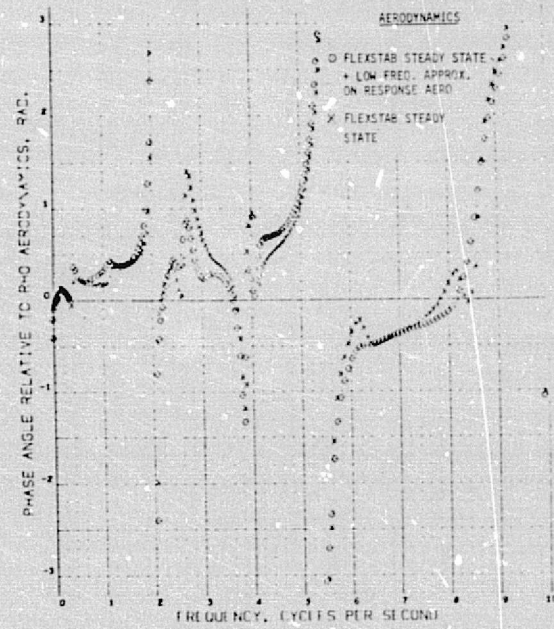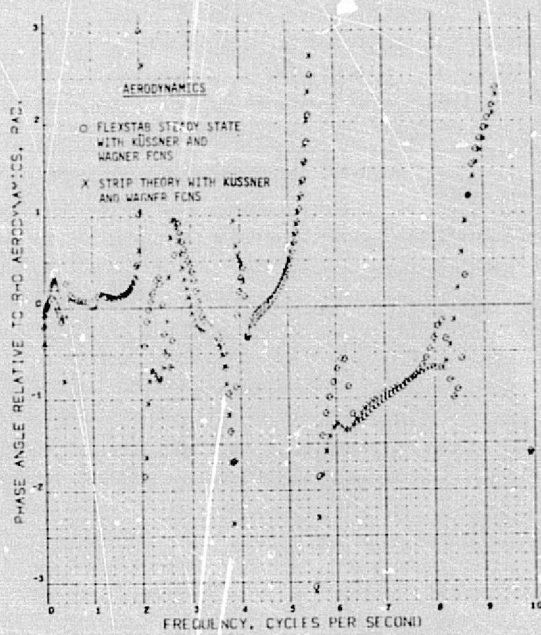
(b) Phase Angles

Figure C-15.—(Concluded)
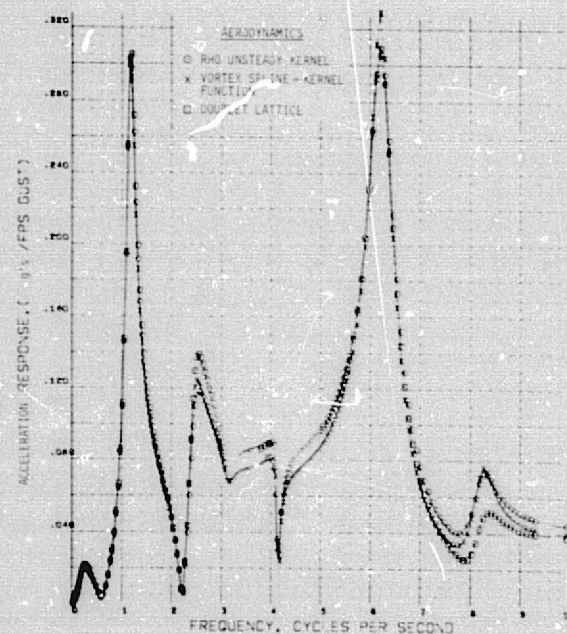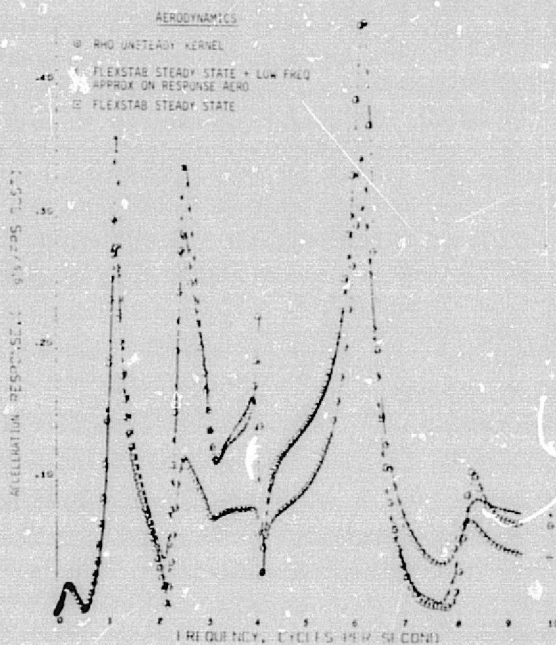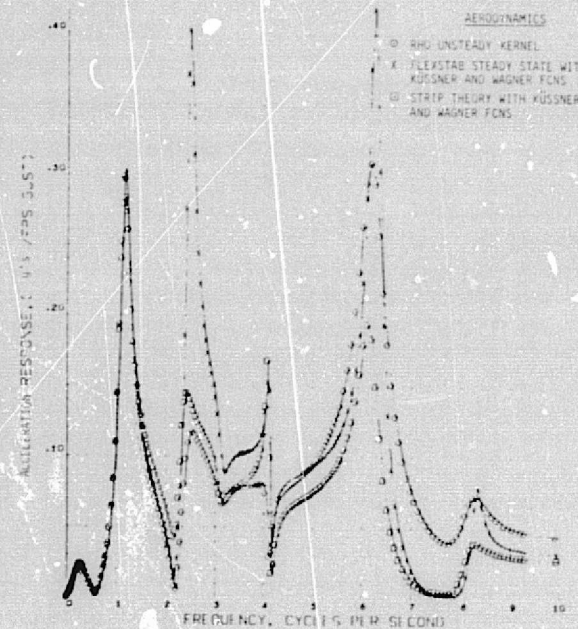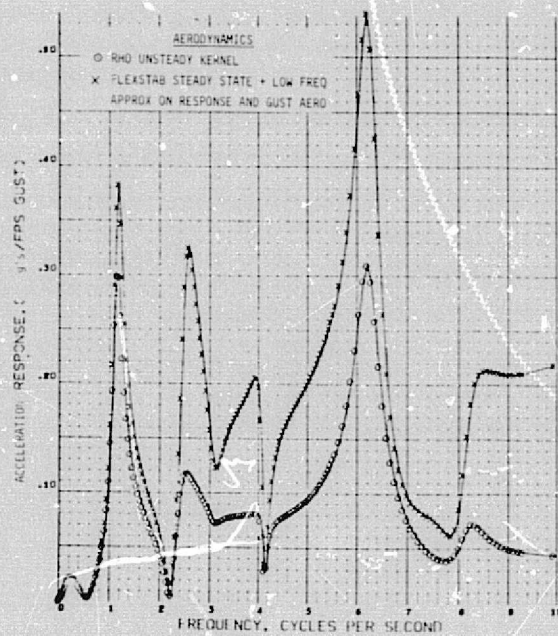
(a) Magnitudes

Figure C-16.—Comparison of Wing Acceleration Frequency Response Function at
Outboard Nacelle Due to Gust Excitation
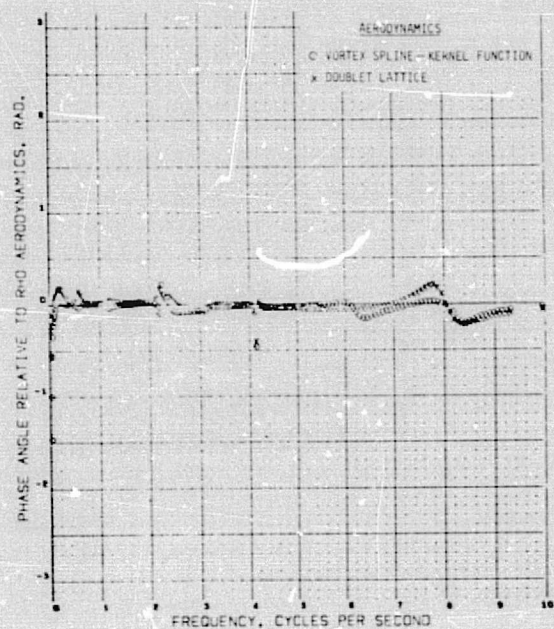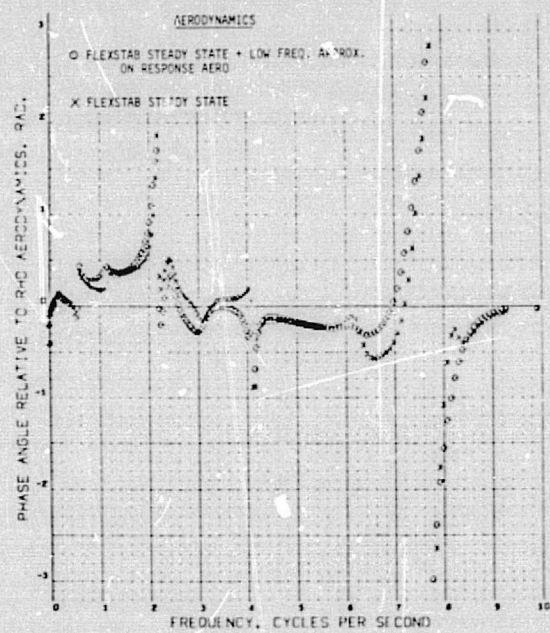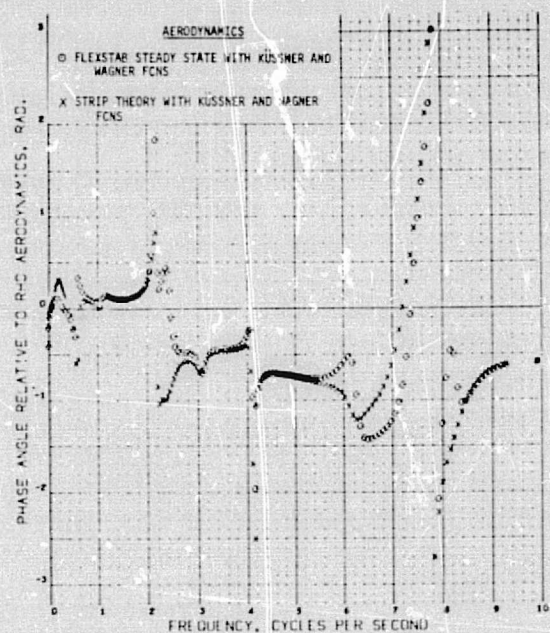
(b) Phase Angles

Figure C-16.—(Concluded)
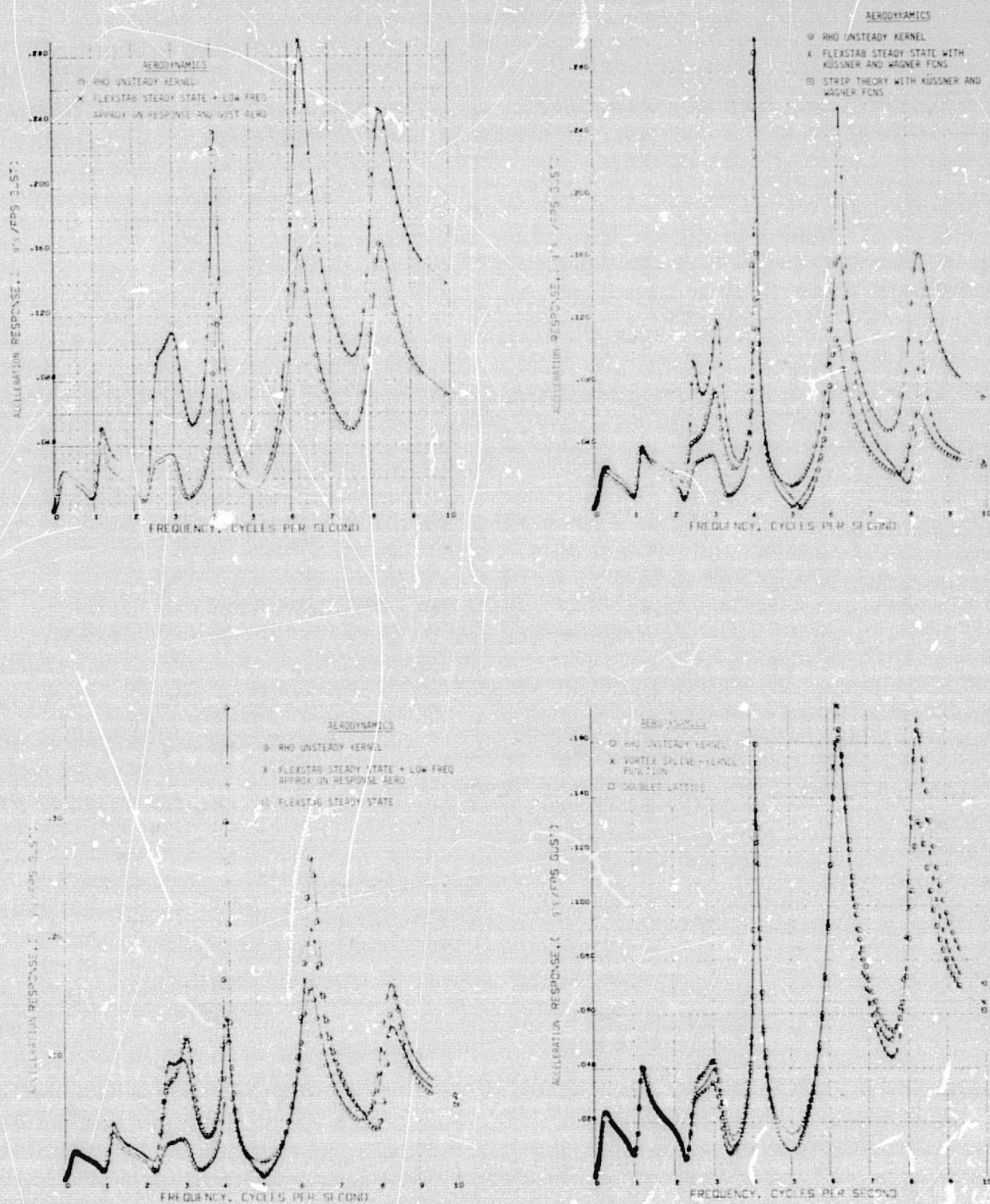
(a) Magnitudes

Figure C-17.—Comparison of Wing Acceleration Frequency Response Function at
Inboard Nacelle Due to Gust Excitation

99
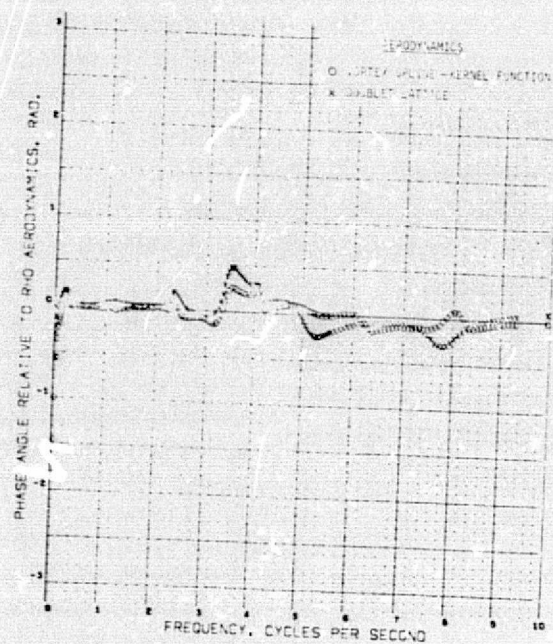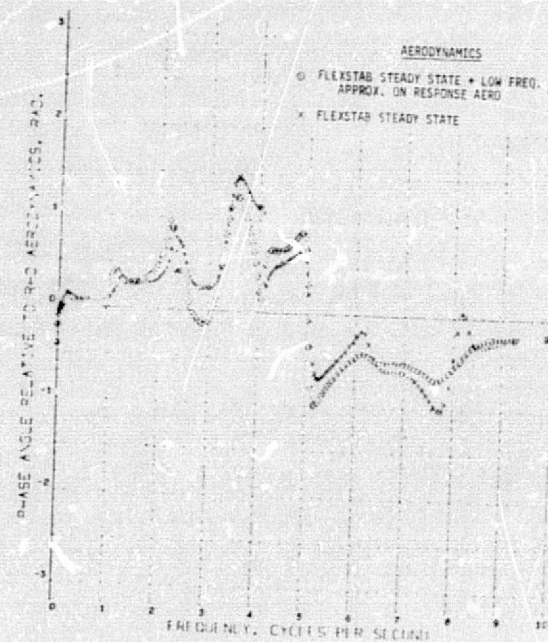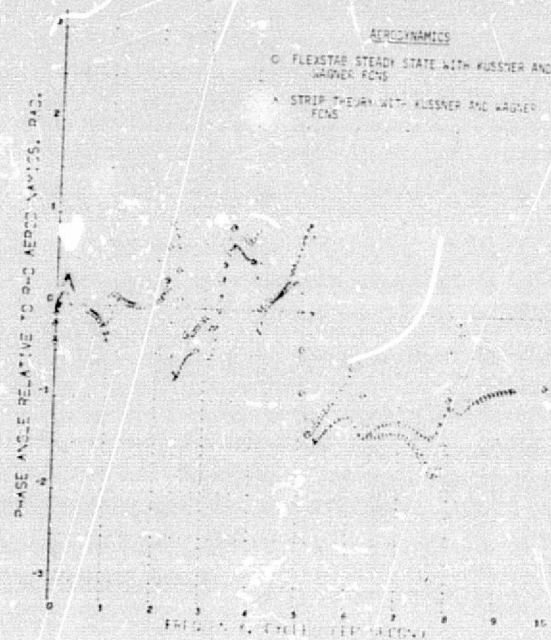
(b) Phase Angles

Figure C-17.—(Concluded)
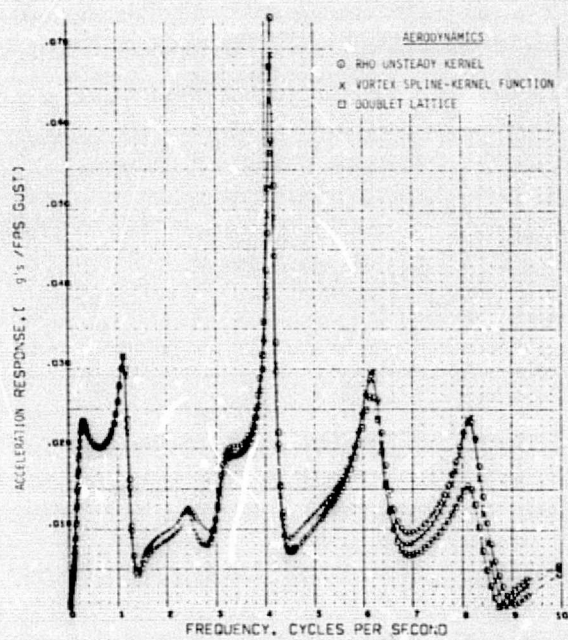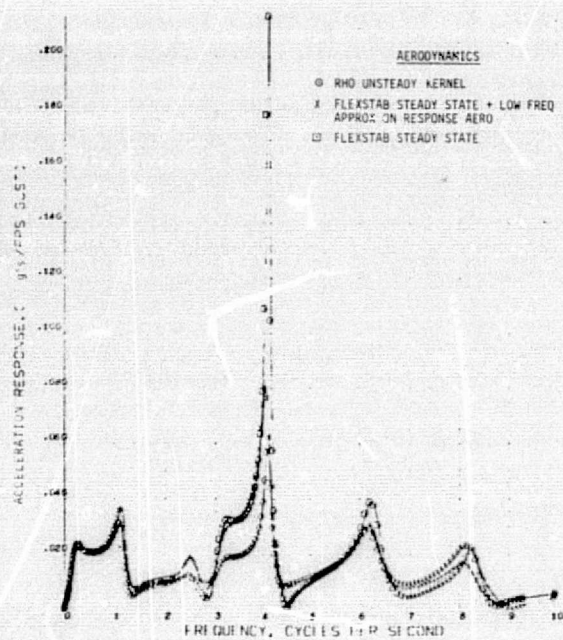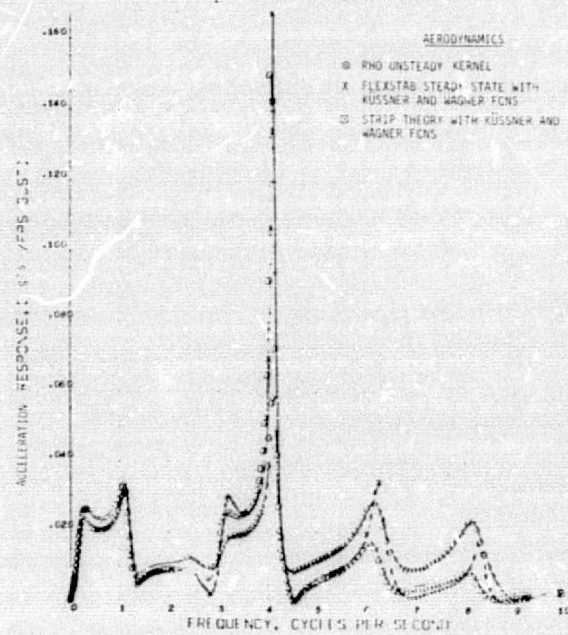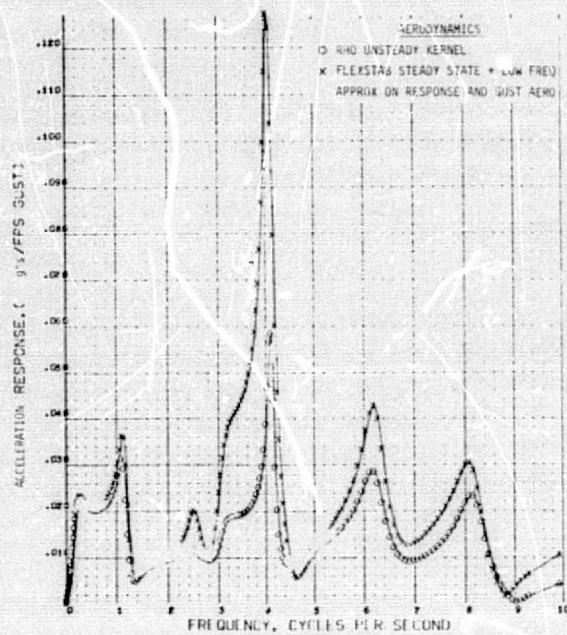
(a) Magnitudes

Figure C-18.—Comparison of Wing Acceleration Frequency Response Function at
Wing Root Due to Gust Excitation

101
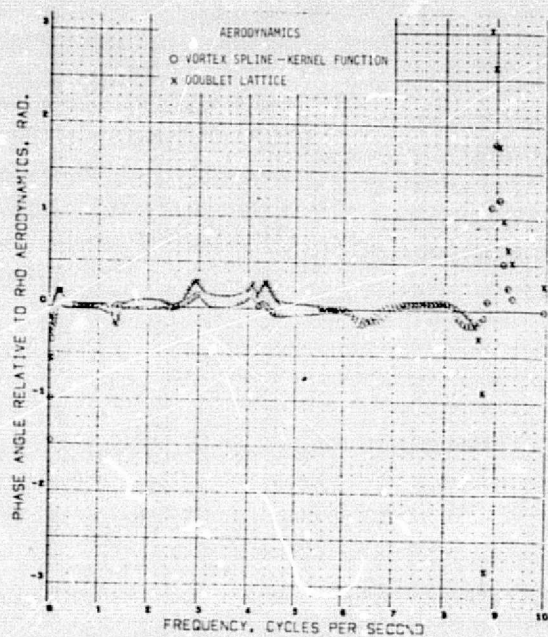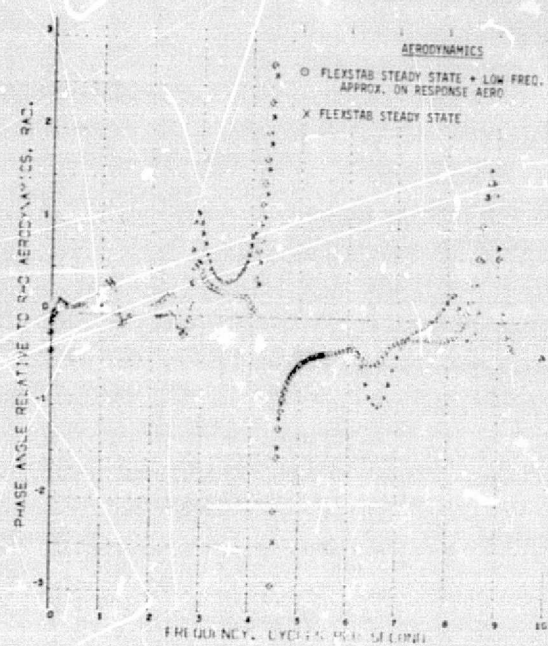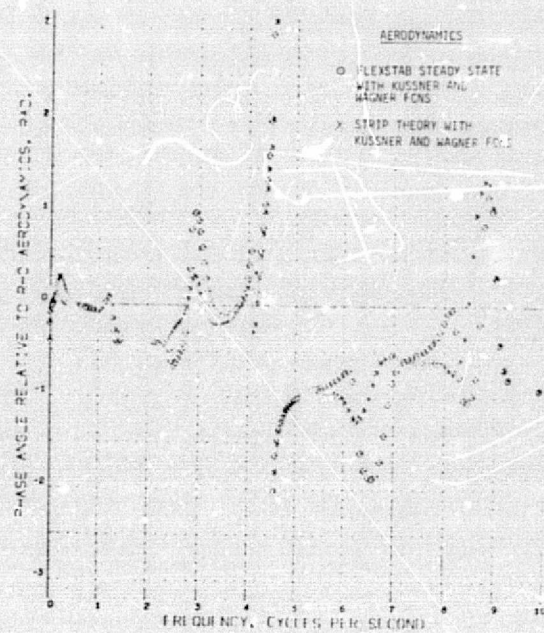
(b) Phase Angles

Figure C-18.—(Concluded)

102
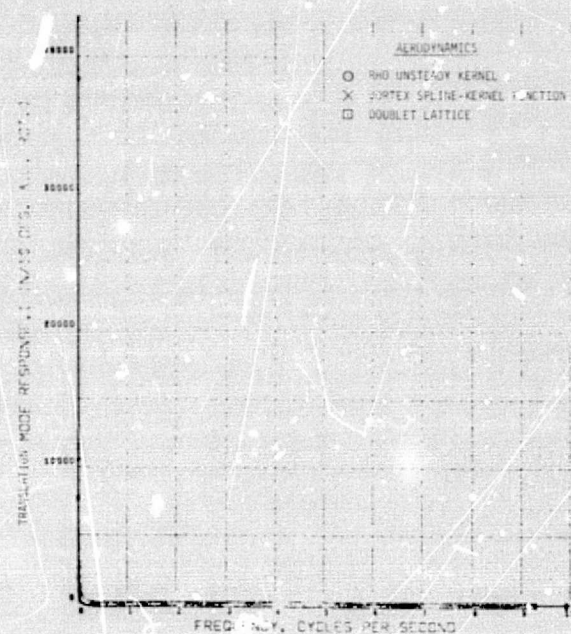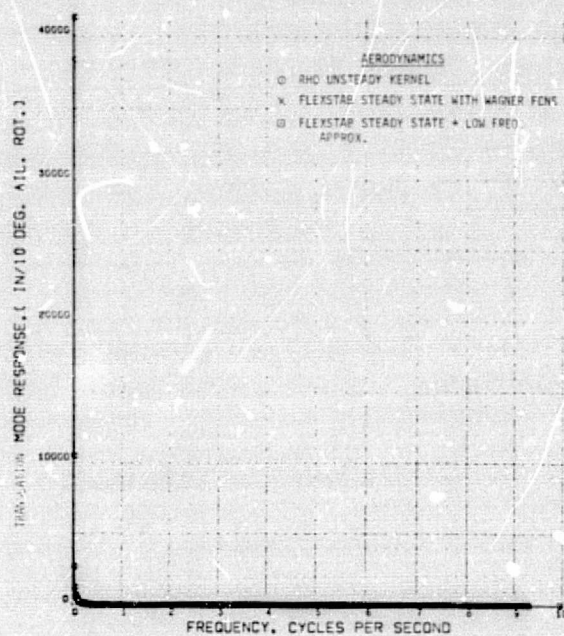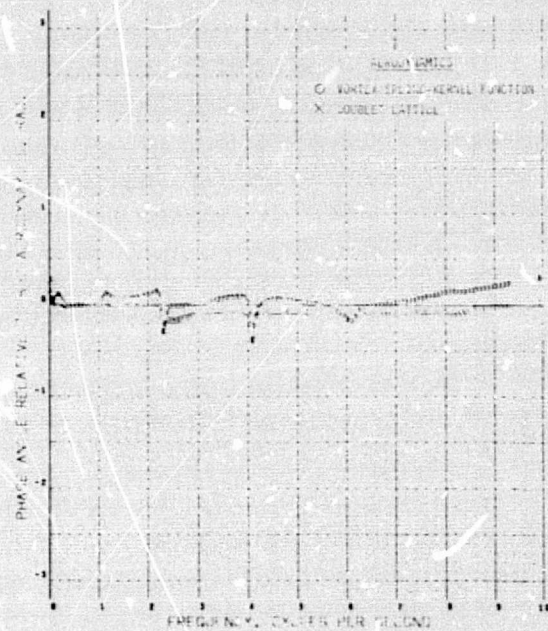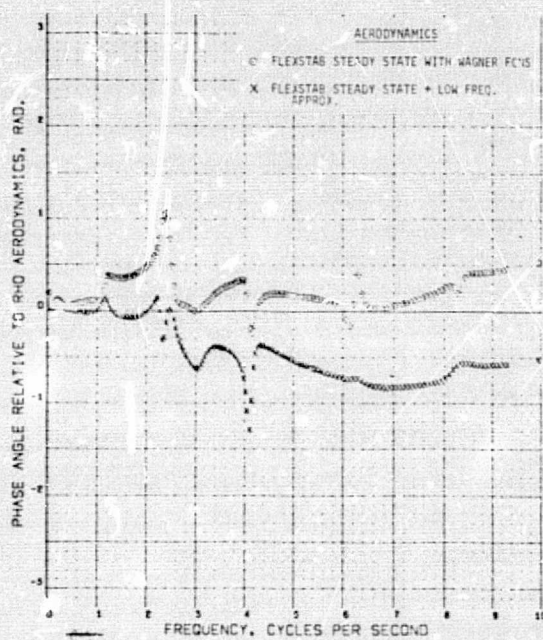
(a) Magnitudes

(b) Phase Angles

Figure C-19.—Comparison of Generalized Coordinate Frequency Response Function
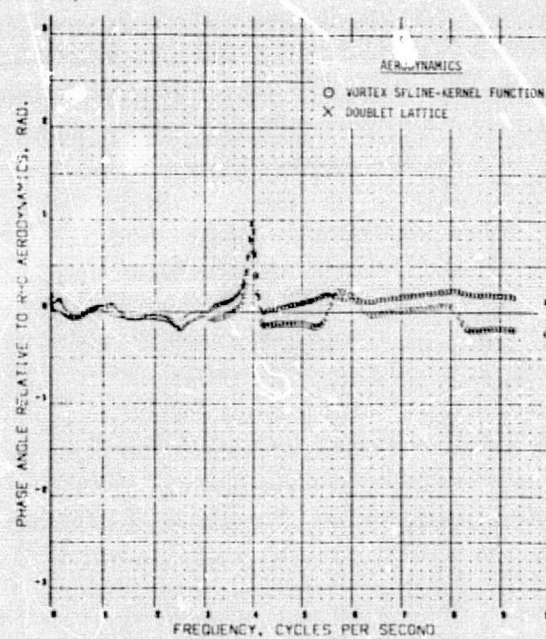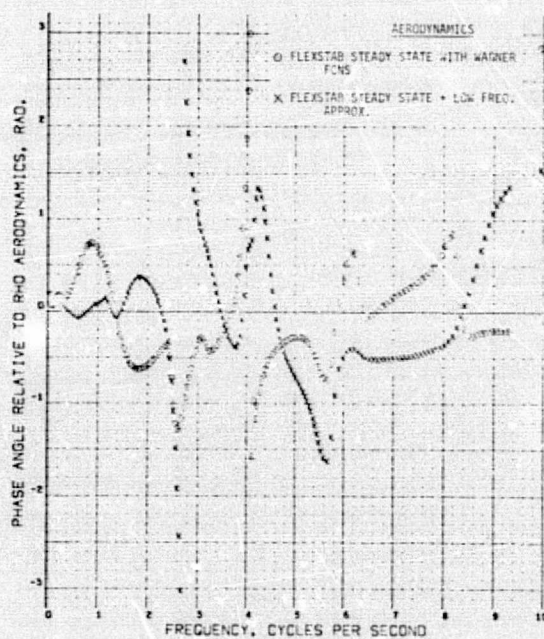Due to Oscillatory Aileron Excitation
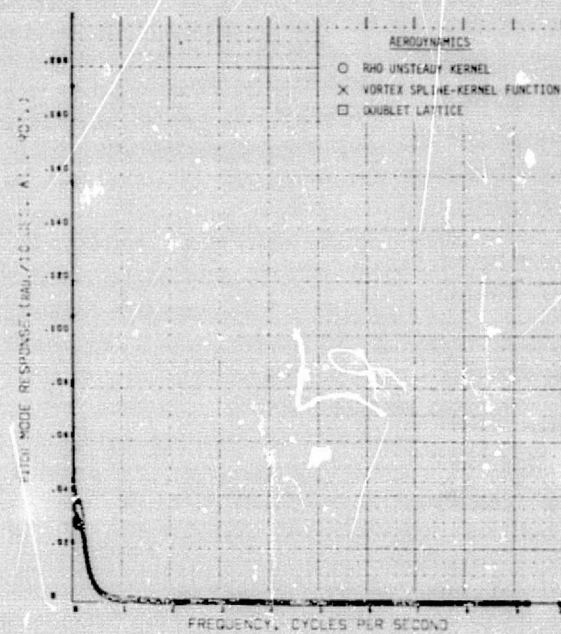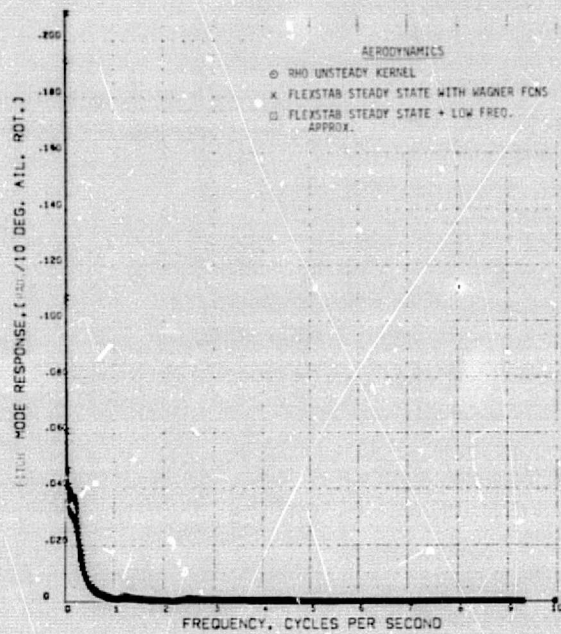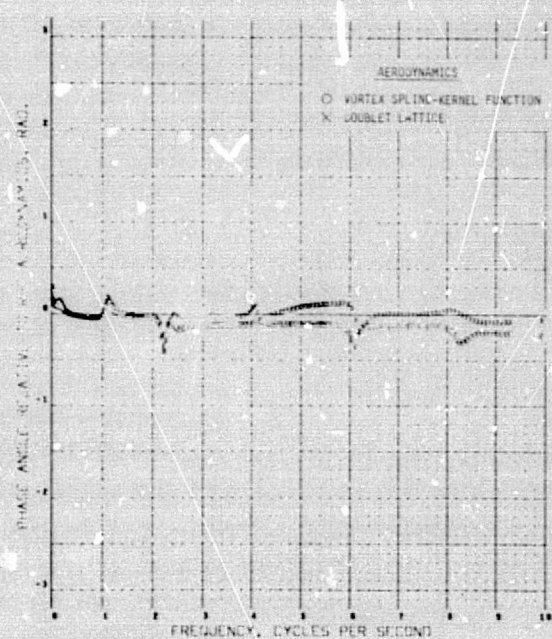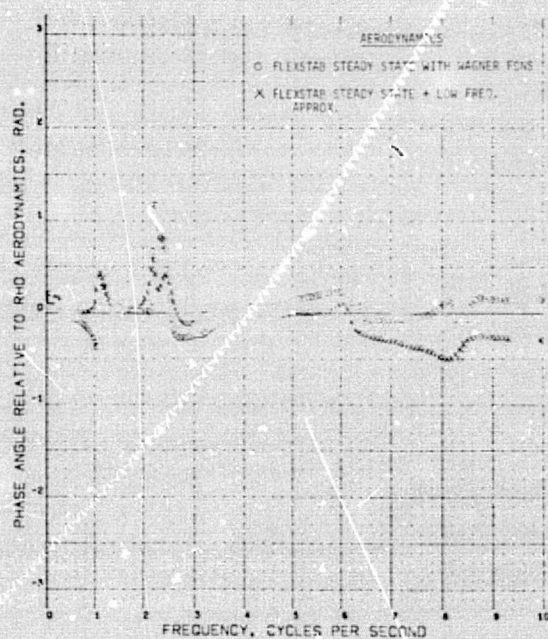
(a) Magnitudes

(b) Phase Angles

Figure C-20.—Comparison of Generalized Coordinate Frequency Response Function
Due to Oscillatory Aileron Excitation

104
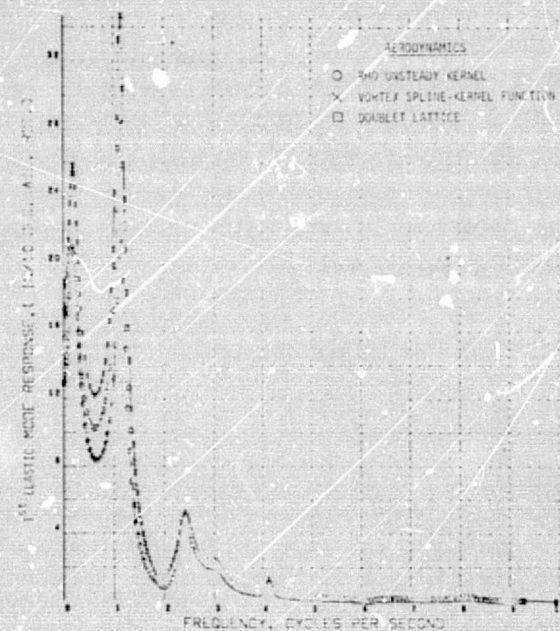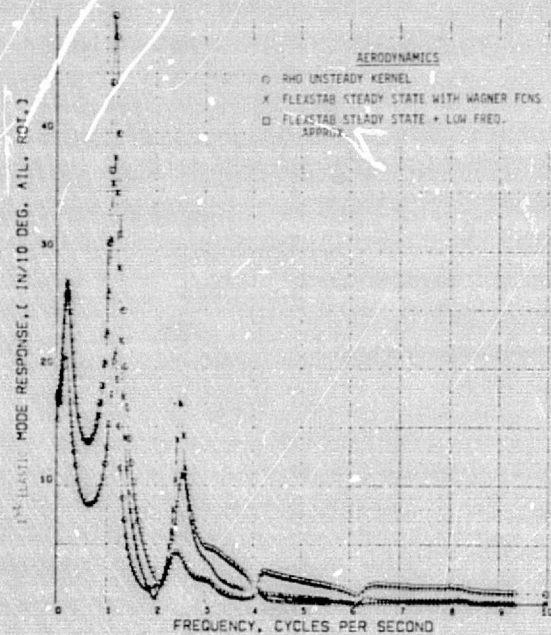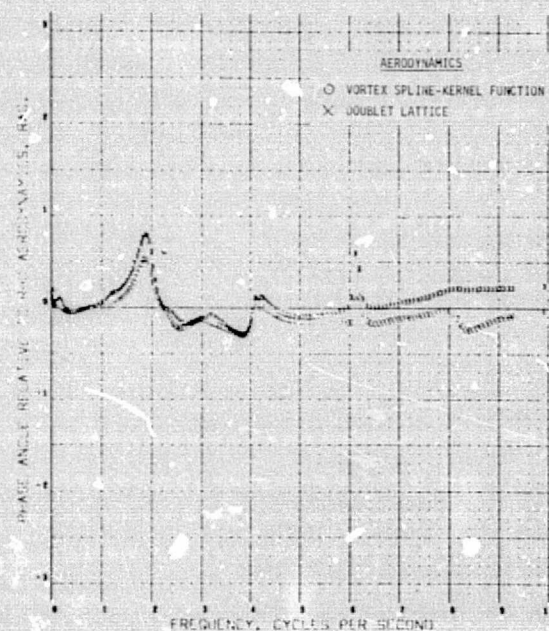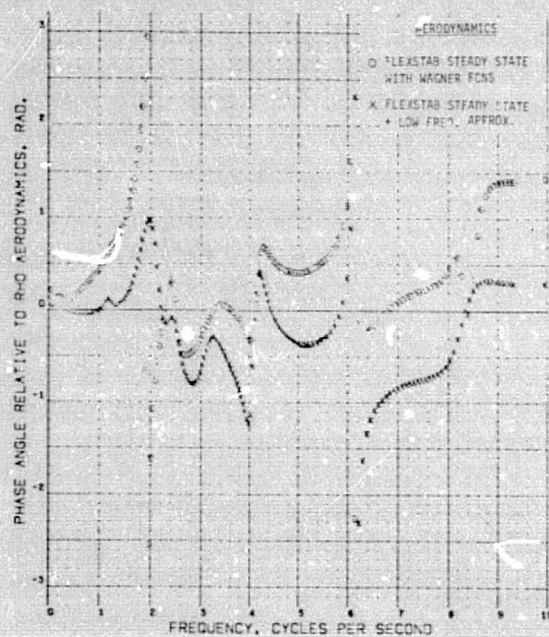
(a) Magnitudes

(b) Phase Angles

Figure C-21.—Comparison of Generalized Coordinate Frequency Response Function
Due to Oscillatory Aileron Excitation

105
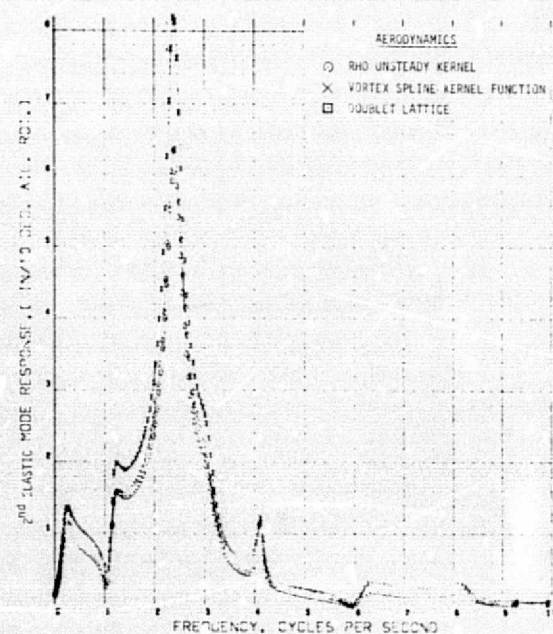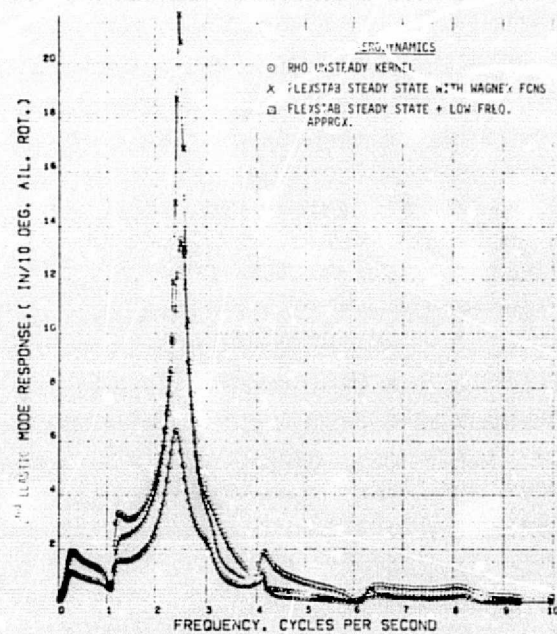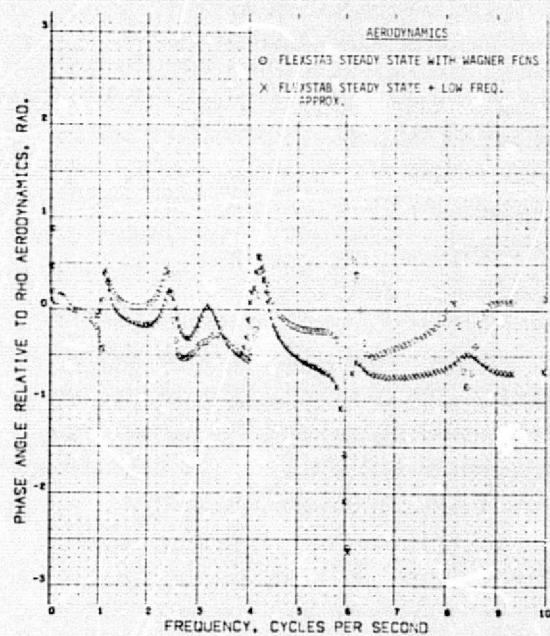
(a) Magnitudes

(b) Phase Angles

Figure C-22.—Comparison of Generalized Coordinate Frequency Response Function
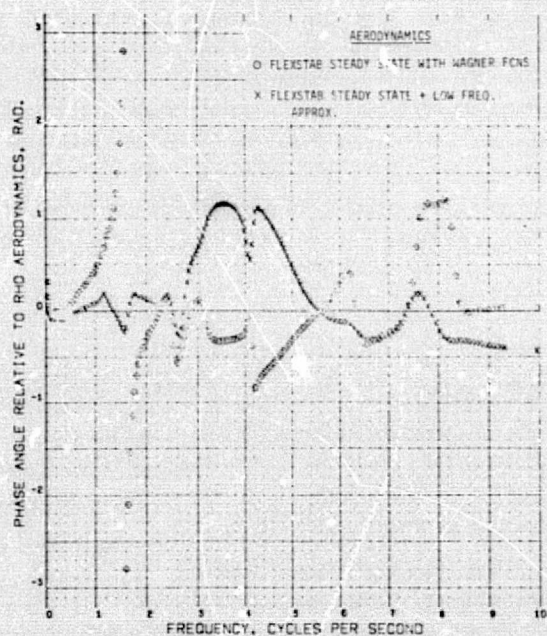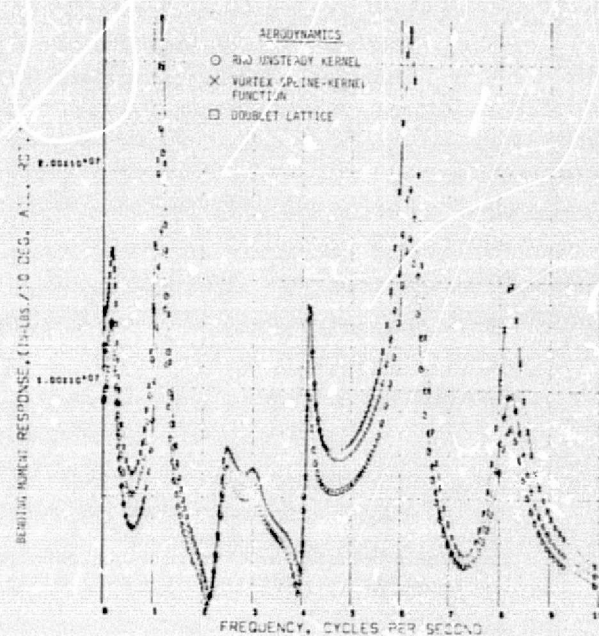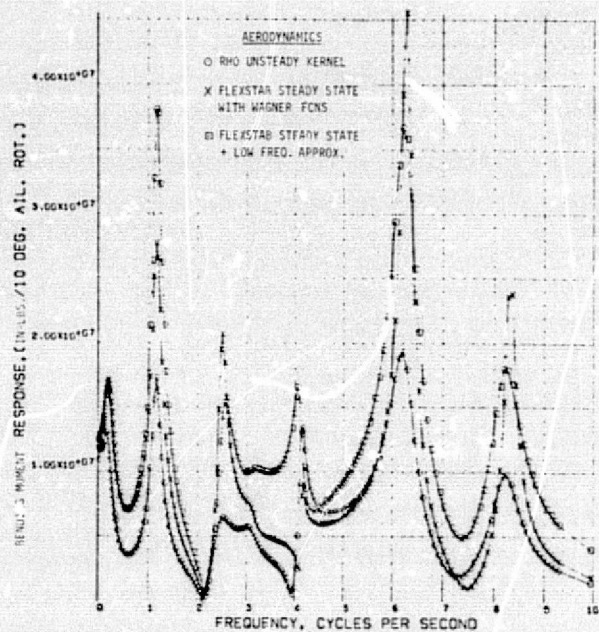Due to Oscillatory Aileron Excitation

106
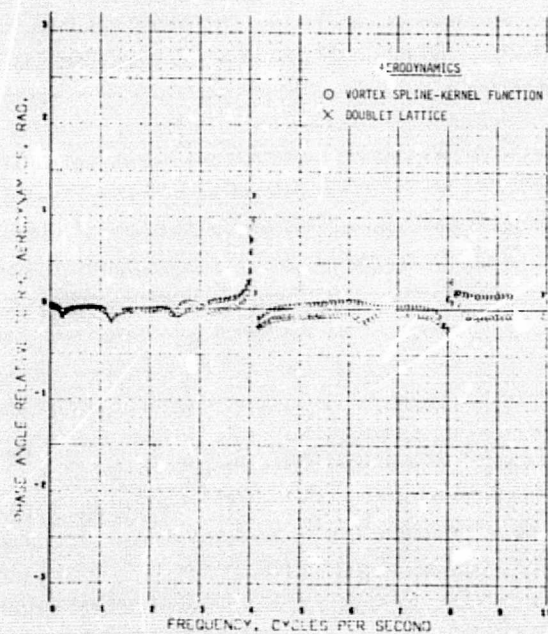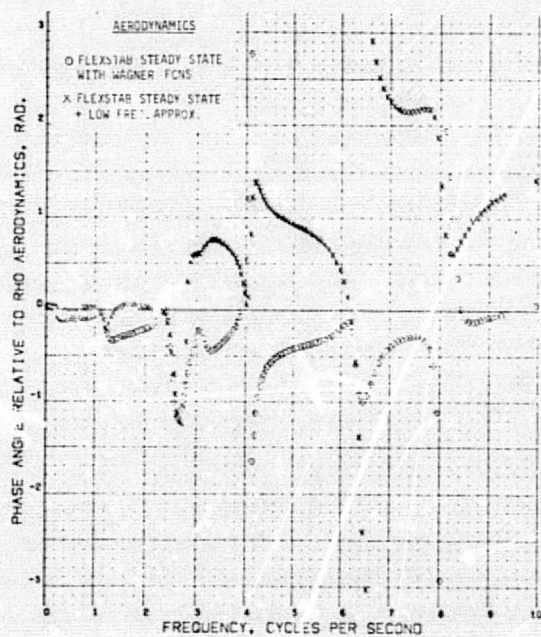
(a) Magnitudes
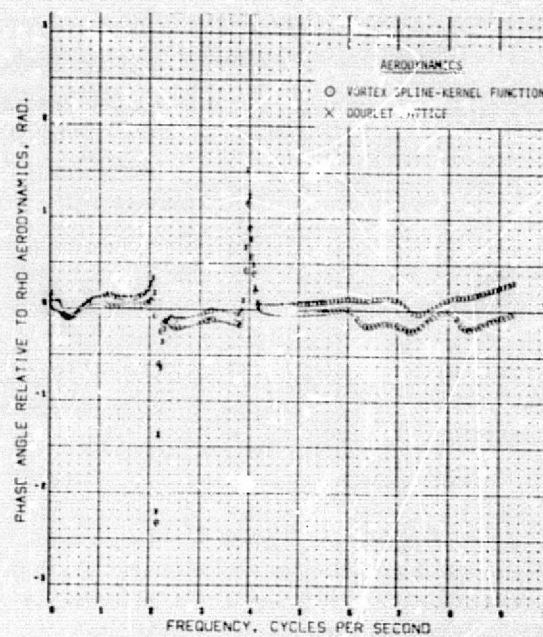

(b) Phase Angles

Figure C-23.—Comparison of Generalized Coordinate Frequency Response Function
Due to Oscillatory Aileron Excitation

107
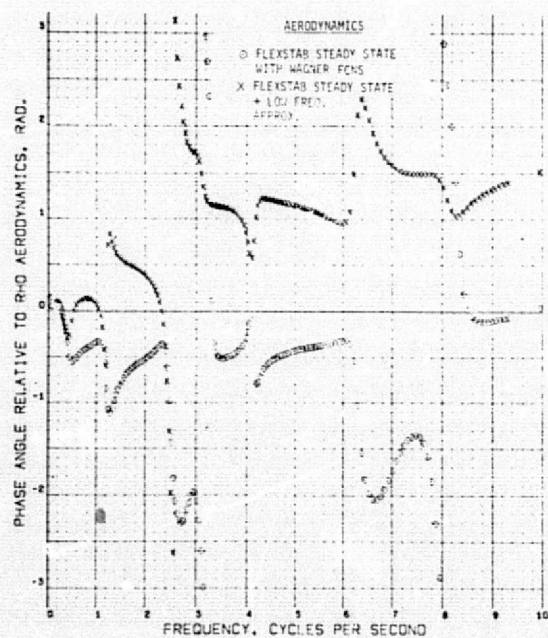
(a) Magnitudes

(b) Phase Angles

Figure C-24.—Comparison of Generalized Coordinate Frequency Response Function
Due to Oscillatory Aileron Excitation

108
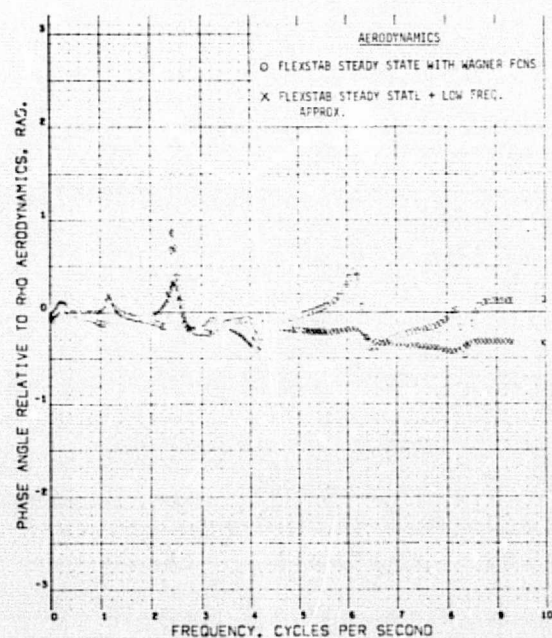
(a) Magnitudes

(b) Phase Angles

Figure C-25.—Comparison of Generalized Coordinate Frequency Response Function
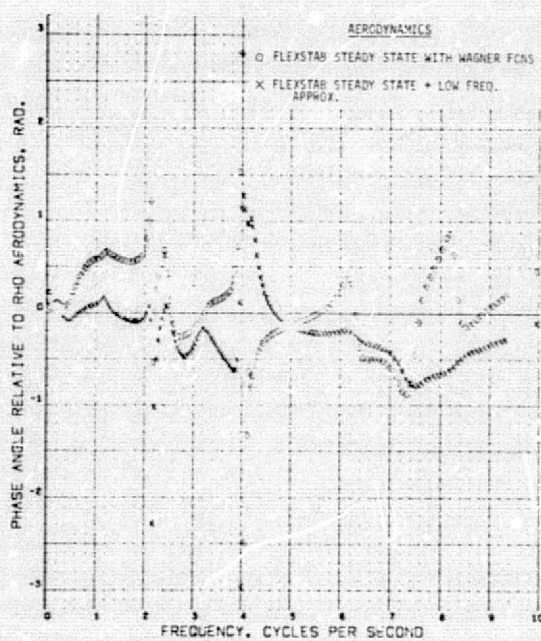Due to Oscillatory Aileron Excitation

109
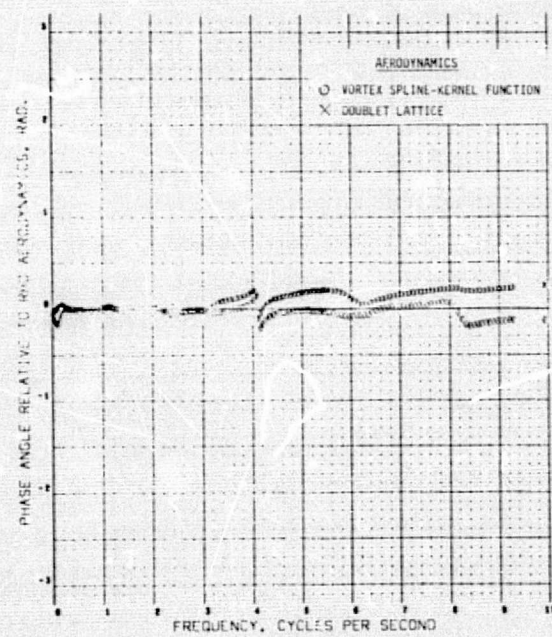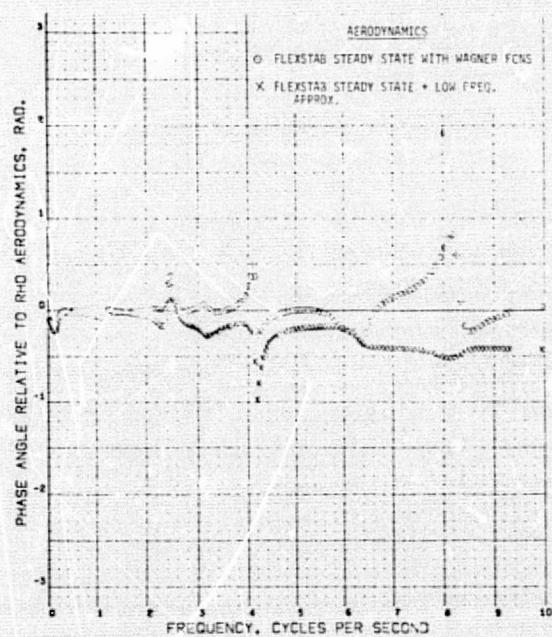
(a) Magnitudes

(b) Phase Angles

Figure C-26.—Comparison of Generalized Coordinate Frequency Response Function
Due to Oscillatory Aileron Excitation

110
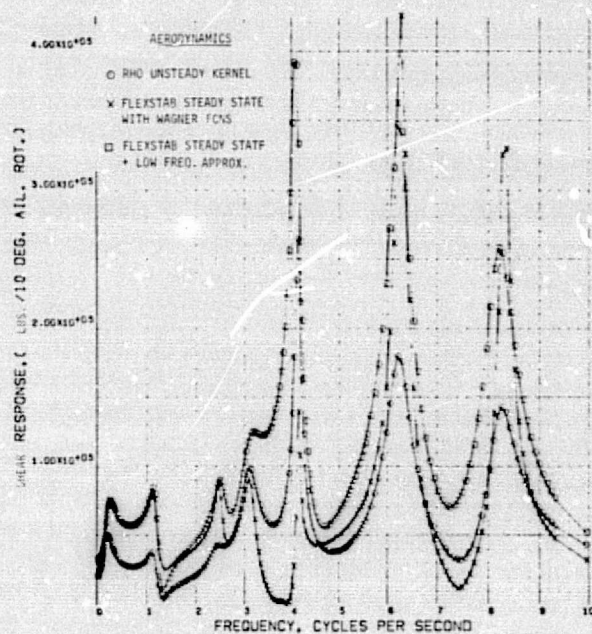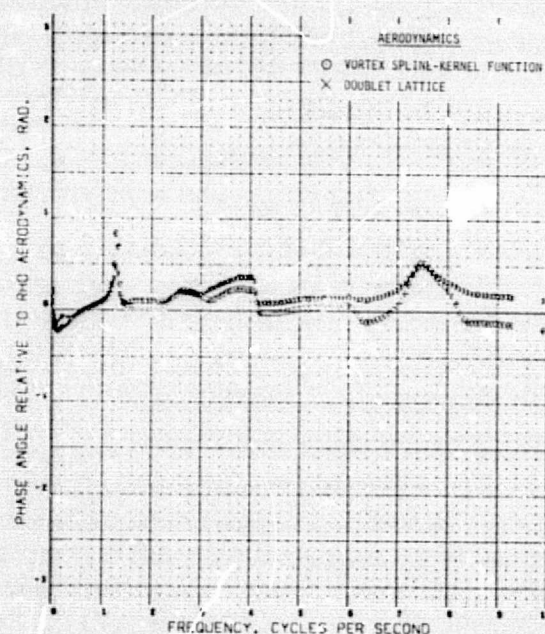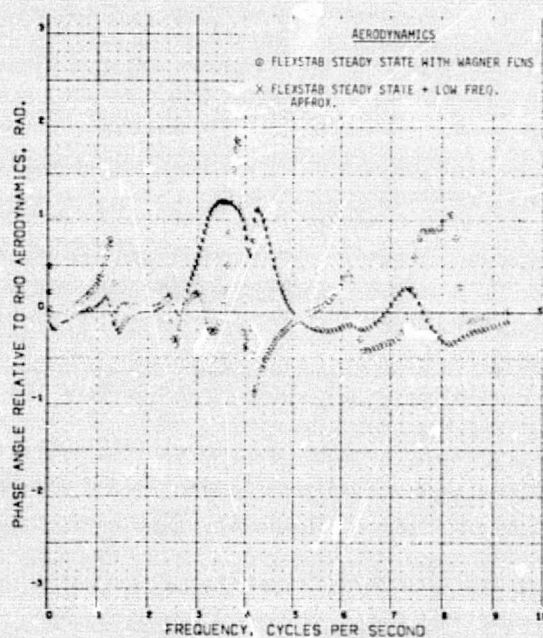
(a) Magnitudes

(b) Phase Angles

Figure C-27.—Comparison of Wing Shear Frequency Response Function at Wing Root
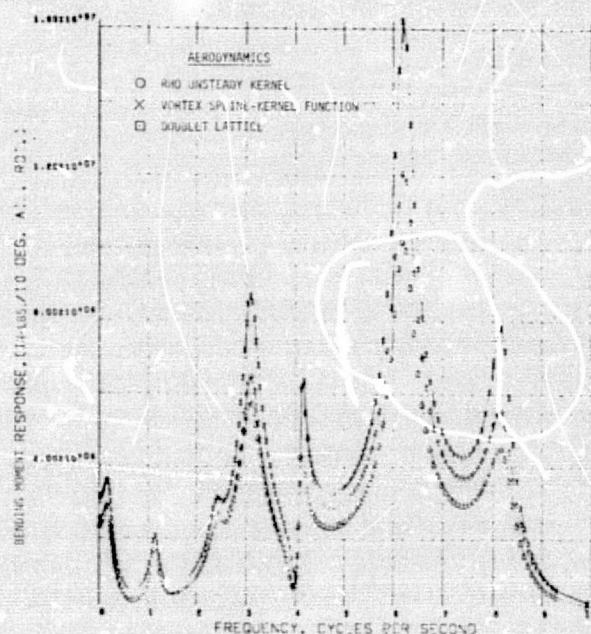Due to Oscillatory Aileron Excitation

111
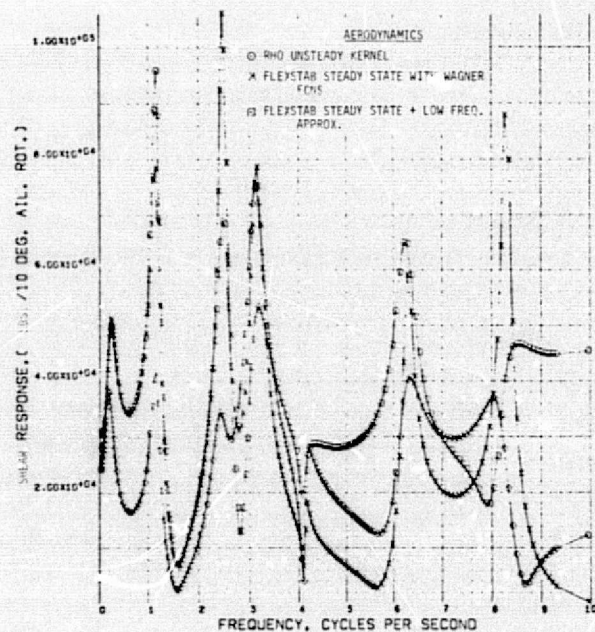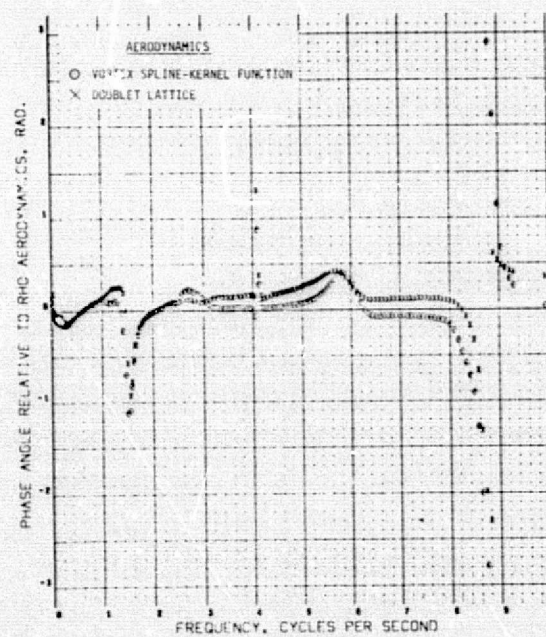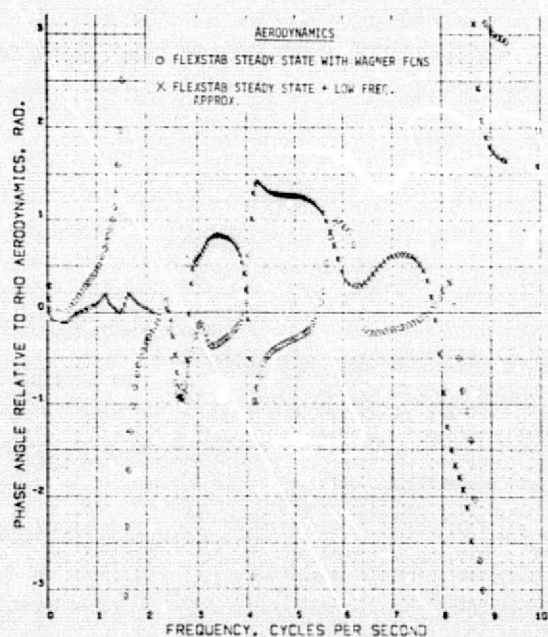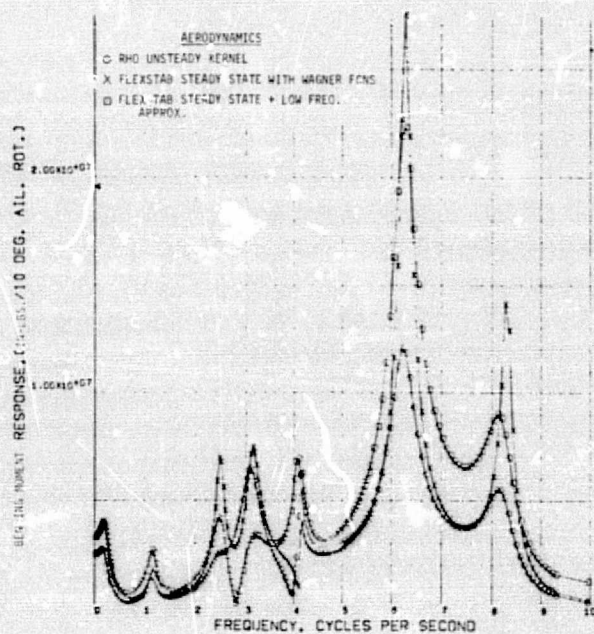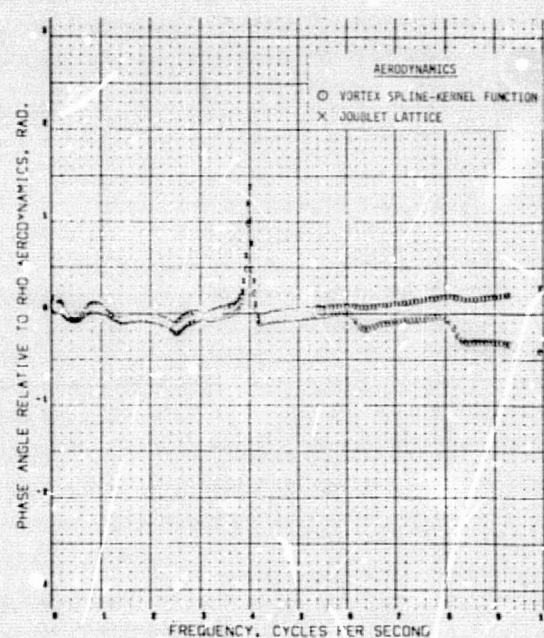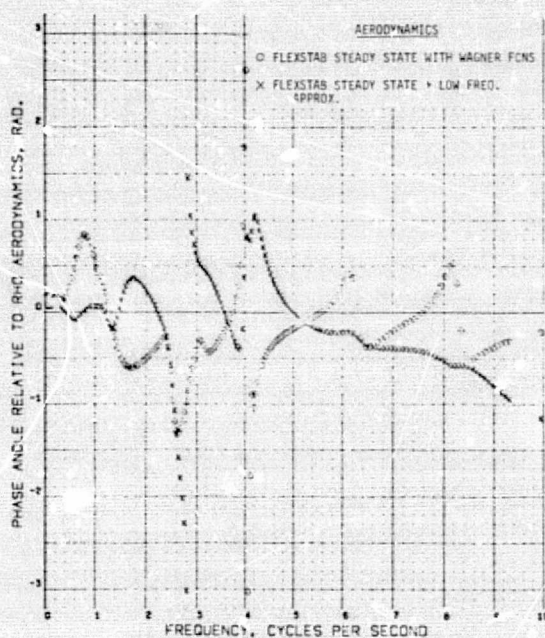
(a) Magnitudes

(b) Phase Angles

Figure C-28.—Comparison of Wing Shear Frequency Response Function at Inboard
Nacelle Due to Oscillatory Aileron Excitation
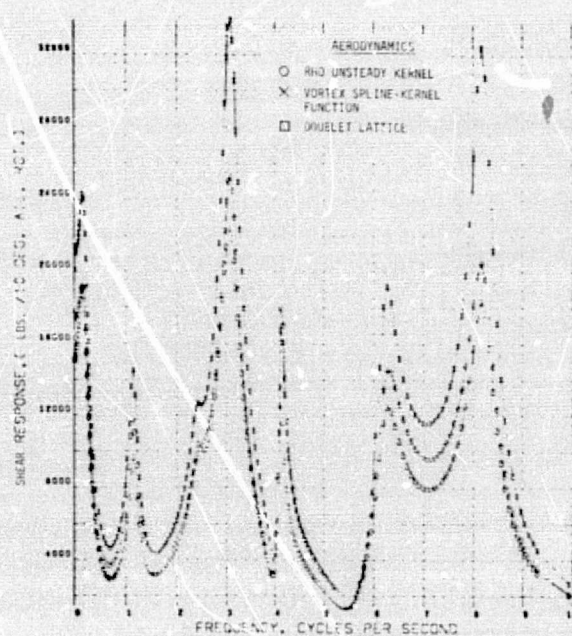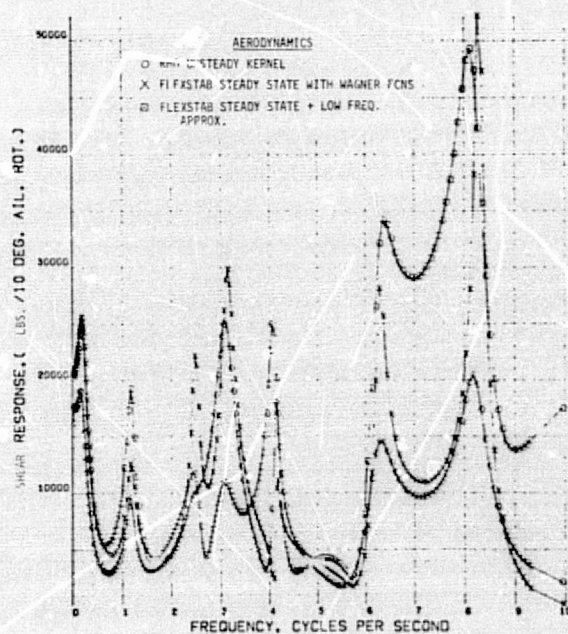
(a) Magnitudes

(b) Phase Angles

Figure C-29.—Comparison of Wing Shear Frequency Response Function at Outboard Nacelle Due to Oscillatory Aileron Excitation
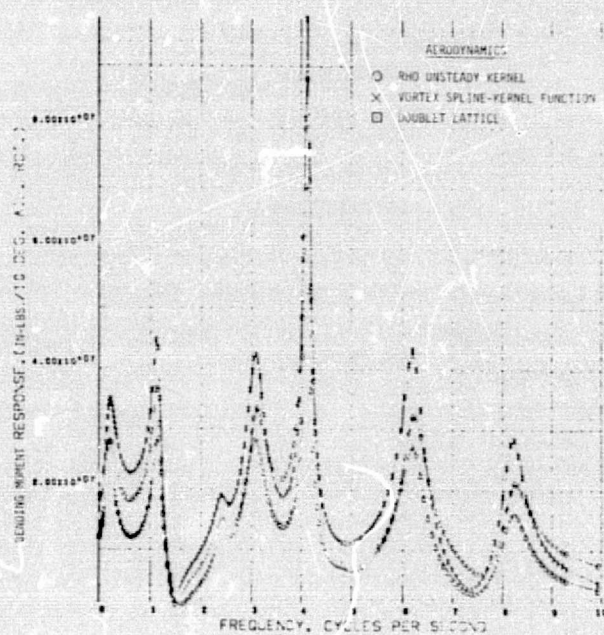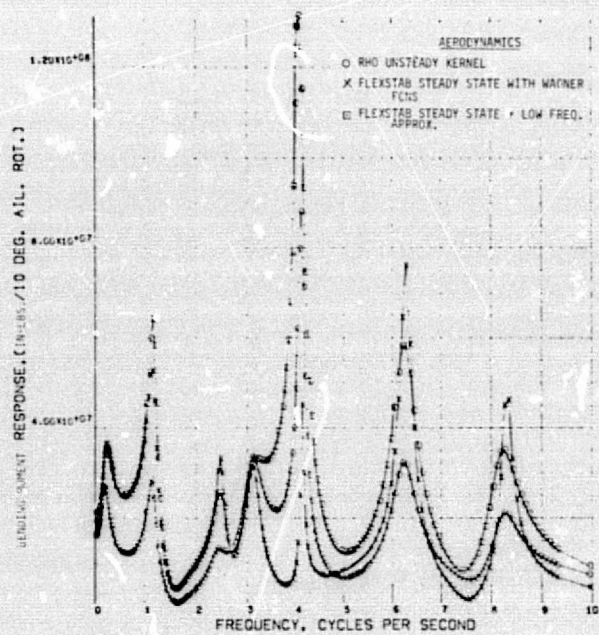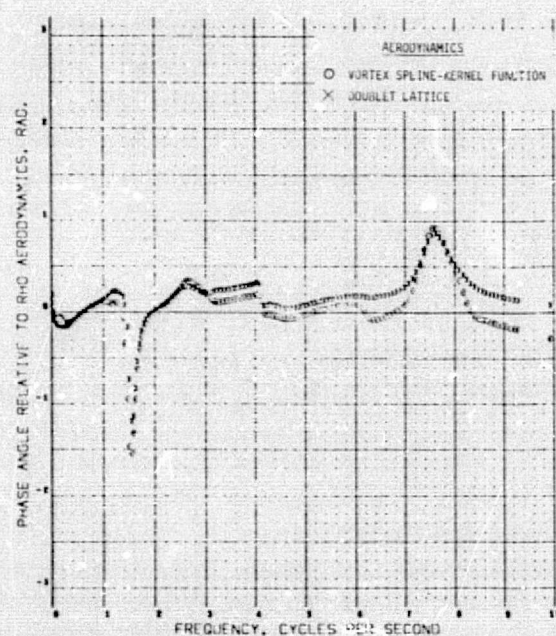
(a) Magnitudes

(b) Phase Angles

Figure C-30.—Comparison of Wing Bending Moment Frequency Response Function at
Wing Root Due to Oscillatory Aileron Excitation

114

(a) Magnitudes

(b) Phase Angles

Figure C-31.—Comparison of Wing Bending Moment Frequency Response Function at
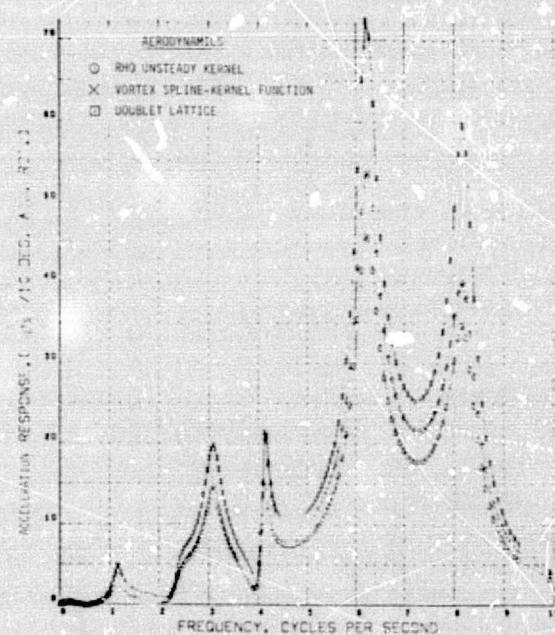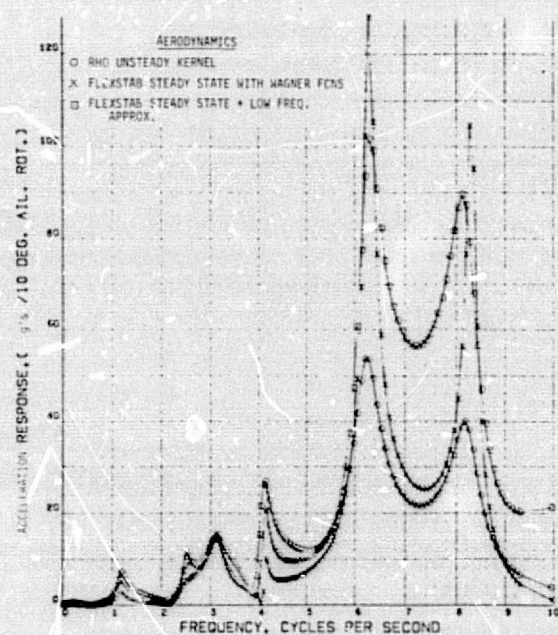Inboard Nacelle Due to Oscillatory Aileron Excitation
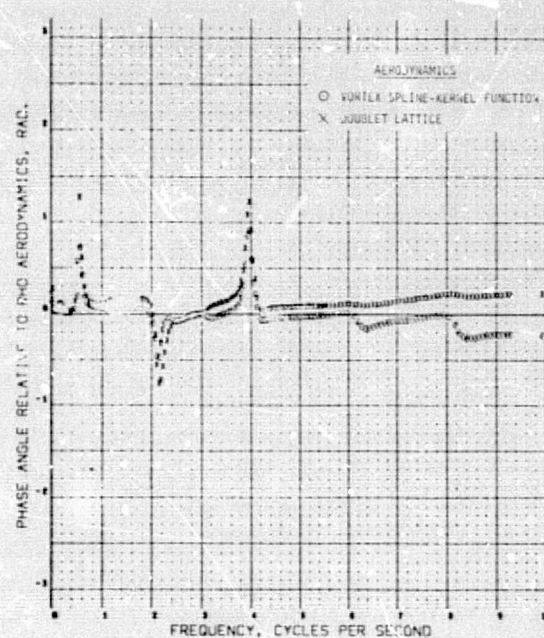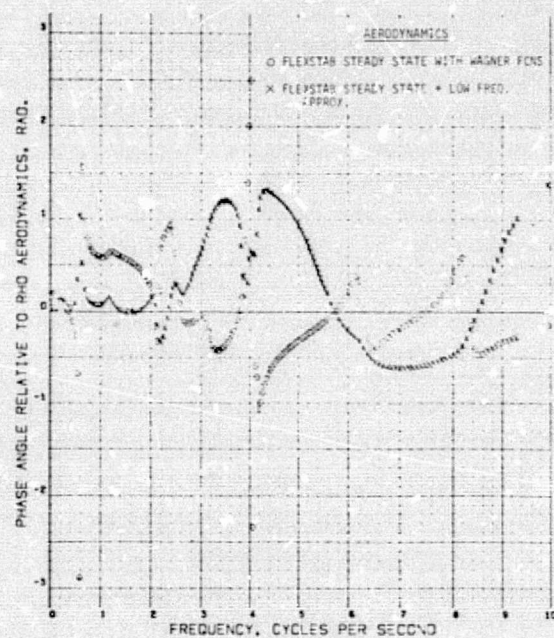
115

(a) Magnitudes

(b) Phase Angles

Figure C-32.—Comparison of Wing Bending Moment Frequency Response Function at
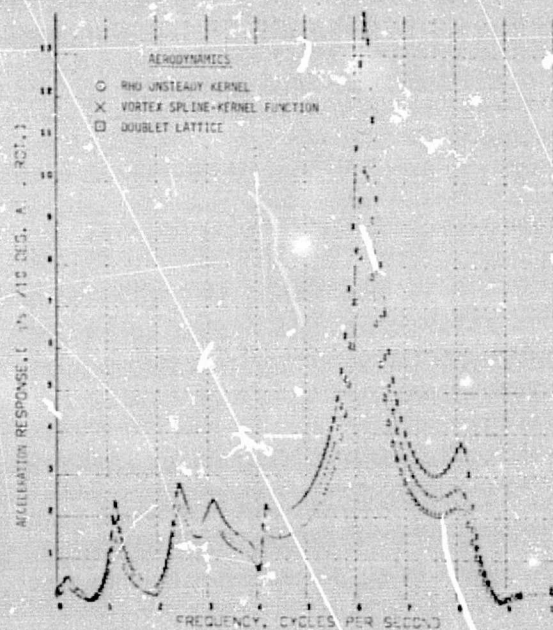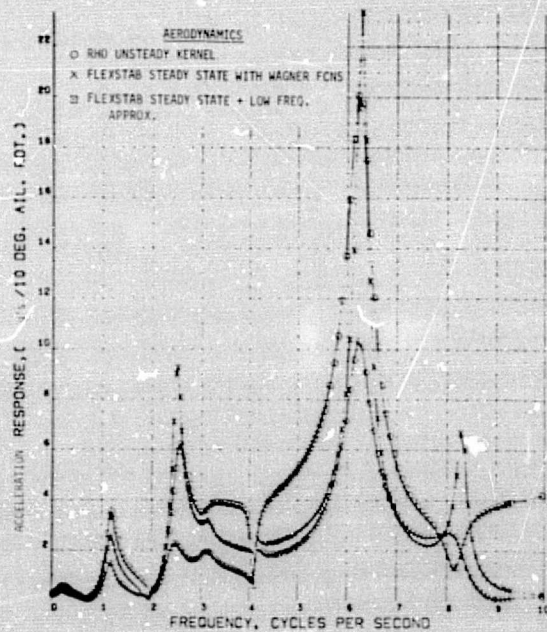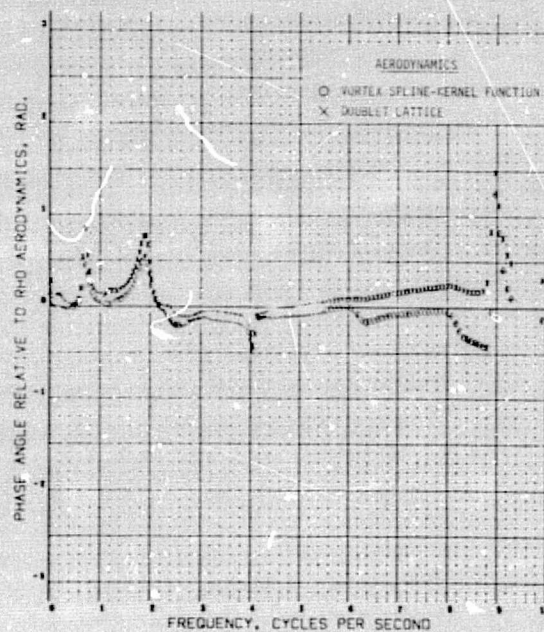Outboard Nacelle Due to Oscillatory Aileron Excitation

116

(a) Magnitudes

(b) Phase Angles

Figure C-33.—Comparison of Wing Acceleration Frequency Response Function at
Wingtip Due to Oscillatory Aileron Excitation

117

(a) Magnitudes

(b) Phase Angles

Figure C-34.—Comparison of Wing Acceleration Frequency Response Function at
Outboard Nacelle Due to Oscillatory Aileron Excitation

118

(a) Magnitudes

(b) Phase Angles

Figure C-35.—Comparison of Wing Acceleration Frequency Response Function at Inboard Nacelle Due to Oscillatory Aileron Excitation
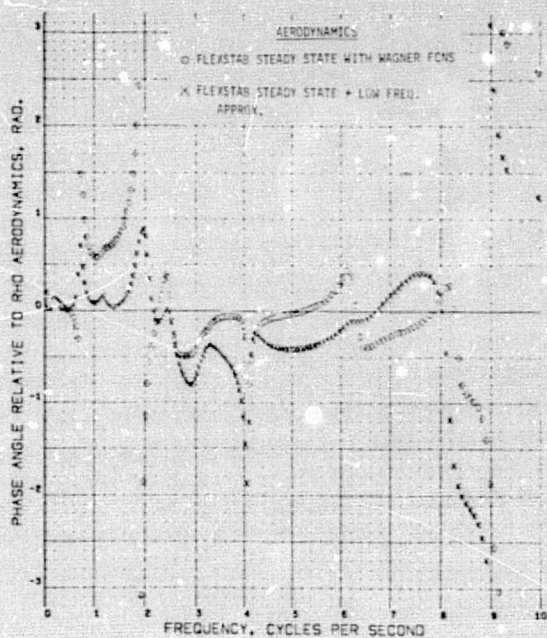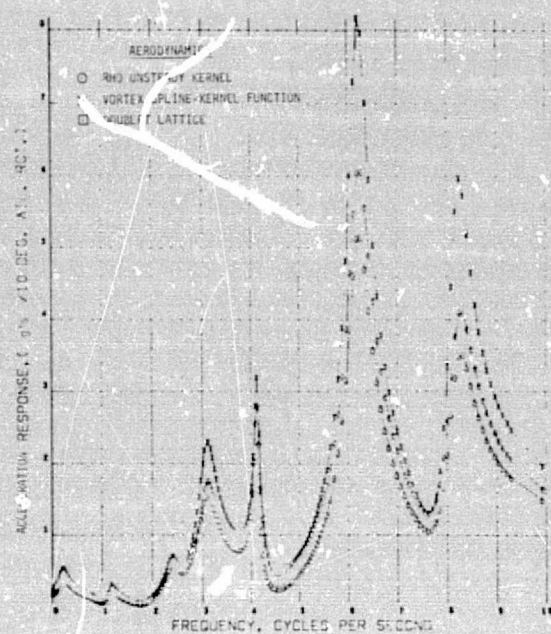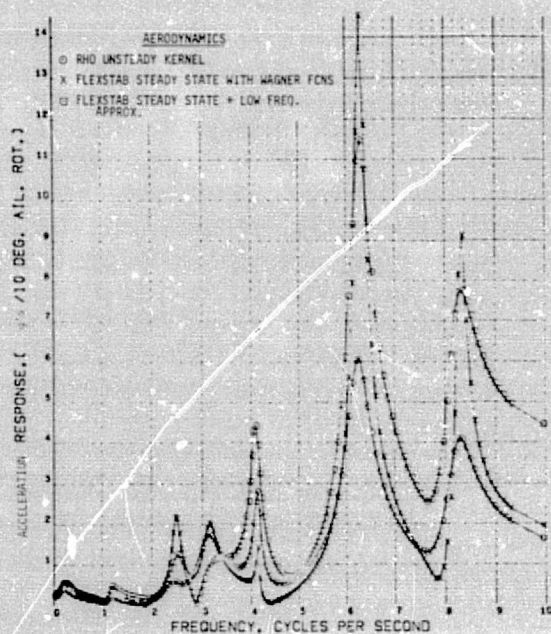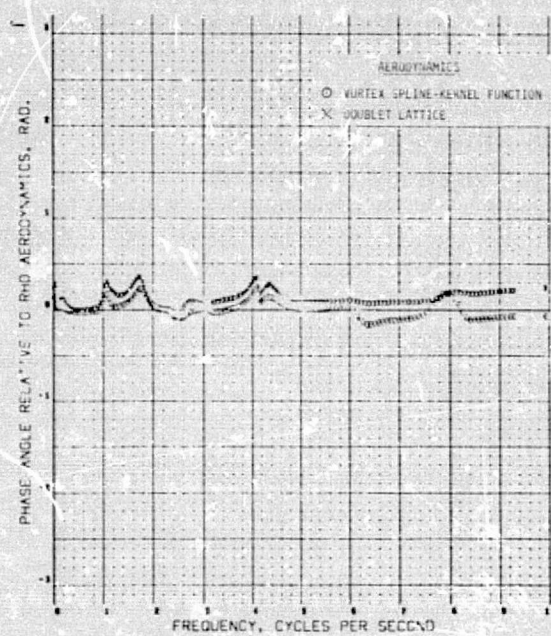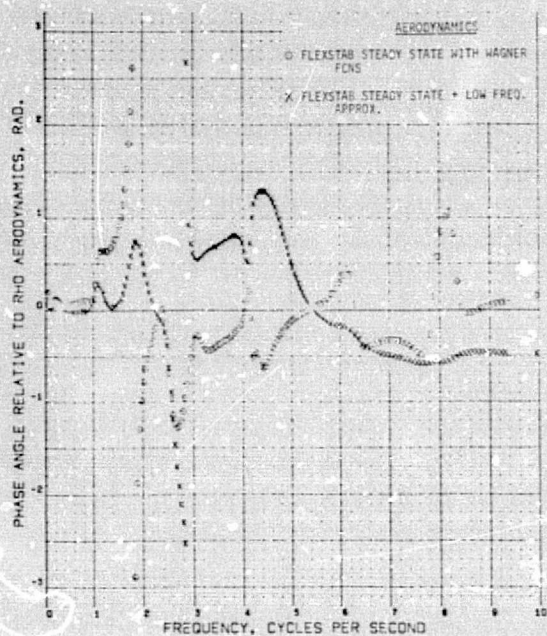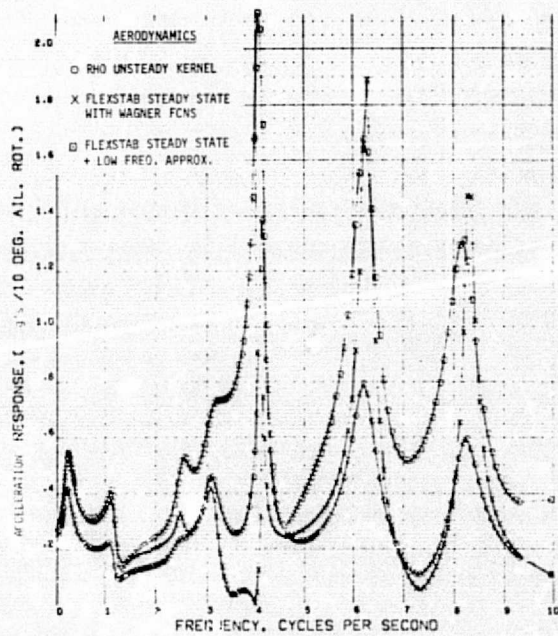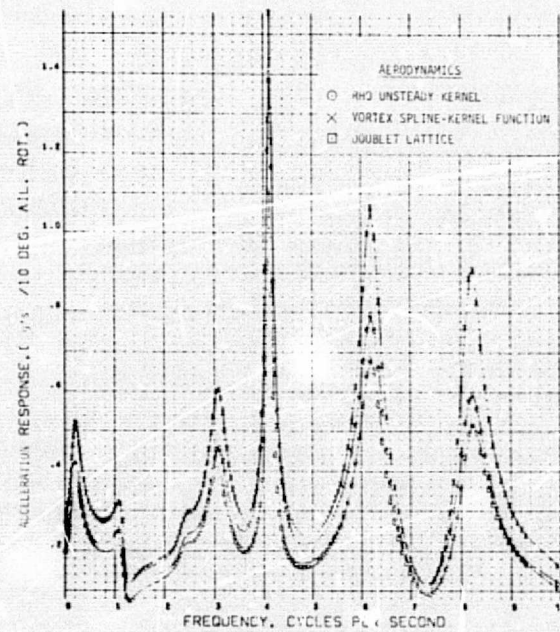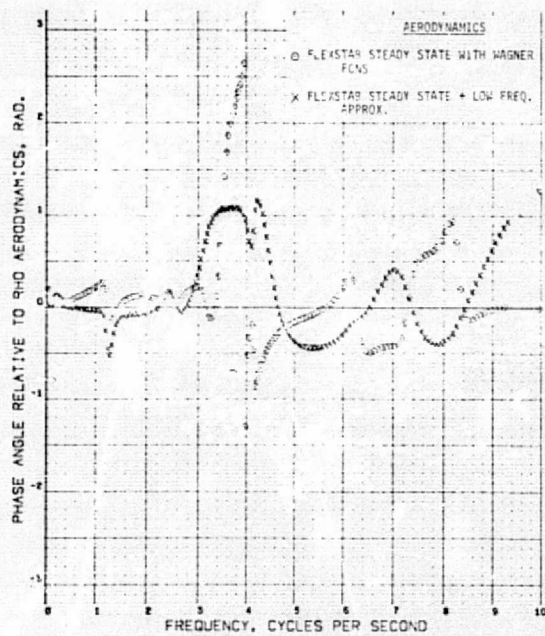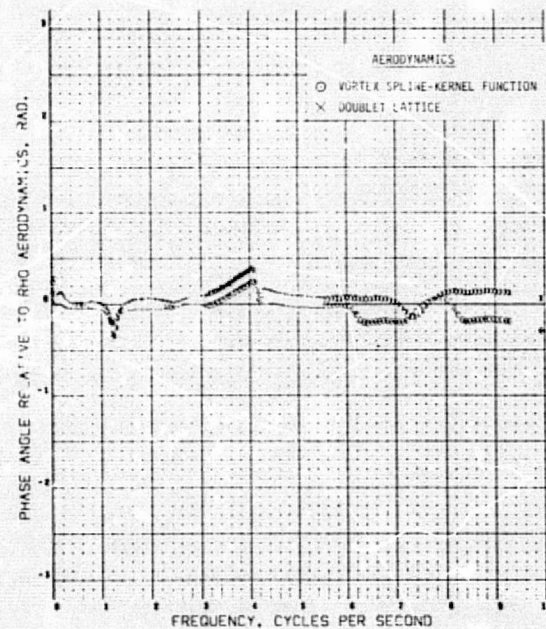
(a) Magnitudes

(b) Phase Angles

Figure C-36.—Comparison of Wing Acceleration Frequency Response Function at
Wing Root Due to Oscillatory Aileron Excitation

120

REFERENCES

1. *A Method for Predicting the Stability Characteristics of an Elastic Airplane*. NASA CR-114712-114715, Vol. 1 through 4, 1974.

   Volume 1–*FLEXSTAB Theoretical Description*. NASA CR-114712.
   Volume 2–*FLEXSTAB 1.02.00 User's Manual*. NASA CR-114713.
   Volume 3–*FLEXSTAB 1.02.00 Program Description*. NASA CR-114714.
   Volume 4–*FLEXSTAB 1.02.00 Demonstration Cases and Results*.
   NASA CR-114715.

2. Fromme, J. A.; and Halstead, D. W.: *Solutions to Kussner's Integral Equation in Unsteady Flow Using Local Basis Functions*. NASA CR-137719, September 1975.

3. Rowe, W. S.; Winther, B. A.; and Redman, M. C.: *Prediction of Unsteady Aerodynamic Loadings Caused by Trailing Edge Control Surface Motions in Subsonic Compressible Flow–Analysis and Results*. NASA CR-2003, June 1972.

4. Giesing, J. P.; Kalman, T. P.; and Rodden, W. P.: *Subsonic Unsteady Aerodynamics for General Configurations, Part I, Direct Application of the Non-Planar Doublet Lattice Method*. AFFDS-TR-71-S, Part I, February 1975.

5. Mercer, J. E.; Weber, J. A.; and Lesferd, E. P.: *Aerodynamic Influence Coefficient Method Using Singularity Splines*. NASA CR-2423, May 1974.

6. Gray, W. L.; and Schenk, K. M.: *A Method for Calculating the Subsonic Steady State Loading on an Airplane With a Wing of Arbitrary Planform and Stiffness*. NACA TN3030, 1953.

7. Miller, R. D.; Richard, M.; and Rogers, J. T.: *Feasibility of Implementing Unsteady Aerodynamics Into the FLEXSTAB Computer Program System*. NASA CR-132530, 1974.

8. Fung, Y. C.: *An Introduction to the Theory of Elasticity*. John Wiley & Sons (New York), 1955.

9. Jones, R. T.: *The Unsteady Lift of a Wing of Finite Aspect Ratio*. NACA Report 681, 1940.

10. Bisplinghoff, R. L.; Ashley, H.; and Halfman, R. A.: *Aeroelasticity*. Addison-Wesley (Reading, Mass.), 1955.

11. Houbolt, J. C.; Steiner, R.; and Pratt, K. G.: *Dynamic Response of Airplanes to Atmospheric Turbulence Including Flight Data on Input and Response*. NASA TRR-199, 1964.

12. Austin, W. H., Jr.: *Development of Improved Gust Load Criteria for United States Air Force Aircraft*. SEG-TR-67-28, 1967.

13. Mitchell, C. G. B.: *Calcualtion of the Response of a Flexible Aircraft to Harmonic and Discrete Gusts by a Transform Method*. Royal Aircraft Establishment Tech. Rep. 65264, November 1965.

14. Goldstein, H.: *Classical Mechanics*. Addison-Wesley, 1959.

15. Greenwood, D. T.: *Principles of Dynamics*. Prentice-Hall, 1965.